ON THE MECHANISM OF LEVATOR ANI MUSCLE INJURY DURING VAGINAL BIRTH

by

Jinyong Kim

A dissertation submitted in partial fulfillment
of the requirements for the degree of
Doctor of Philosophy
(Mechanical Engineering)
in the University of Michigan
2013

Doctoral Committee:

Research Professor James A. Ashton-Miller, Co-Chair
Professor John O. L. DeLancey, Co-Chair
Professor Gregory M. Hulbert
Assistant Professor Mark L. Palmer
Professor Alan S. Wineman

Dedicated to my family

for their love, guidance, and support

ACKNOWLEDGMENTS

First and foremost, I would like to express my earnest gratitude to my advisors, Professor James A. Ashton-Miller and Professor John O. L. DeLancey. Their thoughtful advice, brilliant insight, and patient encouragement guided me to realize how to be not just a good researcher, but a good person. My deep appreciation extends to my committee members, Professor Alan S. Wineman, Professor Gregory M. Hulbert, and Professor Mark M. Palmer for serving on my committee and providing helpful comments and constructive criticism that added to the quality of the overall thesis.

Support for this thesis was provided by the National Institutes of Health, Office of Research on Women's Health grant, "Specialized Center of Research on Sex and Gender Factors Affecting Women's Health", Grant # P50 HD044406 and the Michigan Institute for Clinical and Health Research, Clinical and Translational Service Award, Grant # UL1 RR024986. I would also like to thank Mr. Dean A. Mueller (the Anatomical Donation Program at the University of Michigan) for coordinating body donation, which was inevitable part of this research. Other facilities at the University of Michigan, including the histology core facility of the School of Dentistry, the Microscopy and Image-analysis Laboratory of the Department of Cell & Developmental Biology, and the Virtual Microscopy Facility of the Department of Pathology are gratefully appreciated.

I thank all the Biomechanics Research Laboratory members that I have worked with and shared an office with: Mr. Ali Attari, Ms. Melanie Beaulieu, Mr. Bradley C.

Campbell, Dr. Luyun Chen, Dr. Mark T. Gordon, Mr. Nicholas Groeneweg, Dr. Dejun Jing, Ms. Aliaksandra S. Kapshai, Dr. Hogene Kim, Ms. Yunju Lee, Dr. David Lipps, Dr. Jiajia Luo, Dr. Youkeun Oh, and Mr. Payam Mirshams Shahshahani. It has been a great pleasure to work with you all.

I think that I have been really fortunate to have opportunities to be a part of the Pelvic Floor Research Group as a trainee. The doctors, fellows and staffs of the group inspired me enough with their invaluable knowledge, opinions and suggestions. Thank you all for your interest and ability to introduce the other perspective and force me to question the clinical value of my research. I would like to give my special thanks to Dr. Cornelia Betschart for her help throughout my PhD. She has always been available and incredibly helpful with everything. Most of my work could not have done without her.

Many thanks to my Medical Innovation Fellows, Dr. Courtland K. Keteyian, Dr. David P. Lorch, and Dr. Marius A. Tijunelis. Without their understanding and support, it would not have been possible for me to find a balance between research and the Medical Innovation Center fellowship during the last several months of my PhD.

My deepest thank goes to all my family in Korea, Australia, the United Kingdom, Japan, and the United States for all the love and support they have given me. Finally, I would like to dedicate this thesis to my lovely wife, Ji Yeon, and my precious son, Einu, who mean everything to me.

TABLE OF CONTENTS

LIST OF FIGURES

LIST OF TABLES

ABSTRACT

Vaginal birth is the single largest modifiable risk factor for female pelvic floor disorders; common conditions that include pelvic organ prolapse and excretory incontinence. Magnetic resonance imaging (MRI) has demonstrated defects in the levator ani muscle near its pubic origin immediately after vaginal birth that correlate with a three- to four-fold increase in prolapse later in life. A current knowledge gap concerns the normal anatomy and histology of this attachment region, why the injury apparently occurs at the pubic origin and not elsewhere in the muscle, and accurate measures of second stage labor events.

A series of cadaveric and MRI-based examinations were conducted. An anatomical study of the origin of the pubovisceral portion of the levator ani muscle (PVM) revealed a systematic change in morphology as one moves from the medial to the lateral region (Ch. 2.1): the medial origin formed a direct oblique attachment with the pubic bone, while the lateral origin arose from the catenary-like levator arch. The fiber directions of the different levator ani muscle subdivisions where quantified by tracing fiber directions on 3T MRIs (Ch. 2.2). The projected angle of the PVM fibers was found to differ by an average of 58° from that of the puborectal muscle (PRM) in the mid-sagittal plane. We conclude that the PVM fiber direction exerts a predominantly “lifting” force acting cranially, while the PRM provides “squeezing” force acting more ventrally.

Another histological study revealed that the PVM originates medially from the pubic bone via a fibrous entheses whose collagen fibers arise tangentially from the periosteum of the pubic bone (Ch. 2.3).

The above findings were used to build finite element (FE) models of the pelvic floor to better understand the injury mechanism during vaginal birth. A 2-D FE planar model of a thin ribbon of anisotropic hyperelastic tissue representing the PVM showed a significant strain energy concentration at the inferior margin of the scarf enthesis (Ch. 3.1). This suggests why injury of the levator ani muscle can initiate at that location. A 3-D FE model of vaginal birth corroborated these findings and demonstrated why not only the PVM origin (or PVM enthesis) but also the levator arch were at higher risk of injury than the midsection of the muscle (Ch. 3.2).

Finally, a novel measurement system based on computer vision technique was developed for measuring perineal surface deformation *in vivo* during late second stage of labor (Ch. 4). The results from two women showed that the deformation during the final push was up to twice that of earlier pushes in the second stage.

We conclude that during vaginal birth, not only excessive stretch particularly at the end of the second stage but also characteristic anatomical pattern of the PVM origin at the pubic bone play major roles in causing the injury.

CHAPTER 1

Introduction

Pregnancy and giving birth to a baby are special times in a woman's life. Unfortunately, for certain women, vaginal delivery can result in distressing sequelae that can become lifelong impairments and are associated with considerable socioeconomic costs. These include pelvic organ prolapse and urinary incontinence, two pelvic floor disorders that particularly affect middle-aged and older women. For example, the number of women with pelvic organ prolapse is projected to increase from 3.3 to 4.9 million in the United States in next 40 years (Wu et al. 2009). And some 45 % of women aged between 30 and 90 years suffer from urinary continence (Melville et al. 2005). Both problems are associated with significant decrements in physical activity and quality of life (Subak et al. 2006). The direct cost of treating pelvic organ prolapse in the United States amounts to $ 1,012 million (Subak et al. 2001), while urinary incontinence requires an estimated $26.3 billion annually in societal costs (Wagner and Hu 1998).

These pelvic floor disorders are much more common in women that have given birth than in those who have not (Nygaard et al. 2008), demonstrating a correlation between vaginal childbirth and the underlying pathomechanics of the disorders. This thesis is written in an attempt to better understand this relationship from biomechanical standpoint.

This chapter presents the terminology used throughout this dissertation and female pelvic floor functional anatomy for orientation purposes. Then, we shall discuss prior research on the relationship between vaginal delivery and associated muscular injuries are discussed. Finally, the working hypothesis for the overall investigation and the major specific aims are provided.

1.1 Background and Significance

1.1.1 Pelvic Floor Muscles: Functional Anatomy

The levator ani muscle group is a major structural component of the female pelvic floor. These muscles form the bottom of the abdomino-pelvic cavity and support the pelvic organs by maintaining closure of the urogenital hiatus (i.e., the opening within the levator ani muscle through which the urethra and the vagina pass) (Lawson 1974). The muscles are also activated during a cough in order to dynamically stabilize the pelvic floor and protect the connective tissue from undue stresses. One often finds the term 'pelvic floor' used interchangeably in the literature with the 'levator ani'.

The levator ani muscle consists of three major parts: the pubococcygeal (= pubovisceral), puborectal and iliococcygeal muscles (Federative Committee on Anatomical Terminology 1998). The pubovisceral muscle can be further divided into the puboperineal (inserting into the perineal body), pubovaginal (inserting onto the vaginal wall), and puboanal (inserting into the intersphincteric groove of the anal canal) muscles

(Kearney et al. 2004) (Figs. 1.1 and 1.2). The iliococcygeal portion forms a relatively flat, horizontal shelf and spans the potential gap from one pelvic sidewall to the other. The puborectal muscle forms a sling around and behind the rectum just cephalad to the external anal sphincter. The medial sling of the muscle that arises from the pubic bone is composed of predominantly Type I striated muscle fibers and therefore is suited to maintain constant tone (Critchley et al. 1980). The connective tissue covering on both superior and inferior surfaces is called the superior and inferior fascia of the levator ani. When these muscles and their associated fascia are considered together, the combine structures make up the pelvic diaphragm.

The endopelvic fascia is a dense fibrous connective tissue layer, which surrounds the vagina and attaches it to the arcus tendineus fascia pelvis laterally (DeLancey 1994). The arcus tendineus fascia pelvis in turn is attached to the pubic bone ventrally and to the ischial spine dorsally. The arcus tendineus fascia pelvis is a tensile structure located bilaterally on either side of the urethra and vagina. These structures act like the catenary-shaped cables of a suspension bridge and help support the urethra on the anterior vaginal wall. Although well-defined as a fibrous band near its origin at the pubic bone, the arcus tendineus fascia pelvis becomes a broad aponeurotic structure as it passes dorsally to insert on the ischial spine. It therefore appears as a sheet of fascia as it fuses with the endopelvic fascia, where it merges with the levator ani muscles.

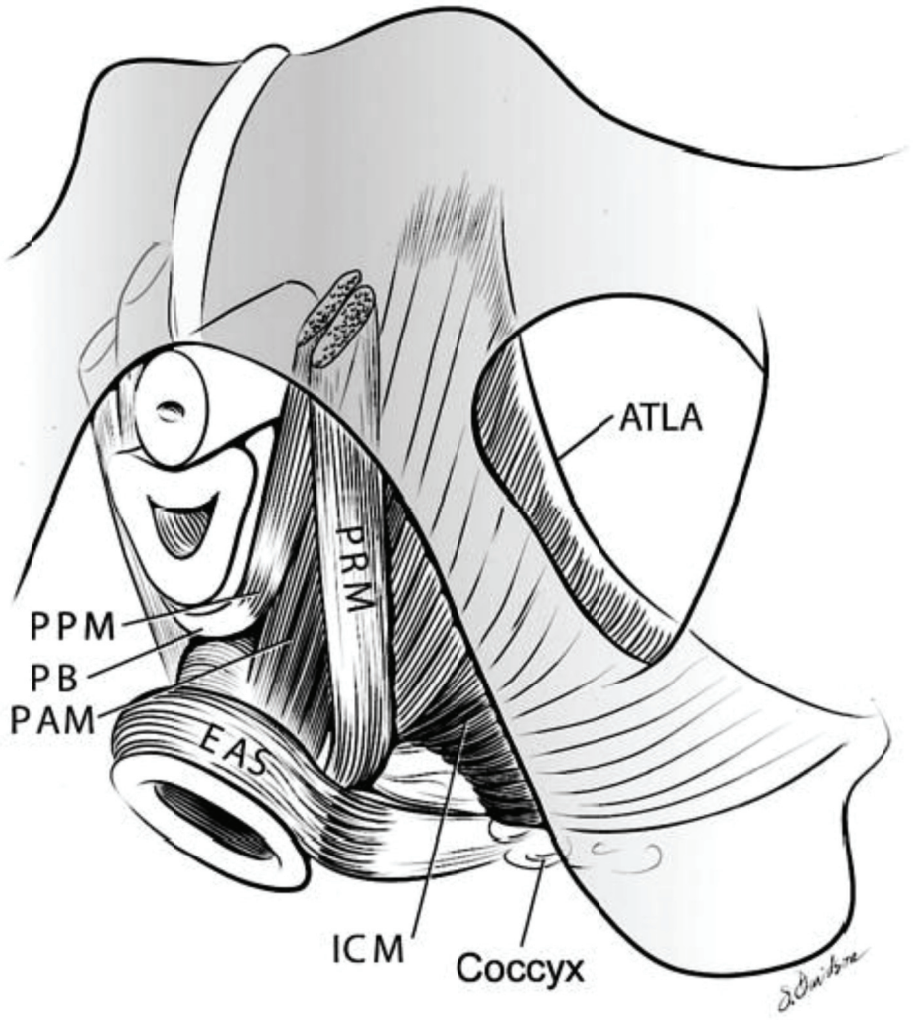

Figure 1.1. Left anteroposterior three-quarter view of the levator ani muscles from below after the vulvar structures and perineal membrane have been removed to show the arcus tendineus levator ani (ATLA); external anal sphincter (EAS); puboanal muscle (PAM); perineal body (PB) uniting the two ends of the puboperineal muscle (PPM); iliococcygeal muscle (ICM); puborectal muscle (PRM). Note that the urethra and vagina have been transected just above the hymenal ring and therefore the perineal membrane is not shown.

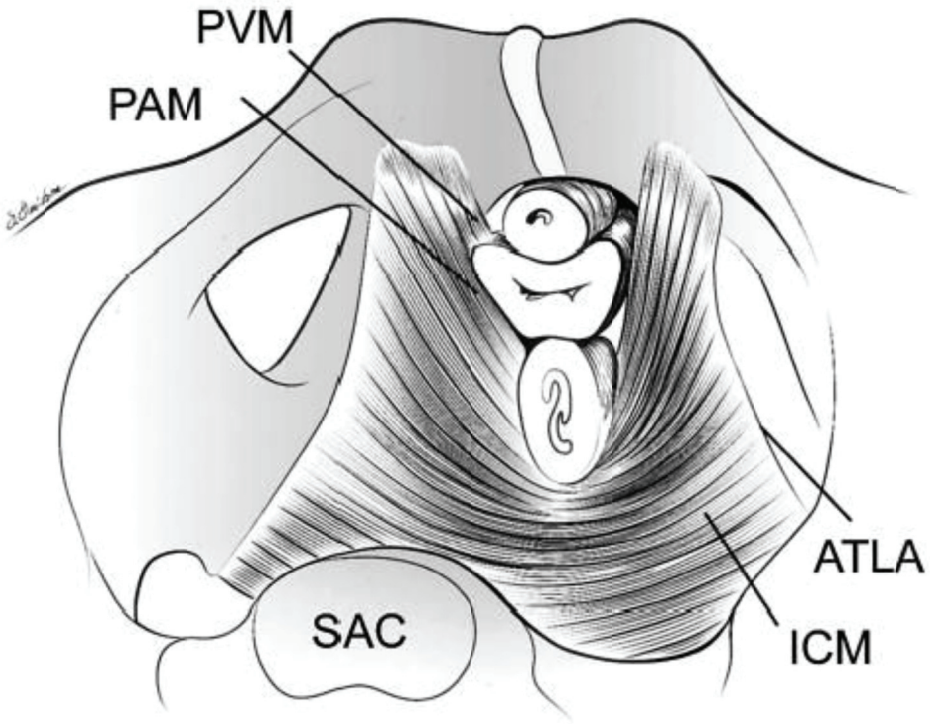

Figure 1.2. Craniocaudal view of the levator ani muscle seen from the right side of the sacral promontory (SAC) and showing the pubovaginal muscle (PVM). The uterus and bladder have been removed to show the urethra, vagina, and rectum have been transected just above the pelvic floor. PAM denotes puboanal muscle; ATLA, arcus tendineus levator ani; and ICM, iliococcygeal muscle. (The internal obturator muscles have been removed to clarify levator muscle origins.) © DeLancey 2003.

1.1.2 Relationship between Vaginal Birth, Muscle Stretch and Levator Muscle Injury

In increased risk for developing pelvic floor dysfunctions (including pelvic organ prolapse or urinary and/or fecal incontinence) has been founding women with to prior vaginal delivery by several epidemiological studies (Foldspang et al. 1992; Mant et al. 1997; Leijonhufvud et al. 2011). Two other observations strengthen this causal relationship between vaginal delivery and pelvic floor impairment:

(1) Women with prolapse are more likely to have major levator ani defects than women without prolapse, with an odds ratio of 7.3 (DeLancey et al. 2007);

(2) Injuries in the levator ani muscles are usually only found in primiparous women but not in nulliparous women (Kearney et al. 2006).

Therefore, it is reasonable to assume that vaginal delivery is responsible for the levator ani muscle structure abnormalities and the accompanying problems.

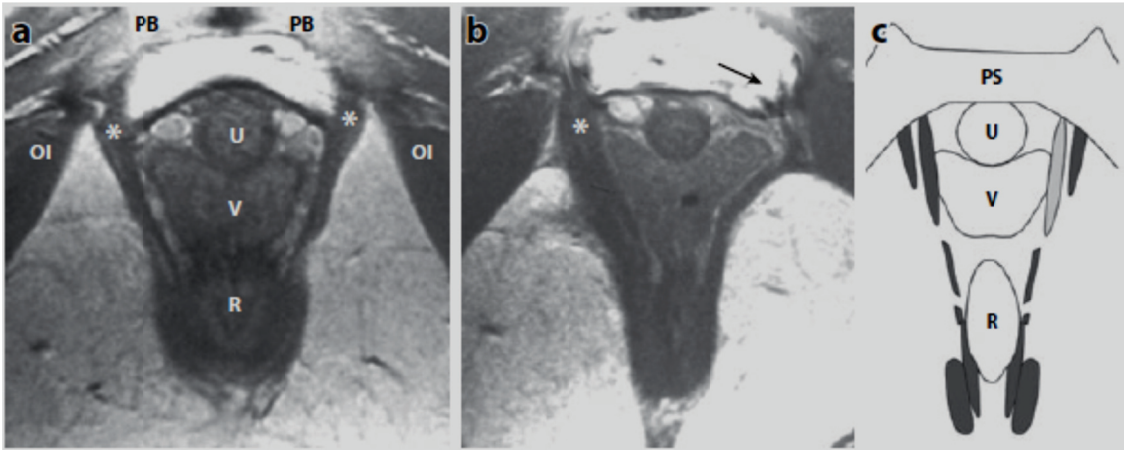

Figure 1.3. (a) Normal anatomy in an axial mid-urethra MR image showing the pubovisceral muscle (asterisks). (b) Woman who have lost a part of the left pubovisceral muscle (displayed on the right side of the image, according to standard medical imaging convention) with lateral displacement of the vagina into the area normally occupied by the muscle. The arrow points to the expected location of the missing muscle. The puborectal muscle is left intact bilaterally. (c) Axial, mid-urethral section through the arch of the pubic bone [see pubic symphysis (PS), top] and the model levator ani muscles at a level corresponding to those from the women shown in panels (a, b). Intact muscles are shown in dark gray and the damaged muscle, light grey. The location of pubovisceral muscle atrophy is illustrated by the light gray shading. OI, Obturator internus muscle; PB, pubic bone; U, urethra; V, vagina; R, rectum. Modified from (Lien et al. 2004).

Where, then, exactly does the levator ani muscle injury occur due to vaginal delivery? Through analyses of MR images, defects have been noted in the pubovisceral

portion of the levator ani muscle that arises from the inner surface of the pubic bone, just lateral to the vagina; this rarely involves the iliococcygeus portion of the muscle (Fig. 1.3) (DeLancey et al. 2003) (Note that the iliococcygeus muscle portion is not likely to be damaged in women with unilateral defects (Margulies et al. 2007)).

Ethical considerations preclude interfering unnecessarily with the process of labor for research purposes. This is because the safety of mother and baby are always prioritized. So, computerized simulation techniques are useful to help clarify what is happening to the pelvic floor and baby during a vaginal delivery. The time course of the pelvic floor deformation during vaginal birth has been simulated by several investigators (Lien et al. 2004; Hoyte et al. 2008; Parente et al. 2008; Li et al. 2010). The main results are that the structure that is stretched the most is the pubovisceral muscle, thereby placing it at the greatest risk for stretch-induced injury of any region of the levator ani muscle. Some variations in the birth process scenario have also been examined, including the effect of fetal head presentation (Parente et al. 2009a; Jing 2010), pelvic floor muscle properties (Parente et al. 2009b), and the energetics of maternal effort during delivery (Lien et al. 2009). Importantly, the work by Lien et al. (2004) and Jing (2010) both identified a high strain region near the pubic origin of the pubovisceral muscle. This will become a focus of the present research.

However, the mechanisms underlying the birth-related injury to the levator ani muscle remain poorly understood. First, more accurate anatomical detail is needed before the exact injury location can be clearly identified by biomechanical analysis. The previous geometrical models simplified the levator ani muscles as either a series of muscle strips or a simple muscle sheet, whereas the levator ani muscle and its

surrounding structures are closely interwoven with each other, forming a multi-layered laminated structure. The detailed morphology of the origin of the levator ani muscle, namely its enthesis (the junction formed with collagenous tissue between the muscle and the bone), needs to be identified and incorporated in the model because there could be features of the junction that might be associated with promoting injury there. Second, we do not yet know whether, during a birth, injury occurs to a pubovisceral muscle in its active or its passive state of muscle activity or both. Third, time-dependent behavior of the levator ani muscle and its influence on the muscle deformation also remains to be elucidated, because a forceps delivery is associated with an elevated risk for injury perhaps because of the increased rate at which the pelvic muscle is stretched (Ashton-Miller and DeLancey 2009). Finally, the complex dynamics of the second stage of labor should be captured, measured, and documented. This kind of rate information will provide clinicians with the specifics of how, when, and in whom levator ani injury is most likely to occur. It will also provide biomechanists with a dataset to validate computer simulation studies.

1.2 Hypothesis and Specific Aims

In this proposal, I hypothesize that birth-related injury of the pubovisceral portion of the levator ani muscle is attributed to the innate morphology of its pubic origin combined with the highly unusual loading conditions that occur during the first vaginal birth in particular, but also on subsequent vaginal births.

The overall goal of this thesis is to identify the pathomechanics of the pubovisceral injury in healthy women giving vaginal birth. The specific aims of the thesis are stated as follows:

- **Aim 1: Anatomical description of the regions of injury of the levator ani muscle and its surrounding structures (Chapter 2)**

Clinically, the regions of injury are known to include several different substructures that come together over a length of about 10 cm across the pelvic sidewall. Although the injury location has been identified on MR scans, the detailed anatomy of this region has still not been clarified as it originates from the pubis. Moreover, the regional differences and the structural role of each of these components remain to be elucidated in both qualitative and quantitative manners. Various analysis methodologies, including cadaveric dissection, histochemical process, and magnetic resonance images, will be adopted to investigate the region of interest from comprehensive to specific levels. The outcome will be valuable for the subsequent biomechanical modeling (Aim 2).

- **Aim 2: Biomechanical modeling for better understanding the mechanisms of injury to the levator ani muscle during vaginal delivery (Chapter 3)**

Given that the opportunities for experiments on women during delivery are limited and that mechanisms of human birth differ significantly from those of experimental animals (Abitbol 1988), finite element analysis will be used to examine the relationship between the risk of birth-related injuries to the levator ani muscle and a variety of factors that may occur during obstetrical events. As a start, a simplified, two-dimensional, anisotropic model will be considered, and then extended to a three-

dimensional, multi-component model. The obstetrical activities will be transformed into a set of predictors, the effect of which will be subsequently assessed with the model using statistical sensitivity analyses. The results of this investigation are expected to provide further insight into the mechanical quantities that are known to correlate with soft-tissue damage. This insight may lead to a better understanding of the factors that determine levator ani muscle injury during vaginal delivery in terms of morphology, loading patterns, and material properties. These in turn may help indicate future opportunities for interventions aimed at preventing these injuries.

- **Aim 3: Development of a 3-D measurement system for the fetal head and the perineal surface movements during the second stage of vaginal delivery (Chapter 4)**

To date, intrapartum measurements of fetal descent have relied on subjective methodologies, such as a tape ruler and stop watch. While convenient and quick, such methods do not have sufficient accuracy and precision so a more objective, non-contact measurement system will be developed. This new system is to be built with the smallest-possible form factor so as to not intimidate the mother-to-be and placed at the bedside for recording the time course of the second stage of labor with minimal assistance by healthcare providers. The amount of the fetal head descent as well as the deformation of the perineal surface should be able to be captured using this system.

1.3 References

Wu, J. M., Hundley, A. F., Fulton, R. G., Myers, E. R. (2009). Forecasting the prevalence of pelvic floor disorders in U.S. Women: 2010 to 2050. *Obstet. Gynecol., 114*(6), 1278-1283. doi: 10.1097/AOG.0b013e3181c2ce96

Melville, J. L., Katon, W., Delaney, K., Newton, K. (2005). Urinary incontinence in US women: a population-based study. *Arch. Intern. Med., 165*(5), 537-542. doi: 10.1001/archinte.165.5.537

Subak, L. L., Brown, J. S., Kraus, S. R., Brubaker, L., Lin, F., Richter, H. E., Bradley, C. S., Grady, D. (2006). The "costs" of urinary incontinence for women. *Obstet. Gynecol., 107*(4), 908-916.

Subak, L. L., Waetjen, L. E., van den Eeden, S., Thom, D. H., Vittinghoff, E., Brown, J. S. (2001). Cost of pelvic organ prolapse surgery in the United States. *Obstet. Gynecol., 98*(4), 646-651.

Wagner, T. H., Hu, T. W. (1998). Economic costs of urinary incontinence in 1995. *Urology, 51*(3), 355-361.

Nygaard, I., Barber, M. D., Burgio, K. L., Kenton, K., Meikle, S., Schaffer, J., Spino, C., Whitehead, W. E., Wu, J., Brody, D. J. (2008). Prevalence of symptomatic pelvic floor disorders in US women. *JAMA, 300*(11), 1311-1316. doi: 10.1001/jama.300.11.1311

Lawson, J. O. (1974). Pelvic anatomy. I. Pelvic floor muscles. *Ann. R. Coll. Surg. Engl., 54*(5), 244-252.

Federative Committee on Anatomical Terminology. (1998). *Terminologia anatomica: international anatomical terminology*. Stuttgart ; New York: Thieme.

Kearney, R., Sawhney, R., DeLancey, J. O. (2004). Levator ani muscle anatomy evaluated by origin-insertion pairs. *Obstet. Gynecol., 104*(1), 168-173.

Critchley, H. O., Dixon, J. S., Gosling, J. A. (1980). Comparative study of the periurethral and perianal parts of the human levator ani muscle. *Urol. Int., 35*(3), 226-232.

DeLancey, J. O. (1994). The anatomy of the pelvic floor. *Curr. Opin. Obstet. Gynecol., 6*(4), 313-316.

Foldspang, A., Mommsen, S., Lam, G. W., Elving, L. (1992). Parity as a correlate of adult female urinary incontinence prevalence. *J Epidemiol Community Health, 46*(6), 595-600.

Mant, J., Painter, R., Vessey, M. (1997). Epidemiology of genital prolapse: observations from the Oxford Family Planning Association Study. *Br. J. Obstet. Gynaecol., 104*(5), 579-585.

Leijonhufvud, A., Lundholm, C., Cnattingius, S., Granath, F., Andolf, E., Altman, D. (2011). Risks of stress urinary incontinence and pelvic organ prolapse surgery in relation to mode of childbirth. *Am. J. Obstet. Gynecol., 204*(1), 70 e71-77.

DeLancey, J. O., Morgan, D. M., Fenner, D. E., Kearney, R., Guire, K., Miller, J. M., Hussain, H., Umek, W., Hsu, Y., Ashton-Miller, J. A. (2007). Comparison of levator ani muscle defects and function in women with and without pelvic organ prolapse. *Obstet. Gynecol., 109*(2 Pt 1), 295-302. doi: 10.1097/01.AOG.0000250901.57095.ba

Kearney, R., Miller, J. M., Ashton-Miller, J. A., DeLancey, J. O. L. (2006). Obstetric factors associated with levator ani muscle injury after vaginal birth. *Obstet. Gynecol., 107*(1), 144-149. doi: 10.1097/01.AOG.0000194063.63206.1c

Lien, K. C., Mooney, B., DeLancey, J. O., Ashton-Miller, J. A. (2004). Levator ani muscle stretch induced by simulated vaginal birth. *Obstet. Gynecol., 103*(1), 31-40. doi: 10.1097/01.AOG.0000109207.22354.65

DeLancey, J. O., Kearney, R., Chou, Q., Speights, S., Binno, S. (2003). The appearance of levator ani muscle abnormalities in magnetic resonance images after vaginal delivery. *Obstet. Gynecol., 101*(1), 46-53. doi: S0029784402024651

Margulies, R. U., Huebner, M., DeLancey, J. O. (2007). Origin and insertion points involved in levator ani muscle defects. *Am. J. Obstet. Gynecol., 196*(3), 251 e251-255.

Hoyte, L., Damaser, M. S., Warfield, S. K., Chukkapalli, G., Majumdar, A., Choi, D. J., Trivedi, A., Krysl, P. (2008). Quantity and distribution of levator ani stretch

during simulated vaginal childbirth. *Am. J. Obstet. Gynecol., 199*(2), 198 e191-195. doi: 10.1016/j.ajog.2008.04.027

Parente, M. P., Jorge, R. M., Mascarenhas, T., Fernandes, A. A., Martins, J. A. (2008). Deformation of the pelvic floor muscles during a vaginal delivery. *Int. Urogynecol. J., 19*(1), 65-71. doi: 10.1007/s00192-007-0388-7

Li, X., Kruger, J. A., Nash, M. P., Nielsen, P. M. (2010). Anisotropic effects of the levator ani muscle during childbirth. *Biomech. Model. Mechanobiol., 10*(4), 485-494. doi: 10.1007/s10237-010-0249-z

Parente, M. P., Jorge, R. M., Mascarenhas, T., Fernandes, A. A., Martins, J. A. (2009a). The influence of an occipito-posterior malposition on the biomechanical behavior of the pelvic floor. *Eur. J. Obstet. Gynecol. Reprod. Biol., 144 Suppl 1*, S166-169. doi: 10.1016/j.ejogrb.2009.02.033

Jing, D. (2010). *Experimental and theoretical biomechanical analyses of the second stage of labor.* PhD. thesis, University of Michigan.

Parente, M. P., Jorge, R. M., Mascarenhas, T., Fernandes, A. A., Martins, J. A. (2009b). The influence of the material properties on the biomechanical behavior of the pelvic floor muscles during vaginal delivery. *J. Biomech., 42*(9), 1301-1306. doi: 10.1016/j.jbiomech.2009.03.011

Lien, K. C., DeLancey, J. O., Ashton-Miller, J. A. (2009). Biomechanical analyses of the efficacy of patterns of maternal effort on second-stage progress. *Obstet. Gynecol., 113*(4), 873-880. doi: 10.1097/AOG.0b013e31819c82e1

Ashton-Miller, J. A., DeLancey, J. O. (2009). On the biomechanics of vaginal birth and common sequelae. *Annu Rev Biomed Eng, 11*, 163-176. doi: 10.1146/annurev-bioeng-061008-124823

Abitbol, M. M. (1988). Evolution of the ischial spine and of the pelvic floor in the Hominoidea. *Am. J. Phys. Anthropol., 75*(1), 53-67. doi: 10.1002/ajpa.1330750107

CHAPTER 2

Anatomical and Histological Studies of the Origin of the Pubovisceral Portion of the Levator Ani Muscle

2.1 Quantitative Description of the Ventral Pubovisceral Muscle and its Origin and Insertion

2.1.1 Introduction

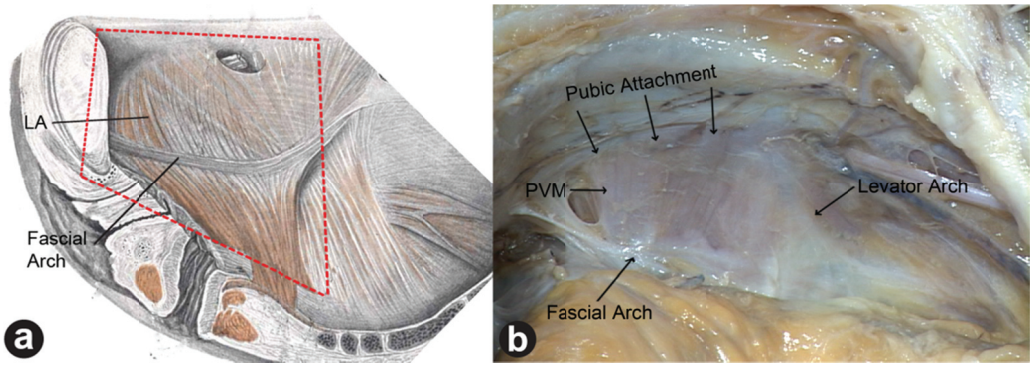

Figure 2.1. **(a)** Left mediolateral view of the anterior pelvic sidewall, with pelvic organs removed, showing the characteristic features of the origin of the pubovisceral muscle. The dotted quadrangle shows the anatomic area of study (Reproduced from Halban and Tandler (1907)). **(b)** A similar view of the right anterior pelvic sidewall of a 50 year old nulliparous fresh cadaver showing the pubovisceral attachments to the pubic bone. The fascial arch lies across the pubovisceral muscle, and the levator arch forms the lateral margin of the pubovisceral muscle as it attaches onto the pelvic sidewall.

Vaginal delivery is known to cause defects visible on magnetic resonance imaging (MRI) in the pelvic floor structures, including the levator ani muscle and the

connective tissue around it (DeLancey et al. 2003; Leijonhufvud et al. 2011). Due to tensile stretch during vaginal delivery that is twice the value tolerated by striated muscle in non-pregnant individuals (Lien et al. 2004), the levator ani muscle is subject to significant structural changes, including muscle tears or even avulsion (DeLancey et al. 2003). These injuries appear to occur in a characteristic "injury zone" on the inner surface of the pubic bone at origin of the pubovisceral but not the puborectal muscle, as evidenced by magnetic resonance image-based studies (DeLancey et al. 2003; Dietz et al. 2007; Margulies et al. 2007; DeLancey et al. 2012). But, there are actually several different constituent parts of the levator ani in this area over a length of about 10 cm across the pelvic sidewall (Kim et al. 2011a). As can be seen in Figure 2.1, the substructures in this anatomical region includes the pubovisceral portion of the levator ani muscle (= pubovisceral muscle, the pubococcygeal muscle), the levator arch (= arcus tendineus levator ani), and the fascial arch (= arcus tendineus fascia pelvis). This raises the possibility of morphological differences in the pubovisceral muscle origin along the pelvic sidewall. Although a number of previous studies have been conducted on this region using histological slides (Lawson 1974; Albright et al. 2005; Grigorescu et al. 2008), morphological differences in the origins of the various sub-parts of the levator ani within this region have not been reported before to the best of our knowledge.

The purpose of this study, therefore, was to establish the gross and microscopic anatomy of the pubic origin of the levator ani muscle involved in birth-induced injury.

2.1.2 Methods

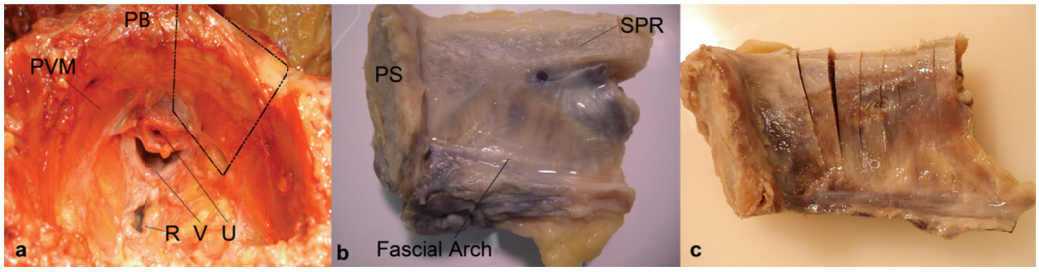

Figure 2.2. **(a)** Superior view of the ventral pelvis after organ removal. The dotted quadrangle shows the area from which histological specimens were acquired. **(b)** An example of an excised specimen block which includes the right side PVM origin from the inner surface of the pubic bone showing the pubic symphysis at left. **(c)** Sectioning strategy used for the PVM origin histology showing the sequential cuts at ~ 5 mm intervals. (PB denotes pubic bone; PVM: pubovisceral muscle; U: urethra; V: vagina; R: rectum; PS: pubic symphysis; SPR: superior pelvis ramus).

Histochemical processing was focused on the pubic origin of the pubovisceral muscle (PVM), which could span from approximately 1 cm lateral from the pubic symphysis laterally to the origin of the levator arch that lies just ventral to the obturator canal (Fig. 2.2). Nine female cadavers, four of which were nulliparous, were collected with the support of the Anatomical Donations Program at the University of Michigan. The cadaveric specimens ranged from 35 to 98 years of age, with a mean age of 66 years of age. Gynecological surgeons with knowledge and experience in evaluation the levator ani muscle and the perineal area (CB and JOLD) assessed all the specimens and none showed signs of major pelvic floor muscle damage associated with maternal birth.

Histological samples were acquired using targeted feature sequential sampling. The purpose of this acquisition strategy was to show the variation of the detailed morphological and structural relationships along the pubic origin of the PVM without

losing important anatomical features, such as the origin of the levator arch and the fascial arch, the merging point of both arches, or the muscle-bone interface of the PVM origin. Once a smaller portion of the sample was excised from the whole pelvis, the sequential precuts on the superior portion of the sample were made at an interval of approximately 5 mm, care being taken to keep the integrity of the structure intact (Fig. 2.2). The detailed fiber orientation, as well as the enthesis or junction between the pubovisceral muscle and the pubic bone, were thoroughly examined using magnification when necessary before the pubic bones and the attached muscles were removed, so that the final sectioning was able to be made parallel to the fiber direction.

Smaller samples were then removed for histochemical processing by cutting them parallel to the PVM fiber direction. The samples were fixed in 10 % neutral buffered formalin, decalcified in 10% formic acid for up to 20 days and stored in 70 % ethanol. Paraffin embedding was then applied followed by serial sectioning of samples less than 7 μm in thickness. Masson's trichrome staining was applied in order to effectively distinguish muscular cells from connective tissue. Finally, digital conversion of the stained slide was conducted using a Super COOLSCAN 5000 ED film scanner (Nikon, Shinjuku, Tokyo, Japan).

2.1.3 Results

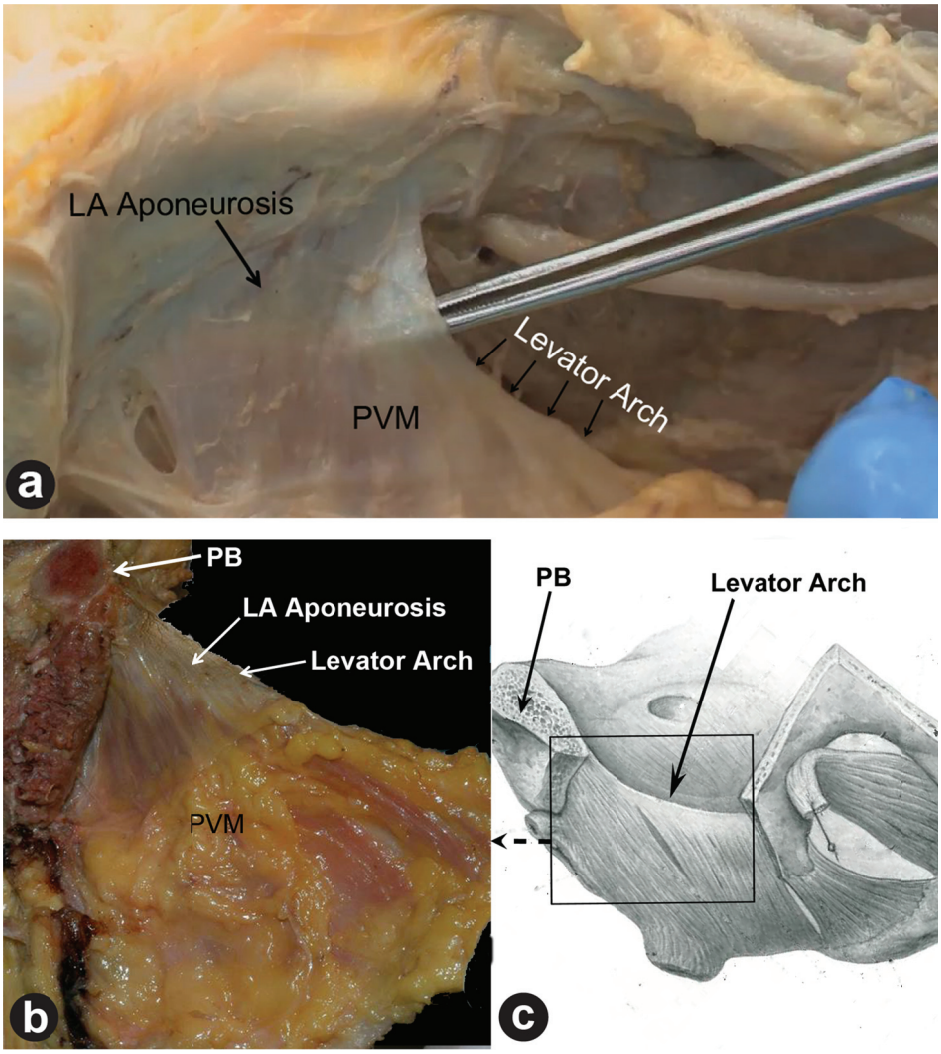

Figure 2.3. **(a)** A view of the inner surface of the right pubic origin of the PVM corresponding to that in Fig. 2.2b. Note how thin the semitransparent levator ani (LA) aponeurosis is (i.e. tips of a clamp being visible through the aponeurosis) as it attaches to the superior pubic ramus. This aponeurosis poses a smooth transition from the muscular area of the PVM to the periosteum of the pubic bone. Medially the muscle can be seen to extend closer to the bone than it is laterally where the aponeurosis widens. **(b)** Left lateral view of the left PVM origin area seen from outside the pelvis after the lateral pelvic bone was removed to reveal the outside of the aponeurotic levator ani muscle. **(c)** To help orient the reader to understand the view in Fig. 2.3b, this drawing also shows a larger left lateromedial field of view of the pelvis with the left pubic ramus removed. Note that the medial portion of the muscle extends to the bone while the more lateral portion has a wide aponeurosis between the muscle and bone. The rectangle shows the view shown in Fig. 2.3b. **(**Reproduced and modified from Anson (1963))

The PVM originates tangentially from the periosteum covering the pubic bone, although importantly its nature changes systematically in morphology from the medial to lateral regions. The PVM origin can therefore be divided into three regions: medial, central, and lateral. Figure 2.3a consists of one picture taken from the inside of the pelvic sidewall. Panel b is a view from outside the pelvis after a lateral portion of the left anterior pubic rami was removed to provide visual access to the PVM as shown in panel c. The PVM origin includes a relatively direct connection between muscle and bone near the midline. Laterally, a thin semitransparent membrane, the thickness of which was no more than 2 mm, is seen. It lies adjacent to the obturator internus muscle, but no fusion between the two muscles was found as they were able to be separated easily by blunt dissection. The lateral portion of the PVM pubic origin blends into the iliococcygeal muscle, which originated from the levator arch that runs from the pubic bone to the ischial spine. The muscle fibers were oriented radially from the levator arch origin.

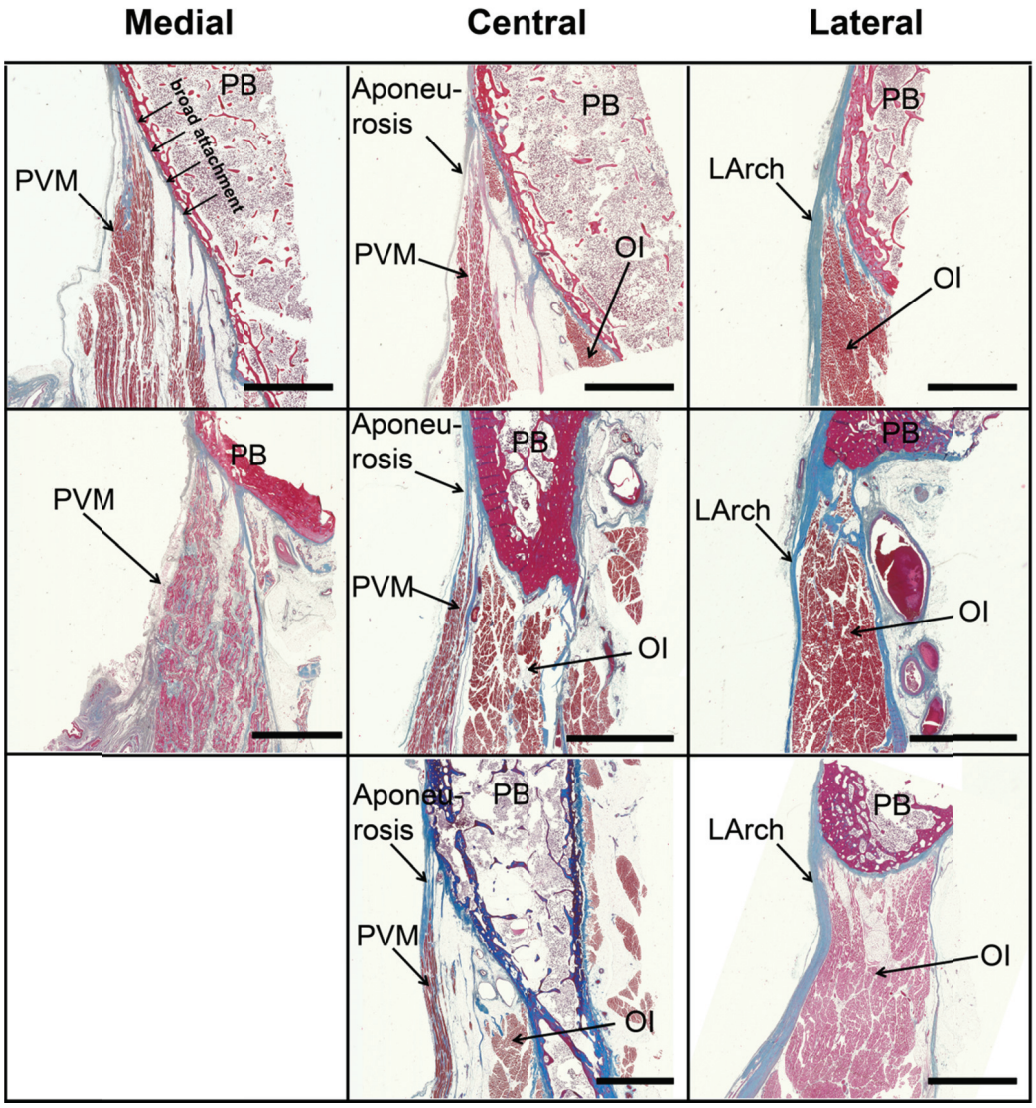

Figure 2.4. Examples of medial, central and lateral region histology of the pubic origin of the PVM. Each row is from a different donor. Histological images showing the pubic origin of the levator ani from medial (column 1), central (column 2), and lateral (column 3) areas with the orientation picture below. All samples shown are stained in Masson's trichrome, and the scale bars are 5 mm. **(Medial)** The medial LA fibers originate from multiple slips attaching in an enthesis to the pubis. Oblique interface between the pubic bone (PB) and the levator ani muscle (LA) can also be observed. The thickness of the LA is greater than in other areas. **(Central)** The central portion originates from the PB in a single aponeurotic attachment, which is noticeably thinner than medial portion. The obturator internus muscle (OI) can be seen lateral to the LA. **(Lateral)** The levator arch (LArch) appears as dense blue connective tissue attaching to the PB and forming the lateral margin of the pubic origin of the LA. Note that relative preponderance of the three portions varies by individual.

Figure 2.4 shows histological cross-sections of the pubic interface of the PVM acquired from cadaveric specimens. Each column shows a different region of origin, from medial to lateral, while the different rows are from different individuals. In the medial region, the muscle fibers attach to the pubic bone by means of short fibrous attachments. In the medial section there is an aponeurosis that bridges a widening distance between the end of the muscle fibers and the periosteum. Laterally, the dense connective tissue band of the levator arch is seen. An angled interface between the muscle and the bone is also evident, especially in the medial region. The aponeurotic PVM widens in the central region resulting in a larger separation between the muscle fascicles and pubic bone. The thickness of the muscle belly thins as one moves laterally.

Figure 2.5 was captured from a video sequence as the perineal area was repeatedly pulled inferiorly in the direction typical of the loading late in a vaginal delivery. Traction created visible tension where the PVM originated from the pubic bone but did not affect the obturator internus muscle. Although tension could be seen all along the muscle origin, it was concentrated most at the point where levator arch attached to the pubic bone.

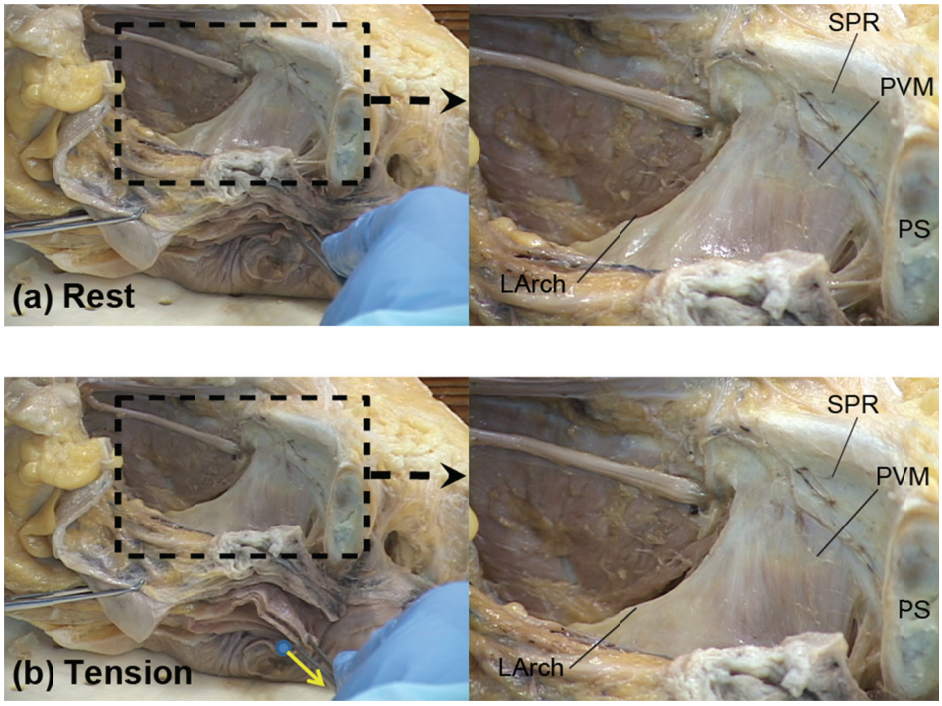

Figure 2.5. Three-quarter view of the inside of the left anterior pelvis of a fresh cadaveric specimen sectioned in the mid-sagittal plane. The views demonstrate how the PVM origin deforms in response to a downward force placed on the perineal structures. Resting position **(a)** and deformed position **(b)** are compared. Tension increases over the pubic origin of the levator ani and the attachment of the levator arch to the pubic bone as the perineal body area is pulled in the direction of loading typical late in a vaginal birth. (SPR denotes superior pubic ramus; PVM: pubovisceral muscle; PS: pubic symphysis; LArch: levator arch)

2.1.4 Discussion

We have found characteristic features of the anatomy of the origin of the PVM in the region where both MRI and computer simulations have shown that birth-induced stretch injury can occur (see Section 2.1.1 Introduction). The lateral margin, which is formed with the levator arch, is a thick collagenous bundle connecting to the pelvic sidewall and the ischial spine with a catenary structure. This attachment pattern contrasts

with the medial margin of the PVM attachment where the muscle is directly attached to the pubic bone via a fibrous enthesis (Benjamin et al. 2002). The medial portion showed yet another characteristic: namely a thin semitransparent muscle aponeurosis. A video shows that when pelvic floor stretch similar to that occurring late in vaginal birth is applied, one can simulate the load on the origins that might occur during vaginal delivery.

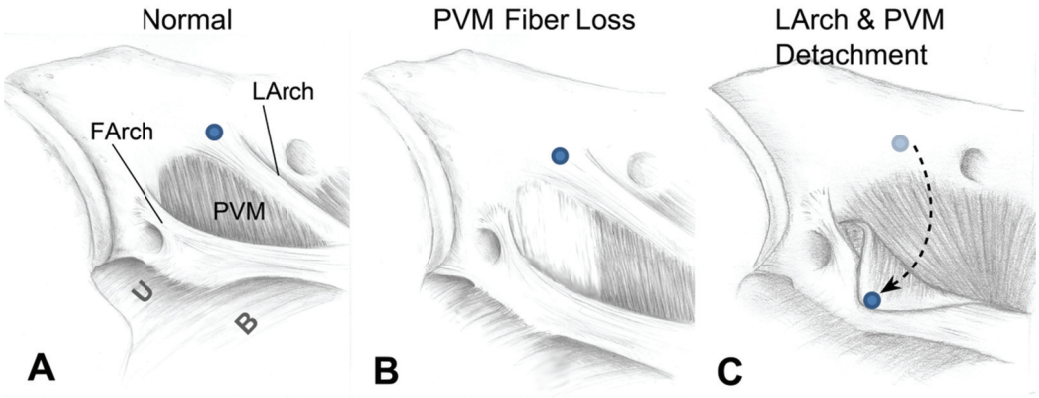

Figure 2.6. Illustrations of the right inner pelvic sidewall showing the fascial and levator arch originating from the pubic bone. (A) Two different types of the PVM origin can be identified: One being direct aponeurotic attachment in anteromedial portion, the other being indirect catenary attachment through the levator arch (LArch) in posterolateral region. Morphological and functional variation in these locations may account for how injury might occur and progress. (B) Aponeurotic attachment can locally be damaged due to excessive stress and strain concentration there, which then leads to muscle atrophy. (C) Detachment of the LArch origin from the pubic bone (dot) observed in 32 year old patient with stress urinary incontinence and history of a traumatic birth (3rd degree laceration). Since there is only a single point of pubic origin at the LArch for the lateral margin of the PVM, detachment of that point (Figure 2.6c) will result in complete offloading of that region of the PVM. (Modified from Fig. 2a of Delancey (2002))

Based on improved understanding of the morphology of this area, we can introduce a conceptual framework that injury to the maternal PVM occurs in a sequential two-step process (Fig. 2.6). In the first step the injury is confined to individual portions of the medial of the PVM in which the portions of the enthesis is partially or completely

torn from the pubic bone. In this defect the levator arch remains intact. Our group has dubbed this interface a 'scarf enthesis' (Kim et al. 2011a), since it is an enthesis where the two heterogeneous materials - the PVM and the pubic bone - meet at an oblique angle. (An oblique junction is often referred to as a scarf joint in the engineering field.) In a computer simulation study that has been conducted to examine how traction on the PVM affects the strain energy distribution in its oblique connection to the pubic bone, the results demonstrated a significant strain energy concentration appearing at the inferior margin of the scarf enthesis (see Chapter 3.1). This suggests a possible location for the initiation of the birth-related avulsive injury which we have designated a “Type I” injury.

The second injury step might be relevant to the ventral attachment of the catenary-like levator arches avulsed from the pubic bone by tension in the iliococcygeal muscle. This would constitute what we call a “Type II” injury and might occur during a subsequent vaginal birth, for example. A characteristic abnormal appearance of the vagina in the same region where damage to the PVM is seen has been reported and involves changes on the overall architecture of this region (Huebner et al. 2008). MR images of women with the architectural distortion showed significant alteration in the levator arch anatomy along with lateral or posterior spill of the vagina from its normal position. Engineering studies of catenary structures also indicate that extra care is needed in designing the cable itself because, as the main load-carrying pathway, failure can lead to catastrophic collapse when it is damaged (Averill 1940; Plaut 2008).

Our methodological approach has several limitations. First, the sample size was small, so generalization of the results should be made with care until the results are corroborated by others, and possible variations with age, parity and/or ethnicity checked.

The availability of nine nulliparous cadavers; a rarity in anatomical donation programs is a strength of this study. Second, the observations of this study were based on cadaveric specimens whose topography is altered by death and the fixation process. We were able to minimize this effect by harvesting the entire pelvis fresh and then fixing by flotation as a whole so that the integrity of the structure was maintained as much as possible. Third, histological descriptions of the study region were focused on geometrical comparisons. More detailed histological descriptions are needed that include different types of collagen, decorin, biglycan, aggrecan and other possible constituents that may form this particular enthesis (Liu et al. 2011). Investigation of the nerve supply to this region might also be worthwhile, since pudendal nerve damage has been noted in women with pelvic floor dysfunction (Smith et al. 1989; Kenton et al. 2011).

The present study has provided a first morphologic and geometric description of the region of birth-related injury near the PVM origin. This may be valuable for a better understanding of the injury mechanism during vaginal delivery (Kim et al. 2011b). The pubic origin of the PVM was examined in terms of three sub-regions or its pubic origin: medial, central, and lateral. Based on the understanding of the structure through cadaver dissections, an analogy to simpler load bearing mechanical elements was made and a hypothetical injury mechanism and injury sequence were offered (i.e., Type I and II injury).

2.1.5 References

Halban, J., Tandler, J. (1907). *Anatomie und aetiologie der genitalprolapse beim weibe*: Braumüller.

DeLancey, J. O., Kearney, R., Chou, Q., Speights, S., Binno, S. (2003). The appearance of levator ani muscle abnormalities in magnetic resonance images after vaginal delivery. *Obstet. Gynecol., 101*(1), 46-53. doi: S0029784402024651

Leijonhufvud, A., Lundholm, C., Cnattingius, S., Granath, F., Andolf, E., Altman, D. (2011). Risks of stress urinary incontinence and pelvic organ prolapse surgery in relation to mode of childbirth. *Am. J. Obstet. Gynecol., 204*(1), 70 e71-77.

Lien, K. C., Mooney, B., DeLancey, J. O., Ashton-Miller, J. A. (2004). Levator ani muscle stretch induced by simulated vaginal birth. *Obstet. Gynecol., 103*(1), 31-40. doi: 10.1097/01.AOG.0000109207.22354.65

Dietz, H. P., Gillespie, A. V., Phadke, P. (2007). Avulsion of the pubovisceral muscle associated with large vaginal tear after normal vaginal delivery at term. *Aust. N. Z. J. Obstet. Gynaecol., 47*(4), 341-344. doi: 10.1111/j.1479-828X.2007.00748.x

Margulies, R. U., Huebner, M., DeLancey, J. O. (2007). Origin and insertion points involved in levator ani muscle defects. *Am. J. Obstet. Gynecol., 196*(3), 251 e251-255.

DeLancey, J. O., Sorensen, H. C., Lewicky-Gaupp, C., Smith, T. M. (2012). Comparison of the puborectal muscle on MRI in women with POP and levator ani defects with those with normal support and no defect. *Int. Urogynecol. J., 23*(1), 73-77. doi: 10.1007/s00192-011-1527-8

Kim, J., DeLancey, J. O., Ashton-Miller, J. A. (2011a). *Why does the pubovisceral muscle fail at its enthesis, and not elsewhere, during the second stage of labor? A computational study*. Paper presented at the 35th Annual Meeting of the American Society of Biomechanics, Long Beach, CA.

Lawson, J. O. (1974). Pelvic anatomy. I. Pelvic floor muscles. *Ann. R. Coll. Surg. Engl., 54*(5), 244-252.

Albright, T. S., Gehrich, A. P., Davis, G. D., Sabi, F. L., Buller, J. L. (2005). Arcus tendineus fascia pelvis: a further understanding. *Am. J. Obstet. Gynecol., 193*(3 Pt 1), 677-681. doi: 10.1016/j.ajog.2005.02.129

Grigorescu, B., Lazarou, G., Olson, T., Downie, S., Powers, K., Greston, W., Mikhail, M. (2008). Innervation of the levator ani muscles: description of the nerve branches

to the pubococcygeus, iliococcygeus, and puborectalis muscles. *Int. Urogynecol. J., 19*(1), 107-116. doi: 10.1007/s00192-007-0395-8

Anson, B. J. (1963). *An atlas of human anatomy*. Philadelphia: Saunders.

Benjamin, M., Kumai, T., Milz, S., Boszczyk, B. M., Boszczyk, A. A., Ralphs, J. R. (2002). The skeletal attachment of tendons--tendon "entheses". *Comp Biochem Physiol A-Mol Integr Physiol, 133*(4), 931-945. doi: 10.1016/S1095-6433(02)00138-1

Delancey, J. O. (2002). Fascial and muscular abnormalities in women with urethral hypermobility and anterior vaginal wall prolapse. *Am. J. Obstet. Gynecol., 187*(1), 93-98.

Huebner, M., Margulies, R. U., DeLancey, J. O. (2008). Pelvic architectural distortion is associated with pelvic organ prolapse. *Int. Urogynecol. J. Pelvic Floor Dysfunct., 19*(6), 863-867. doi: 10.1007/s00192-007-0546-y

Averill, W. (1940). Collapse of the Tacoma Narrows Bridge. *Pacific Builder and Design, 46*, 12.

Plaut, R. H. (2008). Snap loads and torsional oscillations of the original Tacoma Narrows Bridge. *Journal of Sound and Vibration, 309*(3–5), 613-636. doi: 10.1016/j.jsv.2007.07.057

Liu, Y., Birman, V., Chen, C., Thomopoulos, S., Genin, G. M. (2011). Mechanisms of Bimaterial Attachment at the Interface of Tendon to Bone. *Journal of engineering materials and technology, 133*(1). doi: 10.1115/1.4002641

Smith, A. R., Hosker, G. L., Warrell, D. W. (1989). The role of partial denervation of the pelvic floor in the aetiology of genitourinary prolapse and stress incontinence of urine. A neurophysiological study. *Br. J. Obstet. Gynaecol., 96*(1), 24-28.

Kenton, K., Mueller, E., Brubaker, L. (2011). Continent women have better urethral neuromuscular function than those with stress incontinence. *Int. Urogynecol. J., 22*(12), 1479-1484. doi: 10.1007/s00192-011-1447-7

Kim, J., Ramanah, R., DeLancey, J. O., Ashton-Miller, J. A. (2011b). On the anatomy and histology of the pubovisceral muscle enthesis in women. *Neurourol. Urodyn., 30*(7), 1366-1370. doi: 10.1002/nau.21032

2.2 Quantitative 3-D *In Vivo* MRI Measurements of Fiber Orientations in the Female Levator Ani Muscle

2.2.1 Introduction

The importance of the levator ani to pelvic organ support is now well-established pelvic organ support. Injury to the pubovisceral portion of the muscle is seen in 55% of women with prolapse yet only 16% of women with normal support (Delancey 2002; DeLancey et al. 2007; Dietz and Simpson 2008). The most fundamental determinants of a muscle's contractile force are its line-of-action, its fibers' pennation angle (if any), and its physiological cross-sectional area (McMahon 1984). The mechanical consequence of muscle atrophy depends partly on the region of muscle affected, the direction in which the affected fibers contract, and their cross-sectional area.

High resolution magnetic resonance imaging (MRI) allows a detailed analysis of muscle components, ligaments and fascia (Law and Fielding 2008; Morris et al. 2012) in living women. Correlations of cadaver anatomy of the levator ani (Strohbehn et al. 1996) and identification of its levator muscle subdivisions (Margulies et al. 2007) have provided the basis for research in subjects with specific pelvic floor problems. Within the levator ani muscle (LA) muscle fibers have been described both by anatomical dissection (Halban and Tandler 1907; Shobeiri et al. 2008) and imaging (Rociu et al. 2000), and as the most novel technique by diffusion tensor imaging (DTI) (Zijta et al. 2011; Brandão et al. 2012; Rousset et al. 2012). Nonetheless the specific directions and angles of the

different parts of the LA and EAS muscle have not yet measured. The effect of muscle contraction requires an understanding of the angle at which the muscle works.

Two functional characteristics of the levator ani muscle that may affect pelvic floor function have been described. One is a "lifting" action that holds the perineum upwards and failure of this is considered perineal descent (Clark et al. 2010). The other is "squeezing" action where the muscle pull the organs toward the pubic bone to squeeze the levator hiatus closed creating a vaginal high pressure zone (Guaderrama et al. 2005). It is unclear, at present, which component of the levator is responsible for which action. There are two primary candidates, the pubovisceral (= pubococcygeal) muscle and the puborectal muscle.

2.2.2 Methods

A convenience sample of pelvic floor magnetic resonance images (MRI) of 14 healthy women was for this discovery research project drawn from two IRB-approved studies; Evaluating Maternal Recovery from Labor and Delivery; EMRLD (IRB 2005-0011) and Organ Prolapse And Levator; OPAL (IRB 1999-0395). Scans of total of 34 women were reviewed for potential inclusions whose levator ani muscles did not show levator ani injury and who had normal pelvic organ support on examination by a trained examiner to find these scans. Scans were chosen in which the parasagittal images showed the muscle fiber directions with sufficient detail to allow measurements. The eleven MRIs from the EMRLD study were made six months after a first birth and were chosen from women that had no levator ani muscle injury and who had normal pelvic organ

support on examination. Three MRIs of the OPAL2 study were from subjects who served as normal controls in a study searching mechanisms of anterior vaginal wall support failure. Full details of the MRI acquisitions have been previously published (Chou and DeLancey 2001). Briefly, multiplanar two-dimensional proton-density fast-spin images were obtained with an echo time of 15 milliseconds and a repetition time of 4 seconds using a 3-T superconducting magnet (GE Healthcare, Little Chalfont, UK). The slice thicknesses were 4 mm with slice spacing of 1 mm. Demographics were self-reported by the participants.

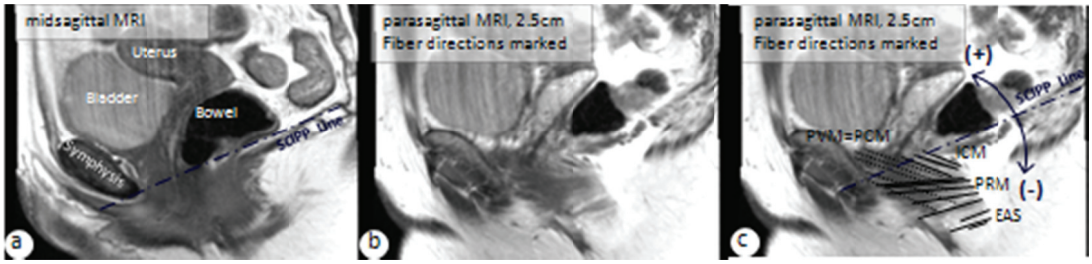

Figure 2.7. (a) Midsagittal MRI showing the midline pelvic organs. The sacro-coccygeal inferior pubic point (SCIPP) line is drawn in the midsagittal plane and transposed to all parasagittal slides up to the pelvic side wall to serve as reference for fiber direction. (b) Fiber bundles were visible (red circles) on this parasagittal slide. (c) Color-coded fibers on a parasagittal slide. Fibers with an angle clockwise to the SCIPP line have a negative sign, fibers with an angle counterclockwise to the SCIPP line have a positive sign.

On sequential 5mm-parasagittal slides on either side of the pelvis, muscle fibers were traced as far laterally as were detectable, up to the pelvic sidewall (Fig. 2.7). For each patient fiber were traced on 12 sequential slides. Muscle fibers were traced in the three Terminologia Anatomica-listed major subdivisions of the LA muscle the pubovisceral muscle (PVM) the puborectalis (PRM), iliococcygeus (ICM) and external anal sphincter muscle (EAS) by the first author (CB) and reviewed and revised as needed

by the senior author (JOLD). For visualization purposes, the muscle fibers were color-coded.. These color-codes were designated as blue for the PVM, green for the PRM, yellow for the ICM; and red for the EAS. The fibers were only traced in the para-sagittal plane as it offers the advantage of being almost parallel to the pubovisceral and puborectal muscle and the images are tangential to the fiber direction.

The angle of the LA fiber tracings relative to the sacrococcygeal-inferior pubic point (SCIPP) line was then automatically measured using custom-made software written in Matlab (Ver. R2012a, MathWorks, Natick, MA). The angles above the SCIPP line were assigned a positive sign (counterclockwise) and below it were assigned a negative sign (clockwise).

Demographics are expressed as mean ± standard deviation (SD). The fiber angles are displayed as mean ± standard error (SE). The ANOVA test was used for the comparison of all muscle lines-of-action and post-hoc two-sided independent samples t-tests were used to make pair-wise comparisons for muscle groups running in the same direction, using SPSS (Ver. 19, IBM Corp., Armonk, NY). A p-value of less than 0.05 was considered statistically significant.

2.2.3 Results

Demographic and clinical data of the women were as follows (mean ± SD): age 35.9±11.4 years, BMI 25.4±3.9 kg/m^2, parity 1.4±0.9, vaginal deliveries 1.1±0.8, ethnicity: Thirteen women were Caucasian, 1 woman was Asian. None had undergone

hysterectomy. No clinically significant defects on the levator ani muscle were present on the MRIs.

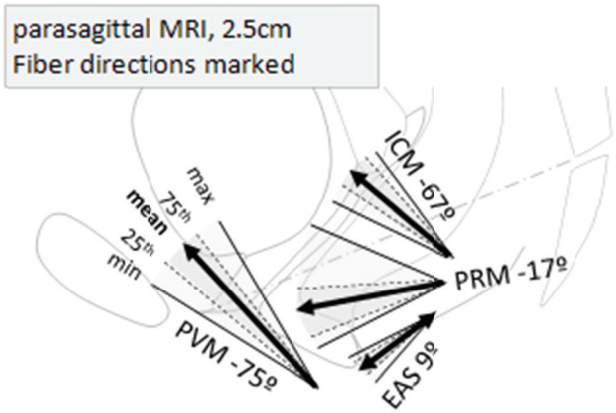

Figure 2.8. Each arrow displays the mean, maximum, minimum and interquartile ranges for fiber direction. The mean values are reported next to the label.

For each muscle the number of fibers counted ranged as follows: PVM: 31 to 71, PRM: 7 to 35, ICM: 29 to 68, and EAS: 7 to 30. The muscle fiber angle of the PVM, ICM, PRM and EAS were normally distributed. The PVM was inclined a mean ± SE angle of -74.6±2.2°. PRM was -17.4±3.7°, the ICM was -66.5±2.3°, and the EAS was 8.6±1.7° relative to SCIPP line of each patient (Fig. 2.8). The fiber angles showed greatest variability for the PRM with an angle range of 49°, followed by the ICM with 29°, the PVM with 26° and the ICM with 24°.

We reject the null hypothesis in that the fiber directions are similar as the PVM, PRM, ICM and EAS muscles were significantly different ($p<0.005$, ANOVA) (Table 2.1). The different lines-of-action of the muscles suggest different muscle functions (Fig. 2.8).

It is noteworthy that angle differences of 58° between the PVM and the PRM, 50° between the ICM and the PRM, and 60° between the PVM and the EAS were found.

Table 2.1. Mean and SD muscle angles across all 14 women. PVM denotes puboviscerali muscle, PRM:puborectalis muscle, ICM:iliococcygeus muscle, EAS:external anal sphincter muscle.

	PVM (in degrees)	PRM (in degrees)	ICM (in degrees)	EAS (in degrees)
Mean	-74.6	-17.4	-66.5	8.6
SD	8.1	13.9	8.7	6.5
SERR	2.2	3.7	2.3	1.7
min	-86.5	-50.5	-80.5	-1.8
max	-60.8	-1.1	-51.9	22.5
range	25.7	49.4	28.6	24.2
5th percentile	-85.2	-38.3	-77.5	0.9
95th percentile	-62.2	-1.8	-54.2	18.2

2.2.4 Discussion

These data show a 58° between the lines-of-action for the PVM and the PRM in these women with normal pelvic organ support with the PRM in a relatively horizontal position and the PVM is more vertically inclined. This suggests the two muscles have different actions. The PVM has a greater lifting component while the PRM has a greater component pulling the perineal structures toward the pubic bone. This is important because the two muscles have different injury patterns: in women with severe pelvic

organ prolapse the PVM portion is injured in 50 of cases, whereas no injury was found in the PRM (DeLancey et al. 2012).

In parallel-fibered muscles such as the PVM and PRM, the angle at which individual muscle fiber shortens is in line with the line-of-action of the muscle (MacIntosh et al. 2006). The information on the angle distribution of the muscles from this study, therefore, reflects the direction in which the muscles close the levator hiatus when they are contracted. If the line-of-action is decomposed into horizontal and vertical components, each of them could be considered as a squeezer and a lifter for the pelvic floor muscle, respectively. Figure 2.9 is redrawn to standing position by putting the SCIPP line to 34° from horizontal line. The PVM and PRM would act at 41° and 17° relative to a horizontal reference line. With trigonometric arithmetic, we can calculate that the squeezing force of the PRM becomes 3.3 (= cotangent 17°) times greater than the lifting force, while the PVM squeezing force is only 1.15 (=cotangent 41°) times greater than the lifting force. Of course normally these muscles contract at the same time so that normally they generate resultant squeezing force in concert.

Another way to compare these *unilateral* muscle actions is that for each 1 N of muscle contractile force, the PVM will provide 1*(cos [41°]) or 0.76 N of squeezing force, whereas the PRM will supply 1*cos [17°]) or 0.95 N of closing force. So the PRM would be the most effective squeezer. Similarly, the PVM will supply 0.65 N of lifting force (calculated as 1*sin [41°]), whereas the PRM will actually depress the pelvic floor with 0.29 N (calculated as 1*sin [-17°]). By comparing these numbers, we see that the PVM is the main lifter, and the PRM is the main squeezer, assisted by the PVM. If they co-contract equally, together they would together generate 1.71 N squeezing force, and a

net lifting force of 0.36 N. These numbers can be compared with the calculations by Morgan et al. (2005) in which the maximal active contributions of *both* sides of the levator ani to a vaginal closure force was ~5 N (to a intravaginal mid-sagittal plane instrumented speculum) in the standing posture.

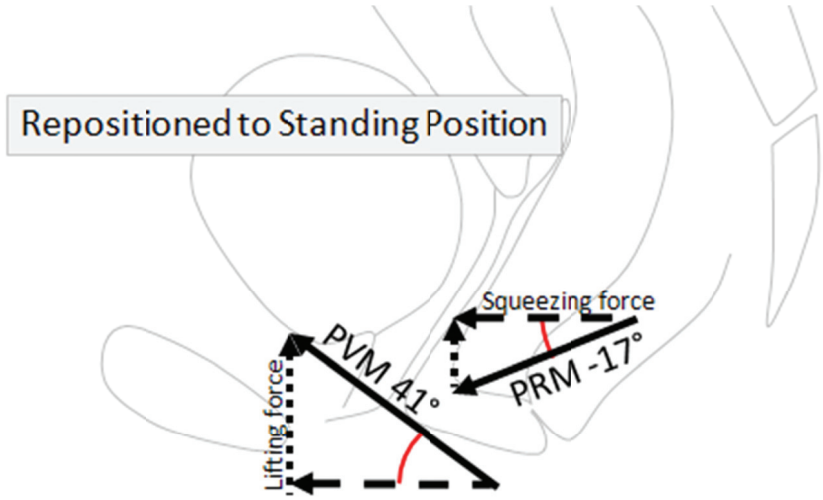

Figure 2.9. The arrows show the average direction of the lines-of-action of the PVM and PRM muscles relative to the putative line of gravity (vertical line). The horizontal components correspond to a squeezing force acting to close the levator hiatus, while the vertical components act to lift (or depress) the pelvic floor. In this configuration, the PRM results to generate 3.3 times greater squeezing force that lifting force, implying the PRM mainly serves as a squeezer. On the other hand, the PVM exerts almost comparable amount of squeezing and lifting forces.

Cadaver dissections can provide excellent detail on structural morphology, but the shape could be distorted by the embalming process. Halban and Tandler (1907) have drawn the muscle fibers of the pubococcygeal muscle as running from the symphysis and the obturator fascia inferiorly and medially. They also mentioned that some of the anterior fibers form a large bow heading posteriorly and get unified from both sides in the

midline. Shobeiri et al. (2008) have identified a different point of insertion for the pubovisceral and iliococcygeus muscle fibers, the latter lying more laterally. The puborectalis muscle fibers, on the other hand, travel perpendicular to the axis of the vagina and the rectum. Recently, advanced MRI technique also has provided a wealth of information related to the morphology and functioning of skeletal muscle. For example, endoanal MR imaging showed sex- and age-related variations in the length and thickness of the anal sphincter and puborectal muscle (Rociu et al. 2000).

The work presented here illustrates the value of MRI in studying the structure of the resting pelvic floor muscles in living women. It clarifies the directions of the muscle fiber lines-of-action and because they are evidently so different, we believe that they have different functions. We found that fiber tracing in 3T MRI scans gave satisfactory representations of the fiber orientations and angles in the sagittal plane because we projected the fiber directions onto the midsagittal plane. This was based on the assumption that the levator ani muscle is bilaterally symmetric. For the present study, we were interested in the morphology of normal muscle whereby the effect of the two sides contracting simultaneously are resolved to a single force in the midsagittal plane. In the future, however, if muscles with a unilateral defect are studied (Chen et al. 2009), this assumption might not be valid.

Conventional MRI is not the appropriate method for measuring fiber curvature because the data are discontinuous and censored by the sequential nature of the images being at 5 mm intervals, rather than having continuous data. This raises the issue of the quality of fiber tracking (Hodgson et al. 2006). Even in DTI, similar issues might be

found where the complex multipennate fiber pattern could decrease the accuracy of fiber orientation measurements (DeLancey et al. 2012).

This study was based on a small sample of young healthy women with no major LA defects. Additional limitations include this study neither being a randomized nor a population-based study. The study was an exploratory study without a priori power analyses. The covariance test of the mixed model structure revealed that the sample size of 14 subjects is powered sufficiently to detect a statistical significance between the muscle groups. Our results apply to healthy young predominantly white women and should not be generalized for other parts of the female population without further work. In the future it would be of interest to classify the muscle direction for a specific age group, parity status, ethnic group, and/or pelvic floor condition (like prolapse).

The distinct difference in orientation between the PVM and the PRM as well as between the ICM and the PRM justifies the classification of the LA muscle into four regions having different names and functions. But the further division of the PVM into the pubovaginalis, puboperinealis and puboanalis subgroup on MRI, however, would not appear to be valid because the muscle fibers cannot reliably be traced according to a knowledge of the anatomical location of origin-insertion pairs (Kearney et al. 2004). New imaging technologies like DTI might be able to provide better information, but that remains to be proven, and automated DTI fiber tracing can produce false positives with muscle fibers appearing to pass through the perineal body which is known anatomically to contain no such fibers (Shafik et al. 2007). Finally, present MRI techniques are not able to allow one to differentiate between fiber types (e.g., Type 1 vs 2) or between bundles of striated vs smooth muscle bundles.

2.2.5 References

Delancey, J. O. (2002). Fascial and muscular abnormalities in women with urethral hypermobility and anterior vaginal wall prolapse. *Am. J. Obstet. Gynecol., 187*(1), 93-98.

DeLancey, J. O., Morgan, D. M., Fenner, D. E., Kearney, R., Guire, K., Miller, J. M., Hussain, H., Umek, W., Hsu, Y., Ashton-Miller, J. A. (2007). Comparison of levator ani muscle defects and function in women with and without pelvic organ prolapse. *Obstet. Gynecol., 109*(2 Pt 1), 295-302. doi: 10.1097/01.AOG.0000250901.57095.ba

Dietz, H. P., Simpson, J. M. (2008). Levator trauma is associated with pelvic organ prolapse. *BJOG, 115*(8), 979-984. doi: 10.1111/j.1471-0528.2008.01751.x

McMahon, T. A. (1984). *Muscles, reflexes, and locomotion*. Princeton, N.J.: Princeton University Press.

Law, Y. M., Fielding, J. R. (2008). MRI of pelvic floor dysfunction: self-assessment module. *AJR. Am. J. Roentgenol., 191*(6 Suppl), S54-59. doi: 10.2214/AJR.07.7113

Morris, V. C., Murray, M. P., Delancey, J. O., Ashton-Miller, J. A. (2012). A comparison of the effect of age on levator ani and obturator internus muscle cross-sectional areas and volumes in nulliparous women. *Neurourol. Urodyn., 31*(4), 481-486. doi: 10.1002/nau.21208

Strohbehn, K., Ellis, J. H., Strohbehn, J. A., DeLancey, J. O. (1996). Magnetic resonance imaging of the levator ani with anatomic correlation. *Obstet. Gynecol., 87*(2), 277-285.

Margulies, R. U., Huebner, M., DeLancey, J. O. (2007). Origin and insertion points involved in levator ani muscle defects. *Am. J. Obstet. Gynecol., 196*(3), 251 e251-255.

Halban, J., Tandler, J. (1907). *Anatomie und aetiologie der genitalprolapse beim weibe*: Braumüller.

Shobeiri, S. A., Chesson, R. R., Gasser, R. F. (2008). The internal innervation and morphology of the human female levator ani muscle. *Am. J. Obstet. Gynecol., 199*(6), 686 e681-686. doi: 10.1016/j.ajog.2008.07.057

Rociu, E., Stoker, J., Eijkemans, M. J., Lameris, J. S. (2000). Normal anal sphincter anatomy and age- and sex-related variations at high-spatial-resolution endoanal MR imaging. *Radiology, 217*(2), 395-401.

Zijta, F. M., Froeling, M., van der Paardt, M. P., Lakeman, M. M., Bipat, S., van Swijndregt, A. D., Strijkers, G. J., Nederveen, A. J., Stoker, J. (2011). Feasibility of diffusion tensor imaging (DTI) with fibre tractography of the normal female pelvic floor. *Eur. Radiol., 21*(6), 1243-1249. doi: 10.1007/s00330-010-2044-8

Brandão, S., Da Roza, T., Parente, M., Ferreira, H. A., Mascarenhas, T., Ramos, I., Jorge, R. N. (2012). *Magnetic resonance tractography as a means to evaluate pubovisceral muscle fibers.* Paper presented at the The 37th Annual Meeting of the International Urogynecological Association, Brisbane, Australia.

Rousset, P., Delmas, V., Buy, J. N., Rahmouni, A., Vadrot, D., Deux, J. F. (2012). In vivo visualization of the levator ani muscle subdivisions using MR fiber tractography with diffusion tensor imaging. *J. Anat., 221*(3), 221-228. doi: 10.1111/j.1469-7580.2012.01538.x

Clark, N. A., Brincat, C. A., Yousuf, A. A., Delancey, J. O. (2010). Levator defects affect perineal position independently of prolapse status. *Am. J. Obstet. Gynecol., 203*(6), 595 e517-522. doi: 10.1016/j.ajog.2010.07.044

Guaderrama, N. M., Nager, C. W., Liu, J., Pretorius, D. H., Mittal, R. K. (2005). The vaginal pressure profile. *Neurourol. Urodyn., 24*(3), 243-247. doi: 10.1002/nau.20112

Chou, Q., DeLancey, J. O. (2001). A structured system to evaluate urethral support anatomy in magnetic resonance images. *Am. J. Obstet. Gynecol., 185*(1), 44-50. doi: 10.1067/mob.2001.116368

DeLancey, J. O., Sorensen, H. C., Lewicky-Gaupp, C., Smith, T. M. (2012). Comparison of the puborectal muscle on MRI in women with POP and levator ani defects with those with normal support and no defect. *Int. Urogynecol. J., 23*(1), 73-77. doi: 10.1007/s00192-011-1527-8

MacIntosh, B. R., Gardiner, P. F., McComas, A. J. (2006). *Skeletal muscle: form and function*. Champaign, IL: Human Kinetics.

Morgan, D. M., Kaur, G., Hsu, Y., Fenner, D. E., Guire, K., Miller, J., Ashton-Miller, J. A., Delancey, J. O. (2005). Does vaginal closure force differ in the supine and standing positions? *Am. J. Obstet. Gynecol., 192*(5), 1722-1728. doi: 10.1016/j.ajog.2004.11.050

Chen, L., Ashton-Miller, J. A., DeLancey, J. O. (2009). A 3D finite element model of anterior vaginal wall support to evaluate mechanisms underlying cystocele formation. *J. Biomech., 42*(10), 1371-1377. doi: 10.1016/j.jbiomech.2009.04.043

Hodgson, J. A., Finni, T., Lai, A. M., Edgerton, V. R., Sinha, S. (2006). Influence of structure on the tissue dynamics of the human soleus muscle observed in MRI studies during isometric contractions. *J. Morphol., 267*(5), 584-601. doi: 10.1002/jmor.10421

Kearney, R., Sawhney, R., DeLancey, J. O. (2004). Levator ani muscle anatomy evaluated by origin-insertion pairs. *Obstet. Gynecol., 104*(1), 168-173.

Shafik, A., Sibai, O. E., Shafik, A. A., Shafik, I. A. (2007). A novel concept for the surgical anatomy of the perineal body. *Dis. Colon Rectum, 50*(12), 2120-2125. doi: 10.1007/s10350-007-9064-8

2.3 A Detailed Investigation of the Pubovisceral Muscle Enthesis

2.3.1 Introduction

An enthesis is the specialized arrangement of connective tissue that by which a striated muscle connects to bone. Two types of entheses have been described: a fibrous enthesis and a fibrocartilaginous enthesis Benjamin et al. (2002). A fibrous enthesis is composed mainly of dense fibrous connective tissues which can be further divided into two regions - periosteal and bony, depending on the site of the tendon attachment. On the other hand, a fibrocartilaginous enthesis appears in the area subjected to compression and shows two more additional zones between connective tissue and bone - an uncalcified fibrocartilage and calcified fibrocartilage region. Entheses are often the sites of musculoskeletal overuse injuries and these include tennis elbow and jumper's knee (Benjamin et al. 2002). Examples of the different types of entheses have been described (Woo et al. 1987; Benjamin et al. 2006; Benjamin et al. 2008; Francois et al. 2001).

The focus of the present paper is the origin of the pubovisceral muscle (PVM, also known as the pubococcygeal muscle as listed in Federative Committee on Anatomical Terminology (1998)) from the pubic bone (Margulies et al. 2007), because it is subject to increased risk for injury during difficult vaginal births (Kearney et al. 2006; Dietz and Lanzarone 2005). This stretch-related injury, which occurs during labor, is thought to be due to the PVM having to stretch to over three times its original length (Lien et al. 2004), or more than twice the value that striated muscle can normally

withstand without injury in non-pregnant individuals (Brooks et al. 1995). More recently, such injuries have been implicated in causing pelvic organ prolapse, a common female pelvic floor impairment that is a common cause of surgical treatment later in life (DeLancey et al. 2007; Dietz and Simpson 2008).

Several attributes of an enthesis can help protect against injury at the junction of the three structures having differing material properties: striated muscle, collagenous connective tissue, and bone. First, dense embedded fibrous fasciae and/or the periosteum can help dissipate stress concentrations and mitigate against the risk of tensile failure or tearing (Benjamin et al. 2008). Second, the enthesis can be anchored to the bone via Sharpey's fibers, which perforate the superficial lamellae of the bone (Woo et al. 1987). Thirdly, elastic fibers could play a role in helping to minimize the effect of abrupt increases in load by deforming under load (Nordin et al. 2001). Finally, certain morphological features, such as a flaring near the bone, could systematically reduce high tensile stresses and/or strains by adding greater cross-sectional area in regions prone to injury (Benjamin et al. 2006). However, to our knowledge the literature contains no descriptions of the morphology or histology of the PVM enthesis.

The first goal of this chapter, therefore, was to classify the PVM enthesis, which specifically corresponds to the medial side of the pubic attachment of the PVM, according to a formal enthesial classification system. A second goal was to test the hypothesis that one or more of the above stress-reduction mechanisms would be observed in the PVM enthesis.

2.3.2 Methods

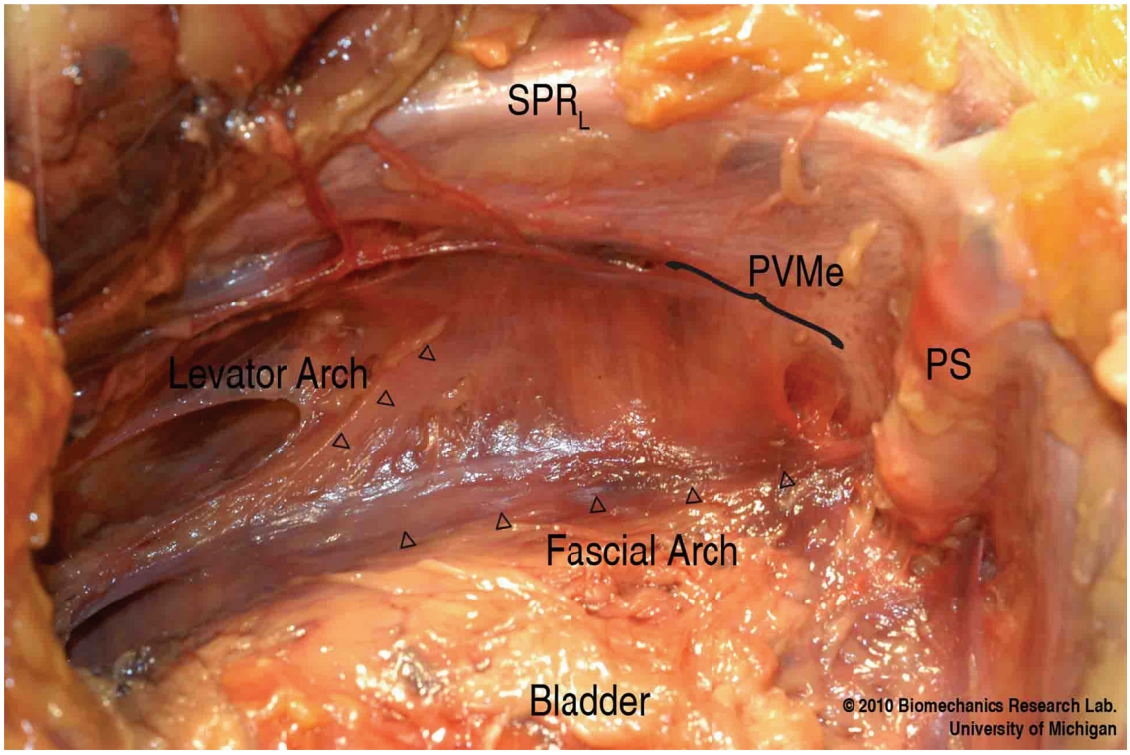

Figure 2.10. View looking down towards the left pelvic sidewall showing the location of the PVM enthesis (PVMe, below bracket). SPR_L denotes superior pelvic ramus (left); and PS, pubic symphysis.

Five female cadavers were dissected to examine the detailed morphology and histology of the origin of the PVM at the pubic bone (Fig. 2.10). The cadaveric specimens ranged in age from 51 to 98 years old (mean 77 years). All the specimens appeared to be parous from inspection of the perineal body and cervix when present. None showed signs of pelvic floor muscle damage associated with maternal birth, as evaluated by a clinician anatomist with experience in evaluating the levator ani muscle (John O. L. DeLancey). Characteristics such as the detailed morphological and structural relationships around the PVM and its attachment area, and the specific fiber orientation

and connection of the PVM enthesis were examined before the pubic bones and the attached muscles were removed. The fiber direction in the region where PVM injury is known to occur (Kearney et al. 2006; Margulies et al. 2006; Shobeiri et al. 2008) was determined by visual inspection, using magnification when necessary.

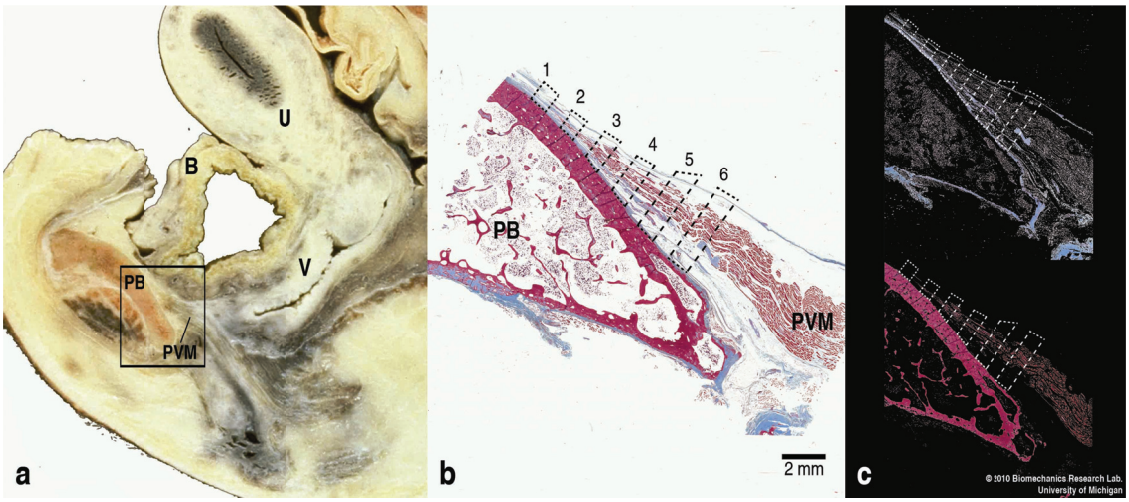

Figure 2.11. (a) Lateral view of a parasagittal section through a female cadaveric pelvis for orientation. The rectangular box shows an area that includes the pubic bone and the origin of the pubovisceral muscle on which detailed histological and quantitative analyses were performed. (b) The pubovisceral muscle origin showing the sampling bands (dashed quadrangles) at 6 different locations along the pubovisceral muscle, where color-based segmentation was conducted. (Masson's trichrome stain, scale bar = 2 mm). [Note: this specimen is from a different cadaver from that shown in (a)]. (c) After the image is filtered by color, the pre-defined sampling bands were quantitatively analyzed to compute unit area and relative composition of the collagenous tissue (blue; top image) and the muscle (red, bottom image). In this and the following images, PVM denotes the pubovisceral muscle; OIM, obturator internus muscle; PB, pubic bone; B, bladder; U, uterus; and V, vagina.

Smaller samples were removed for histochemical processing by excising them parallel to the PVM fiber direction. The samples were fixed in 10 % neutral buffered formalin, decalcified in 10 % formic acid, and dehydrated in 70 % ethanol. Paraffin

embedding was then applied followed by serial sectioning of samples less than 7 μm in thickness. Sections were stained with hematoxylin and eosin, Masson's trichrome, and Verhoeff-Van Gieson according to standard procedures for selected slides for analyzing muscle/connective tissue composition and elastic fiber pattern. A ScanScope XT digital slide scanner (Aperio Technologies, Vista, CA) and a Super COOLSCAN 5000 ED film scanner (Nikon, Shinjuku, Tokyo, Japan) were used to convert the slides into digital images.

For the quantitative observation, custom designed software written in Matlab (The MathWorks, Natick, MA) was developed to allow the interactive selection of the quadrangular sampling bands to be assessed. It permitted analysis of changes within the muscles and connective tissue along the PVM enthesis (Fig. 2.11) at 2 mm intervals, resulting in 6–7 sampled locations depending upon the length of the enthesis in each sample. The location where no muscle was present was defined as the origin of the measurement. At each location, bands with 1 mm width were placed perpendicular to the PVM line-of-action and used to collect pixel image information in the sampling bands. Color based segmentation using the k-means clustering technique was applied to the trichrome digital images of the specimens to distinguish the muscle (stained in red) from the connective tissue (stained in blue). Descriptive statistics were generated as mean and SD.

2.3.3 Results

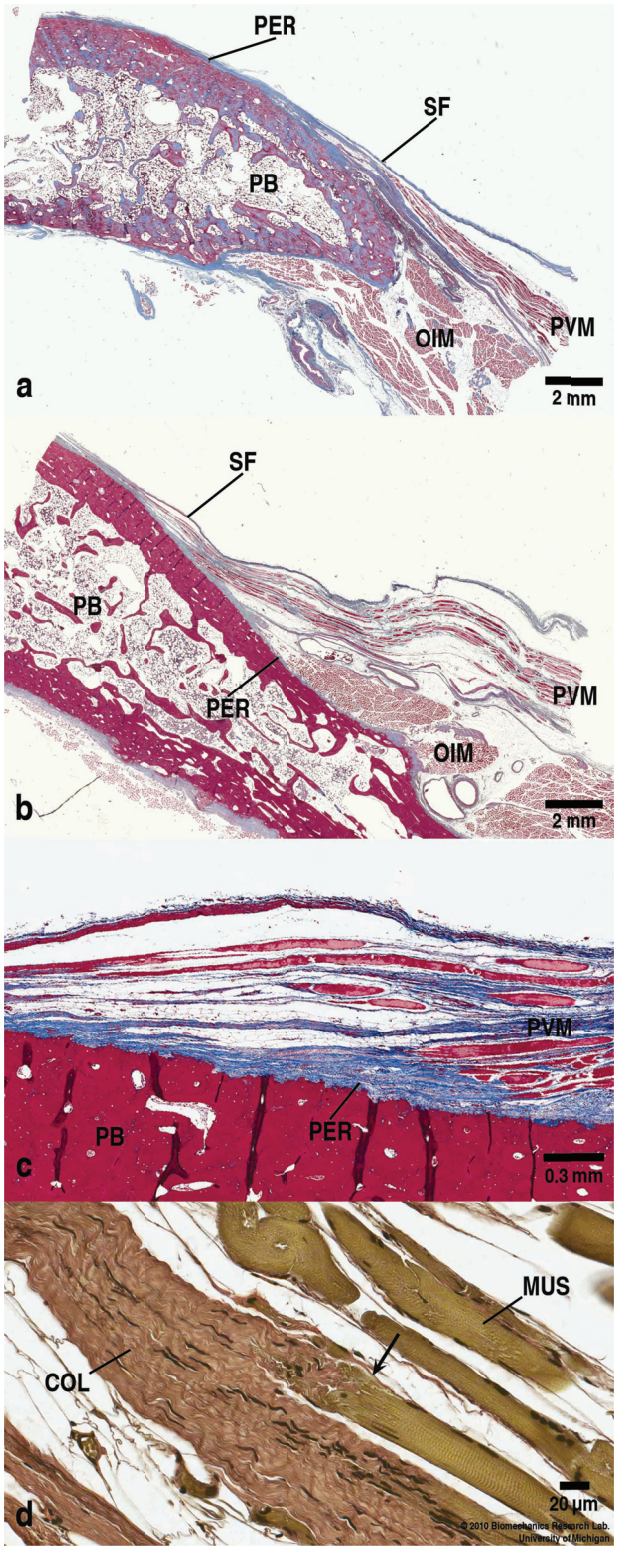

f entheses:
through
bone 2-3
m the
e PVM
e pubic
ly to the
the PB

VM.
ale bars =
tal section
e pubic
. Note the
ic bone
cations as
mples.
ale bars =
ion view
ving the
ers from
riosteum
be seen
ne surface
of
nto the

lines in
ue folding
ing. Also
rotated
trichrome
)
v) of the
ious tissue
stain,
es superior
nd PER,
igures,
ers, and

Figure 2.12 a and b illustrate the geometric relation of the PVM origin to its surrounding structures. The striated PVM muscle fibers mainly insert tangentially onto the periosteum of the superior pubic rami and the posteroinferior margin of the body of the pubic bone (Fig. 2.12d). The width of the attachment extends over a length of about 30 mm. The length of the tendinous fibers linking the PVM to the pubic bone ranges from tens of micrometers to a few millimeters (Fig. 2.12c). The PVM is bounded by the superior fascia of the pelvic diaphragm on both its ventral and dorsal surfaces until each merges with the periosteum 5–10 mm apart. No flaring of the PVM enthesis was observed in the sagittal plane as it attached onto the pubic bone. The fiber direction in the superficial region of the PVM ran perpendicular to the arcus tendineus fascia pelvis, passing lateral to the tendinous arch on its way to attach to the perineal body. Immediately lateral to the PVM enthesis lies the medial origin of the obturator internus muscle, the fiber direction of which is unmistakable since it runs perpendicular to that of the PVM.

As can be seen in Fig. 2.12c, the PVM enthesis appears as a fibrous enthesis rather than a fibrocartilaginous enthesis, because neither the fibrocartilaginous zone nor the tidemark — a basophilic line separating the fibrocartilage into the calcified zone and the uncalcified zone — was present. The PVM attaches to the pubic bone at an acute angle. While the superficial layer of the collagenous fibers blends with the periosteum of the pubic bone, penetration of the deeper collagen through the periosteum directly to the pubic bone was not seen. The thickness of the periosteum in the region of the PVM enthesis does not appear to be different than elsewhere on the pubic bone. No Sharpey's fibers extending into the bone itself were observed anywhere in the enthesial region.

Figure 2.13 demonstrates the change in composition of the muscle fibers and the connective tissue in the PVM in the sampling quadrangles. Moving from the muscle towards the bone, the unit area occupied by the muscle fibers gradually decreases as it goes towards the bone. The connective tissue area shows a lesser change than the muscle fiber does. It is notable that the areas of the connective tissue and the muscle become equal in location 5, which is approximately 8 mm apart from the origin. The table also shows that muscular composition increases from about 2 % at the origin to approximately 60 % at the last sampling band.

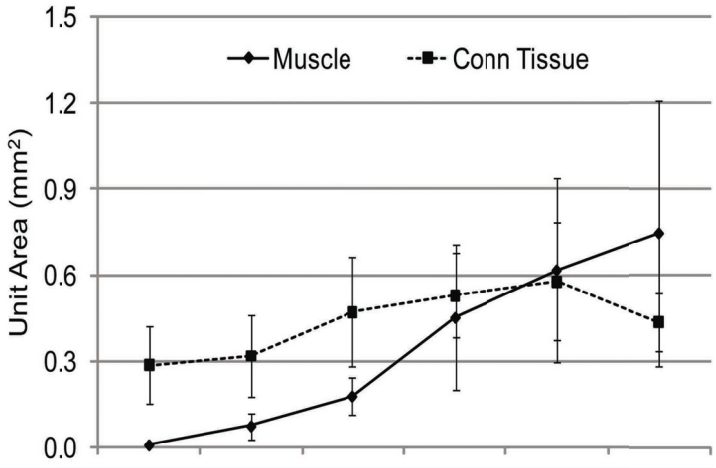

Sampling Band Location	1	2	3	4	5	6
Muscle Composition (%)	2.3	20.0	29.0	44.2	50.1	59.6

Figure 2.13. Longitudinal distribution of the muscle and the connective tissue at the sampling bands along the PVM from its origin. Values are mean (bars indicate SD) areas within the 1 mm-wide sampling bands taken normal to the line-of-action of the PVM. The table shows the composition of the muscle in each location. The unit area of the muscle matches that of the connective tissue at a point approximately 8 mm (location 5) from the pubic bone origin.

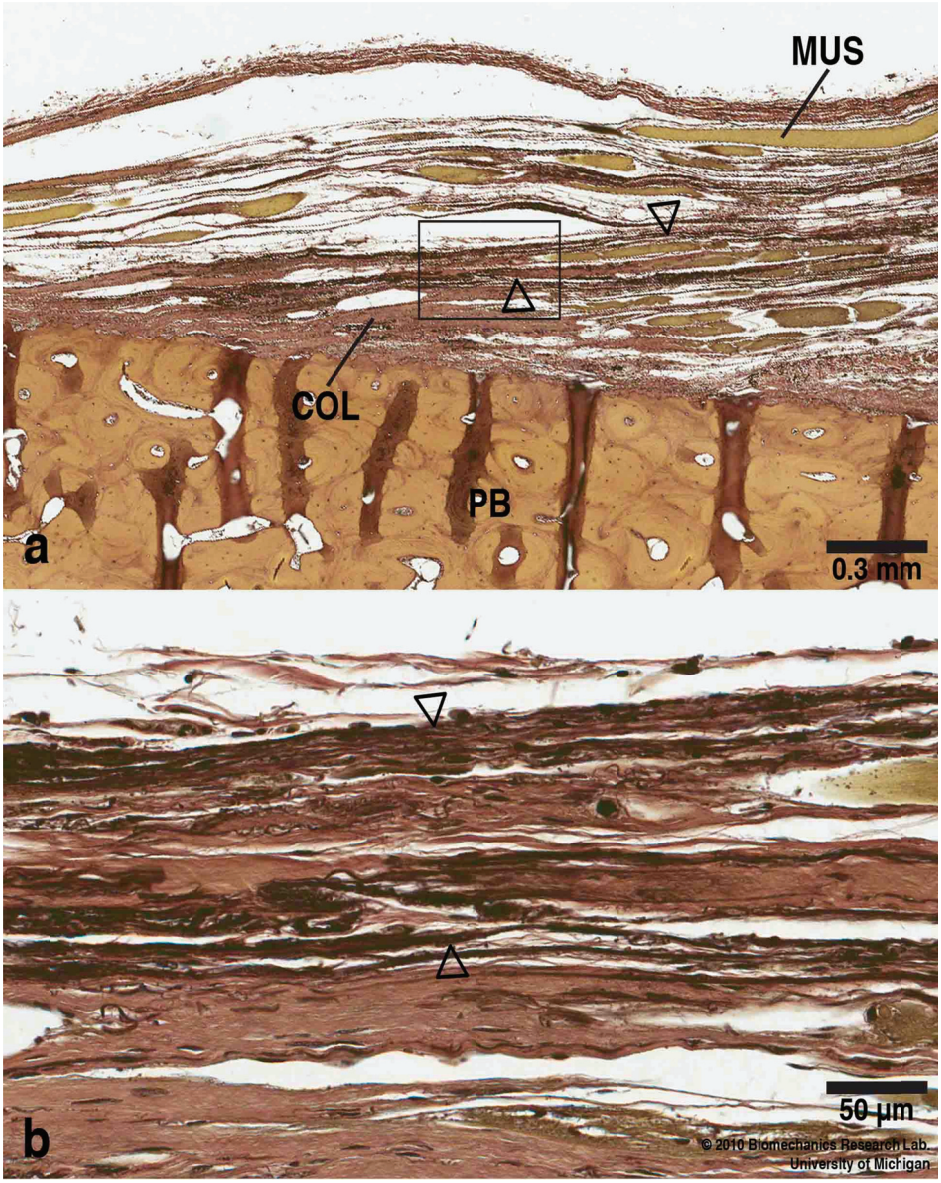

Figure 2.14. Elastic fibers (stained in black, arrowhead) are sparsely distributed in a fibrillar form along the collagenous fibers (red). (Verhoeff-Van Gieson stain, Scale bar = 0.3 mm). (b) Higher power view of the boxed region in (a) showing the elastic fibers in more detail. (Verhoeff-Van Gieson stain, Scale bar = 50 µm).

Figure 2.14 shows the myotendinous junction stained with Verhoeff-Van Gieson staining method, which renders elastic fibers black. The elastic fibers appear at widely

spaced intervals. They are found in very small amounts in fibrillar form in tendons in general.

2.3.4 Discussion

The present study has shown that the PVM originates from the pubic bone via short collagenous fibers, the proximal ends of which form a fibrous enthesis without any evidence of fibrocartilaginous zones or a tidemark. Quantitative analysis demonstrates that the proportion of muscular tissue becomes equal to that of the connective tissue at location 5, about 8 mm away from the osteotendinous junction. Neither flaring of the enthesis at the muscle-bone interface nor Sharpey's fibers penetrating into the bone was observed in enthesial region. Therefore, the hypothesis that flaring and Sharpey's fibers form an important part of its structure was rejected. Finally, elastic fibers appear to be widely, yet sparsely, distributed along the tendinous fibers.

The anatomy of the levator ani muscle has been described by several authors and these findings have been summarized by Kearney et al. (2004). The findings of our research extend the earlier studies on the PVM anatomy and its surrounding area (Margulies et al. 2007; Lawson 1974; Albright et al. 2005) by describing the detailed histology of the PVM origin from the pubic bone. The overall morphological features of the levator hiatus including the PVM have been demonstrated with the help of magnetic resonance as well as three-dimensional ultrasound imaging (Margulies et al. 2007; Dietz and Lanzarone 2005). These studies show the loss of muscle that occurs after vaginal birth in certain individuals. However, lack of resolution precludes and examination of the

precise details of the muscle fiber connection to the bone. The present study was more concerned with the nature of the origin of the intact PVM from the bone with a view to better understanding the structures that are likely to be involved in the injury.

The PVM enthesis arises tangentially from the periosteum of the pubic bone to which it is connected through a fibrous enthesis in the manner of the insertion of the pronator teres on the mid-shaft of the radius (Benjamin et al. 2006). Taking into account that form is derived from structure and function (Benjamin et al. 2006; Benjamin et al. 2008), the absence of the tidemark and the fibrocartilaginous zones in the PVM enthesis might mean that tensile loading rather than compressive loading is predominant in this area. This makes sense considering that the PVM is subjected to considerable posteroinferior stretch during vaginal delivery (Lien et al. 2004).

There is growing knowledge concerning injury to the portion of the levator ani muscle that originates from the pubis. For example, an avulsion injury has been associated with the development of pelvic organ prolapse (DeLancey et al. 2007; Dietz and Simpson 2008), and arises as a result of vaginal birth (Kearney et al. 2006; Dietz and Lanzarone 2005). In addition the nature of the levator ani damage itself may not be the only consideration. Recent observations have disclosed “architectural distortion”, which may be defined as a characteristic abnormal appearance of the vagina on axial magnetic resonant scans that is associated with an increased occurrence of pelvic organ prolapse compared to women who have muscle injury but no distortion (Huebner et al. 2008; Larson et al. 2011). It is possible that the architectural distortion signifies that connective tissues and the muscles around the PVM, which are responsible for pelvic organ support, become impaired or even detached at the time of a birth-related PVM avulsion injury.

These structural elements are connected to one another by the periosteum of the pelvis, the arcus tendineus fascia pelvis, the arcus tendineus levator ani, and other fasciae. Therefore, if one of these structures is affected by abnormal external loading, the input work can be transmitted to others.

Several methodological limitations of this research should be considered. First, the sample size is modest and the samples were likely parous individuals who, although not having any distortion or injury to a trained eye, might have some changes secondary to birth. Therefore, the results of the present study might have been affected by possible histological changes subsequent to a vaginal delivery. Studies on younger nulliparous women would be ideal, but thankfully young nulliparous cadavers are rare in anatomical donation programs. Second, the sample age ranges from 51 years and up, so one cannot necessarily extrapolate the results to younger individuals. Thirdly, more detailed histological descriptions are needed including the different types of collagens, decorin, biglycan, aggrecan and other constituents that may form this particular type of enthesis (Thomopoulos et al. 2003). Fourthly, considering the size of elastic fibers being on the order of a few micrometers, observation through a scanning electron microscope could give more comprehensive images of these fibers along the collagenous tissue.

The enthesial region of the PVM lies in the region where avulsion injury is known to occur during the second stage of labor (Dietz and Lanzarone 2005; Dietz et al. 2007). The details of the exact injury mechanism have not yet been fully elucidated. The present research provides a detailed structural description of the pubic origin of the PVM and suggests hypotheses that might be helpful in predicting that failure location. It seems likely that it would occur in the muscular portion of the enthesis before the cross-

sectional area of the enthesis becomes big enough to endure the external loads. This is because collagenous tissues are known to be approximately two orders stronger than striated muscle (Brooks and Faulkner 1996; Woo and Levine 1998). In addition, they should be more resistant to stretch-related injuries than muscle, because they are highly aligned in the enthesis. Now that the anatomical details of this region are apparent, research can progress to add further detail to our growing understanding. For example, one can incorporate the detailed morphology from the present study to create micromechanical models of the PVM enthesis and explore the factors that might cause injury of the PVM enthesis medially and its aponeurosis laterally (see Chapter 2.1).

2.3.5 References

Benjamin, M., Kumai, T., Milz, S., Boszczyk, B. M., Boszczyk, A. A., Ralphs, J. R. (2002). The skeletal attachment of tendons--tendon "entheses". *Comp Biochem Physiol A-Mol Integr Physiol, 133*(4), 931-945. doi: 10.1016/S1095-6433(02)00138-1

Woo, S. L., Maynard, J., Butler, D., Lyon, R., Torzilli, P., Akeson, W., Cooper, R., Oakes, B. (1987). Symposium on injury and repair of the musculoskeletal soft tissues. In S. L. Woo & J. A. Buckwalter (Eds.), *Injury and repair of the musculoskeletal soft tissues* (pp. 133-166). Savannah, GA: American Academy of Orthopaedic Surgeons.

Benjamin, M., Toumi, H., Ralphs, J. R., Bydder, G., Best, T. M., Milz, S. (2006). Where tendons and ligaments meet bone: attachment sites ('entheses') in relation to exercise and/or mechanical load. *J. Anat., 208*(4), 471-490. doi: 10.1111/j.1469-7580.2006.00540.x

Benjamin, M., Kaiser, E., Milz, S. (2008). Structure-function relationships in tendons: a review. *J. Anat., 212*(3), 211-228. doi: 10.1111/j.1469-7580.2008.00864.x

Francois, R. J., Braun, J., Khan, M. A. (2001). Entheses and enthesitis: a histopathologic review and relevance to spondyloarthritides. *Curr. Opin. Rheumatol., 13*(4), 255-264.

Federative Committee on Anatomical Terminology. (1998). *Terminologia anatomica: international anatomical terminology*. Stuttgart ; New York: Thieme.

Margulies, R. U., Huebner, M., DeLancey, J. O. (2007). Origin and insertion points involved in levator ani muscle defects. *Am. J. Obstet. Gynecol., 196*(3), 251 e251-255.

Kearney, R., Miller, J. M., Ashton-Miller, J. A., DeLancey, J. O. L. (2006). Obstetric factors associated with levator ani muscle injury after vaginal birth. *Obstet. Gynecol., 107*(1), 144-149. doi: 10.1097/01.AOG.0000194063.63206.1c

Dietz, H. P., Lanzarone, V. (2005). Levator trauma after vaginal delivery. *Obstet. Gynecol., 106*(4), 707-712. doi: 10.1097/01.AOG.0000178779.62181.01

Lien, K. C., Mooney, B., DeLancey, J. O., Ashton-Miller, J. A. (2004). Levator ani muscle stretch induced by simulated vaginal birth. *Obstet. Gynecol., 103*(1), 31-40. doi: 10.1097/01.AOG.0000109207.22354.65

Brooks, S. V., Zerba, E., Faulkner, J. A. (1995). Injury to muscle fibres after single stretches of passive and maximally stimulated muscles in mice. *J. Physiol.-London, 488 (Pt 2)*, 459-469.

DeLancey, J. O., Morgan, D. M., Fenner, D. E., Kearney, R., Guire, K., Miller, J. M., Hussain, H., Umek, W., Hsu, Y., Ashton-Miller, J. A. (2007). Comparison of levator ani muscle defects and function in women with and without pelvic organ prolapse. *Obstet. Gynecol., 109*(2 Pt 1), 295-302. doi: 10.1097/01.AOG.0000250901.57095.ba

Dietz, H. P., Simpson, J. M. (2008). Levator trauma is associated with pelvic organ prolapse. *BJOG, 115*(8), 979-984. doi: 10.1111/j.1471-0528.2008.01751.x

Nordin, M., Lorenz, T., Campello, M. (2001). Biomechanics of tendons and ligaments. In M. Nordin & V. H. Frankel (Eds.), *Basic biomechanics of the musculoskeletal system* (pp. 102-125). Philadelphia: Lippincott Williams & Wilkins.

Margulies, R. U., Hsu, Y., Kearney, R., Stein, T., Umek, W. H., DeLancey, J. O. (2006). Appearance of the levator ani muscle subdivisions in magnetic resonance images. *Obstet. Gynecol., 107*(5), 1064-1069.

Shobeiri, S. A., Chesson, R. R., Gasser, R. F. (2008). The internal innervation and morphology of the human female levator ani muscle. *Am. J. Obstet. Gynecol., 199*(6), 686 e681-686. doi: 10.1016/j.ajog.2008.07.057

Kearney, R., Sawhney, R., DeLancey, J. O. (2004). Levator ani muscle anatomy evaluated by origin-insertion pairs. *Obstet. Gynecol., 104*(1), 168-173.

Lawson, J. O. (1974). Pelvic anatomy. I. Pelvic floor muscles. *Ann. R. Coll. Surg. Engl., 54*(5), 244-252.

Albright, T. S., Gehrich, A. P., Davis, G. D., Sabi, F. L., Buller, J. L. (2005). Arcus tendineus fascia pelvis: a further understanding. *Am. J. Obstet. Gynecol., 193*(3 Pt 1), 677-681. doi: 10.1016/j.ajog.2005.02.129

Huebner, M., Margulies, R. U., DeLancey, J. O. (2008). Pelvic architectural distortion is associated with pelvic organ prolapse. *Int. Urogynecol. J. Pelvic Floor Dysfunct., 19*(6), 863-867. doi: 10.1007/s00192-007-0546-y

Larson, K., Luo, J., Yousuf, A., Ashton-Miller, J., Delancey, J. (2011). Measurement of the 3D geometry of the fascial arches in women with a unilateral levator defect and "architectural distortion". *Int. Urogynecol. J.*(In Press). doi: 10.1007/s00192-011-1528-7

Thomopoulos, S., Williams, G. R., Gimbel, J. A., Favata, M., Soslowsky, L. J. (2003). Variation of biomechanical, structural, and compositional properties along the tendon to bone insertion site. *J. Orthop. Res., 21*(3), 413-419. doi: 10.1016/S0736-0266(03)00057-3

Dietz, H. P., Gillespie, A. V., Phadke, P. (2007). Avulsion of the pubovisceral muscle associated with large vaginal tear after normal vaginal delivery at term. *Aust. N. Z. J. Obstet. Gynaecol., 47*(4), 341-344. doi: 10.1111/j.1479-828X.2007.00748.x

Brooks, S. V., Faulkner, J. A. (1996). The magnitude of the initial injury induced by stretches of maximally activated muscle fibres of mice and rats increases in old age. *J Physiol, 497 (Pt 2)*, 573-580.

Woo, S. L., Levine, R. E. (1998). Ligament, tendon and fascia. In J. Black & G. W. Hastings (Eds.), *Handbook of biomaterial properties* (pp. 59-65). London, UK: Chapman & Hall.

CHAPTER 3

Computational Finite Element Simulation Studies of the Levator Ani Muscle Injury Mechanism Associated with Vaginal Birth

3.1 A 2-D Pubovisceral Muscle Model

3.1.1 Introduction

Of the 3 million women giving birth vaginally in the U.S. each year, approximately one in ten (or approximately 300,000) will suffer an injury to the pubovisceral portion of their levator ani muscle (PVM; also known as the pubococcygeal muscle, as listed in Terminologia Anatomica) (Kearney et al. 2006). Women with pelvic organ prolapse, a condition that results in major surgery for 200,000 women annually, are three- to four-times more likely to have injuries at this location than women with normal pelvic organ support (DeLancey et al. 2007). Little is known about the mechanism of these injuries.

Clinical observations have demonstrated the PVM ruptures at or the near its origin to the pubic bone, rather than mid-substance or at its junction posteriorly with the perineal body (DeLancey et al. 2003; Dietz et al. 2007), while one might posit that birth-related injury should be equally probable at any of these three locations. The fact that the

injury almost always occurs at the origin, and not elsewhere, suggests an inherent weakness at this location. We are not aware of any studies that have explored why this might be so, whether from a theoretical perspective or an experimental approach.

Figure 3.1. (A) Normal anatomy in an axial mid-urethra proton density magnetic resonance image showing the pubovisceral muscle (*). (B) Woman who has lost a part of the left pubovisceral muscle (displayed on the right side of the image, according to standard medical imaging convention) with lateral displacement of the vagina into the area normally occupied by the muscle. The arrow points to the expected location of the missing muscle. (A,B: redrawn with permission from Lien et al. (2004). (OI = obturator internus; PB = pubic bone; U = urethra; V = vagina; R = rectum.). (C) Parasagittal cross-section through the PVM origin at the pubic bone (PB), approximately 1 cm lateral to the midline, redrawn with permission from Kim et al. (2011). (D) Geometry of the PVM model based on (C).

Does the geometric form of the PVM-pubic bone interface itself might contribute to the risk of the injury in that region of the PVM. Our group has examined this location histochemically (Kim et al. 2011), which showed a similarity between the geometry of this muscle-bone connection, or enthesis (Benjamin et al. 2002), and that of a scarf joint (Fig. 3.1). Therefore, we termed this connection a 'scarf enthesis'. It is known that scarf joints significantly increase mechanical stresses in the vicinity of the joint (Williams 1952; Lubkin 1957). However, determining the stress and deformation fields in the vicinity of the singular point analytically or even numerically is a non-trivial problem. Geometrical and material nonlinearities, which correspond to the birth-associated loading to the PVM, add further complexity to the already difficult problem. A scarf joint has been analyzed using infinitesimal strain theory in order to identify the singular stress field under tension and bending in both two- and three-dimensions (Liu and Fleck 1999; Qian and Akisanya 1999; Chaudhuri, R. A. and Chiu 2009). Finite strain theory has also been utilized to study the crack tip of hyperelastic materials and the asymptotic stress field around it (Geubelle and Knauss 1994; Long et al. 2011). However, to the best of our knowledge, the behavior of a scarf joint involving a hyperelastic material under finite deformation has not been studied.

The primary goal of this study, therefore, was to model the histology of the PVM at its fibrous enthesis and perform a finite element (FE) analysis of the stress and strain energy fields of the anisotropic hyperelastic PVM model placed under various types of loading that might transpire during obstetrical events. A FE analysis of the oblique corner of a scarf joint, however, can give rise to considerable numerical problems including lack

of convergence and poor accuracy (Dempsey and Sinclair 1981). In order to circumvent these problems, we employed the overall strain energy as a convergence criterion (Marks and Gardner 1993) along with a FE formulation that has been reported to detect asymptotic stress fields (Benzley 1974; Brink and Stein 1996). We hypothesized that strain energy is an appropriate predictor of the PVM failure for two reasons. Strain energy brings mathematical effectiveness in circumventing the problems regarding the singular point because finite strain energy in the bounded portions of a body is proved when equilibrium displacement fields exist in elastic bodies (Wilcox 1979; Chaudhuri, R. 2000). In addition, strain energy has been widely used in physiological studies to estimate the severity of muscle injury (Brooks et al. 1995; Wang et al. 1997). Since many aspects of PVM composition and loading are presently uncertain during the second stage of labor, our second goal was to conduct a sensitivity analysis of the effects of five loading or morphological factors, including maximum stretch ratio, angle of the scarf joint, direction of distraction, and PVM material properties (matrix and collagen fiber), on the strain energy distribution in a scarf enthesis loaded under tension.

3.1.2 Methods

Details of the transversely isotropic, hyperelastic material model (Gasser et al. 2006) utilized in this study are explained in this section. The constitutive model of this type of material can be characterized by a strain-energy function (also referred to as a Helmholtz free-energy function) Ψ per unit reference volume, and expressed as a

function of the right Cauchy-Green tensor **C** and the tensor product (or the dyad) of the unit fiber direction vector at the reference configuration $\mathbf{a}_0 \otimes \mathbf{a}_0$,

$$\Psi = \Psi\left(\mathbf{C}, \mathbf{a_0} \otimes \mathbf{a_0}\right) = c_1\left(I_1(\mathbf{C}) - 3\right) + \frac{k_1}{2k_2}\left[\exp\left\{k_2 \overline{E}^2\right\} - 1\right] - \frac{1}{2}p\left(I_3(\mathbf{C}) - 1\right)$$

where

$$\overline{E} := \kappa I_1(\mathbf{C}) + (1 - 3\kappa) I_4\left(\mathbf{C}, \mathbf{a_0} \otimes \mathbf{a_0}\right) - 1$$

Here, $I_1(\mathbf{C})$ is the principal invariant of **C** and $I_4\left(\mathbf{C}, \mathbf{a_0} \otimes \mathbf{a_0}\right)$ is the pseudo-invariants of **C** and $\mathbf{a_0}$, which are given by

$$I_1(\mathbf{C}) = \mathrm{tr}\mathbf{C} \quad ,$$

$$I_4\left(\mathbf{C}, \mathbf{a_0} \otimes \mathbf{a_0}\right) = \mathbf{a_0} \cdot \mathbf{C}\mathbf{a_0} = \lambda^2 \quad .$$

c_1, k_1, and k_2 are material parameters and κ is the level of dispersion in the fiber directions, ranging from 0 (corresponding to an ideal alignment of collagen fibers) to 1/3 (corresponding to an isotropic distribution). Note that I_4 is equal to the square of the stretch λ in the fiber direction $\mathbf{a_0}$, which describes the property of the fiber family and its interaction with the other material constituents.

Multiple linear regression model of the statistical analyses may be further explained as followings in a matrix/vector representation:

$$\mathbf{y} = \mathbf{X}\boldsymbol{\beta} + \boldsymbol{\varepsilon} \qquad \text{or} \qquad y_i = \beta_0 + \beta_j x_{ij} + \varepsilon_i$$

where $\mathbf{y} = \left(y_1, \ldots, y_i, \ldots, y_n\right)^{\mathrm{T}}$, $\boldsymbol{\varepsilon} = \left(\varepsilon_1, \ldots, \varepsilon_i, \ldots, \varepsilon_n\right)^{\mathrm{T}}$, $\boldsymbol{\beta} = \left(\beta_0, \beta_1, \ldots, \beta_j, \ldots, \beta_p\right)^{\mathrm{T}}$, and

$$\mathbf{X} = \begin{pmatrix} 1 & x_{11} & \cdots & x_{1p} \\ 1 & x_{21} & \cdots & x_{2p} \\ \vdots & \vdots & x_{ij} & \vdots \\ 1 & x_{n1} & \cdots & x_{np} \end{pmatrix}, \qquad i = 1, \ldots, n \quad , \quad j = 1, \ldots, p \quad .$$

Here, y_i is the output variable (or response), x_{ij} is the input variable (or predictor), β_i is the parameter, ε_i is the error term, n is the number of cases in the dataset, and p is the number of input variables (or parameters). The column of ones in $\mathbf{X}$ incorporates the intercept term β_0.

The output variable, Area Ratio, is defined to measure the degree of strain energy concentration to the model. Consider $S\left(\Omega\right)$ as a continuous (or at least piecewise continuous) function representing the area occupied by continuum particles in region Ω. The output variable can then be expressed as:

$$y_i := \frac{S\left(\Omega_{\mathrm{C}}\right)}{S\left(\Omega_0\right)}$$

where Ω_0 contains the entire mesh elements of the model, while Ω_C is the control volume consisting of the elements that include the largest 5 % of the element-wise strain energy density. Therefore, the smaller y_i the model has, the smaller the area covering 5 % of the total strain energy given to the system. Note that p equals to 5 in the first degree, and 20 in the second degree model.

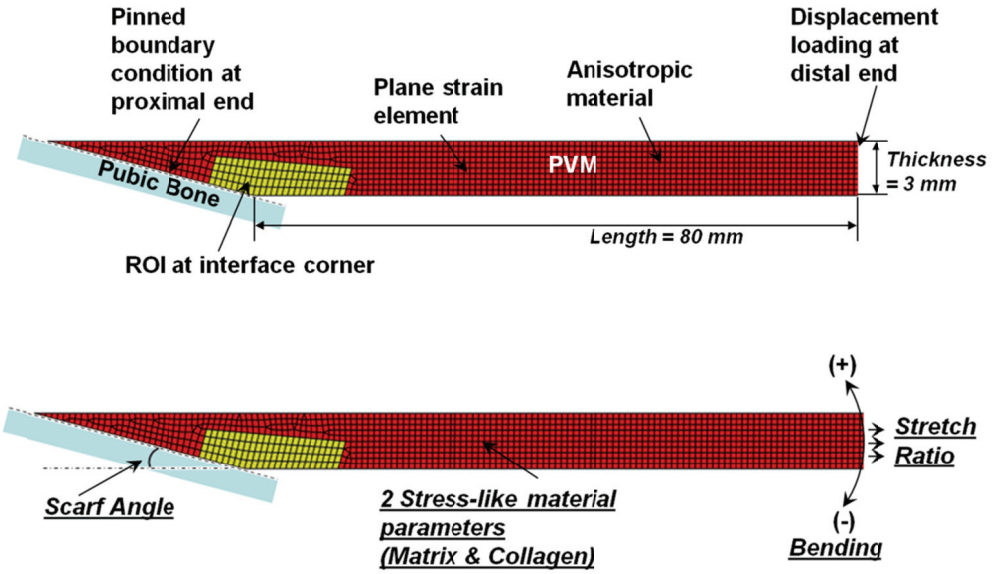

Figure 3.2. (a) The finite element model of a two-dimensional pubovisceral muscle model, along with the model definitions. (b) Schematic showing the five input parameters used in the multiple regression and sensitivity analysis. The scarf enthesis is at left.

The geometry of the PVM scarf enthesis was simplified to a two-dimensional trapezoid with an inclined proximal edge to form a scarf enthesis (Fig. 3.2). Based on the examination of the cadaver specimens and the histological cross-sections of the PVM (Kim et al. 2011), the thickness and the length of the PVM bundle were specified as 3 mm and 80 mm, respectively. Since this study included the sensitivity analysis for the selected variables, which yielded a total of 243 different combinations, geometry changes

due to scarf angle, loading conditions, and material properties of the model were systematically established and adjusted for each trial.

As for the FE model definitions (Fig. 3.2 (a)), the pubic bone was modeled as a rigid body connected to the proximal end of the PVM model via its oblique attachment area. The proximal end, which was modeled as a straight inclined line as with a scarf joint interface, was assumed to have pinned boundary conditions, because the micromechanical features suggest that this type of fibrous enthesis is primarily loaded in tension and is not sensitive to the direction of loading (Subit et al. 2008). The distal end of the PVM was placed under displacement loading, the direction of which was determined by the loading strategy of the sensitivity analysis (See Section ' Sensitivity Analysis of Strain Energy Concentration at PVM Enthesis' for more details). Also, given that the dimension in the PVM in the lateral direction is much greater than the thickness of the PVM (Kim et al. 2011), we hypothesized the direction of this dimension is constrained (the state of plane strain).

A transversely isotropic, hyperelastic material model (Gasser et al. 2006) was adopted to describe the mechanical behavior of the PVM as a fiber-reinforced matrix. The constitutive model of this type of material can be characterized by a strain-energy function (also referred to as a Helmholtz free-energy function) Ψ per unit reference volume, and expressed as a function of the right Cauchy-Green tensor $\mathbf{C}$ and the tensor product (or the dyad) of the unit fiber direction vector at the reference configuration $\mathbf{a}_0 \otimes \mathbf{a}_0$,

$$\Psi = \Psi\left(\mathbf{C}, \mathbf{a_0} \otimes \mathbf{a_0}\right) = c_1\left(I_1(\mathbf{C}) - 3\right) + \frac{k_1}{2k_2}\left[\exp\left\{k_2 \bar{E}^2\right\} - 1\right] - \frac{1}{2}p\left(I_3(\mathbf{C}) - 1\right)$$

The micromechanical morphology of the soft biological tissue is incorporated in the material model, with the first term describing the isotropic matrix behavior and the second term characterizing the mechanical anisotropy corresponding to the collagenous fibers. The collagen fibers were assumed to be crimped under no load and tensed if the strain of the fibers is large enough. The stretching behavior is largely explained by the exponential function, as can be seen in the second term. This results in the PVM stiffness being much greater in the fiber direction than in directions orthogonal to the fibers. In the last term, since the state of incompressibility of the isotropic matrix material is assumed ($I_3(\mathbf{C}) = 1$), the free energy Ψ is enhanced by an indeterminate Lagrange multiplier $p/2$, which may also be identified as a hydrostatic pressure. The three parameter values (c_1 = 0.3532 MPa, k_1 = 0.0827 MPa, and k_2 = 0.3242) were taken from biaxial *in vitro* tensile tests of female PVM (Jing, D. 2010). The level of dispersion in the fiber direction (κ) was approximated to an ideal case ($\kappa = 0$) to be perfectly aligned for the simplification purpose.

The simulations were performed with Abaqus 6.10-EF1 Implicit (Dassault Systemes, Vélizy-Villacoublay, France) FE analysis software along with HyperMesh 10.0 (Altair Engineering, Troy, MI, USA) pre-processor. In order to avoid the singular behavior of a purely displacement-based solution (Simo and Armero 1992), mixed formulation elements were carefully chosen for the PVM FE model. The FE simulation was verified by confirming that convergence in strain energy is achieved within the

pentagonal region of interest (ROI) around the inferior oblique interface corner with mesh refinement (Marks and Gardner 1993). The total strain energy of an element is computed from the strain energy density and volume of each integration point using the Abaqus output variable identifiers. Since the singularity pattern at the oblique interface corner needs to be suitably captured, the contour plot of the stress field was also checked.(Brink and Stein 1996) Contour plots for the element-wise strain energy density were examined to identify the location of concentrated strain energy in an attempt to predict the location of avulsive PVM injury initiation. Finally, we investigated the relative amount of strain energy carried by the ground material and the collagen fibers in the ROI at the different levels of stretch ratio applied to the model.

Table 3.1. The five input parameters and three levels of their variation that were used for the sensitivity analysis.

Input Variable	**Unit**	**Variation**		
Scarf Angle	(Deg)	10	15	20
Bending	(Deg)	-15	0	15
Stretch Ratio	N/A	1.25	2.25	3.25
Matrix Property	(MPa)	0.1766	0.2649	0.3532
Collagen Property	(MPa)	0.0414	0.0620	0.0827

One can speculate that the occurrence of an injury at the PVM scarf enthesis during vaginal birth is associated both with innate anatomical characteristics as well as intrapartum deformation patterns. Such speculation is presently in order given the practical and ethical difficulties of making any actual measurements during vaginal birth. Changes in the PVM soft tissue properties might also be possible to play a role in the injury mechanism. In order to identify the relationship between these factors and the

possibility for injury initiation, a total of five different independent variables were defined, including Scarf Angle, Bending, Stretch Ratio, and two stress-like material properties from Matrix and Collagen fibers, respectively (Fig. 3.2 (b) and Table 3.1). The Scarf Angle is related to the innate shape of an individual's musculoskeletal architecture at the pubic origin of the PVM. Since, there exist no studies reporting the scarf angle of the PVM, we used a set of the values measured from our cadaver specimens (Kim et al. 2011); these ranged from 10° to 20°. Bending has to do with how perineal descent occurs during the second stage of labor and Stretch Ratio is proportional to the size of the fetal head that engages the PVM late during the second stage (Ashton-Miller and DeLancey 2009). The ranges for these input variables were determined from previous computer birth simulation data (Jing, D. 2010; Lien et al. 2004). Finally, the Matrix and Collagen material properties were reduced by 25 % and 50 % to reflect possible ripening of the pelvic floor muscles during delivery. The default values were acquired from the *in vitro* testing on human PVM (Table 3.1) (Jing, D. 2010). Each of the five input variables was assigned three levels of variation. The ranges of these input variables were evaluated by a clinician anatomist with experience in evaluating the levator ani muscle (John O. L. DeLancey).

Using R 2.13.0 (R Devolopment Core Team 2011), multiple linear regression analyses were performed for modeling the relationship between the output variable and five input variables assigned to the FE model. The regression equation is written in a matrix/vector representation:

$$\mathbf{y} = \mathbf{X}\boldsymbol{\beta} + \boldsymbol{\varepsilon}$$

where, **y** is the output variable (or response), **X** is the input variable (or predictor), **β** is the parameter, and **ε** is the error term. Then, the problem becomes finding the least square estimate of **β**, called $\hat{\boldsymbol{\beta}}$:

$$\hat{\boldsymbol{\beta}} = \left(\mathbf{X}^{\mathrm{T}}\mathbf{X}\right)^{-1}\mathbf{X}^{\mathrm{T}}\mathbf{y}$$

which is the minimized sum of the squared errors, as well as containing information as to the magnitude of the effect of each input variable. The output variable, Area Ratio, is defined by the ratio of area consisting of the elements that include the largest 5 % of the element-wise strain energy density to entire area of the model. This output variable was designed to capture the degree of strain energy concentration to the model when it is subjected to tensional loading. For example, the smaller **y** the model has, the smaller the area covering 5 % of the total strain energy given to the system. For ease of comparison all the variables were converted to standard units (mean 0 and variance 1). Whether each parameter is statistically significant in the regression model was evaluated through the two-tailed t-test and ANOVA. A p-value of less than 0.05 was considered significant. In order to improve the fit and to ensure the normality of the residual, the polynomial terms was also added to the term **Xβ** and compared to the first degree regression model.

3.1.3 Results

Figure 3.3 demonstrates the amount of strain energy collected in the oblique interface corner ROI. The sum of the strain energy appears to converge, confirming that little is to be gained by further mesh refinement. Therefore, the result supports the validity of the presented simulation results.

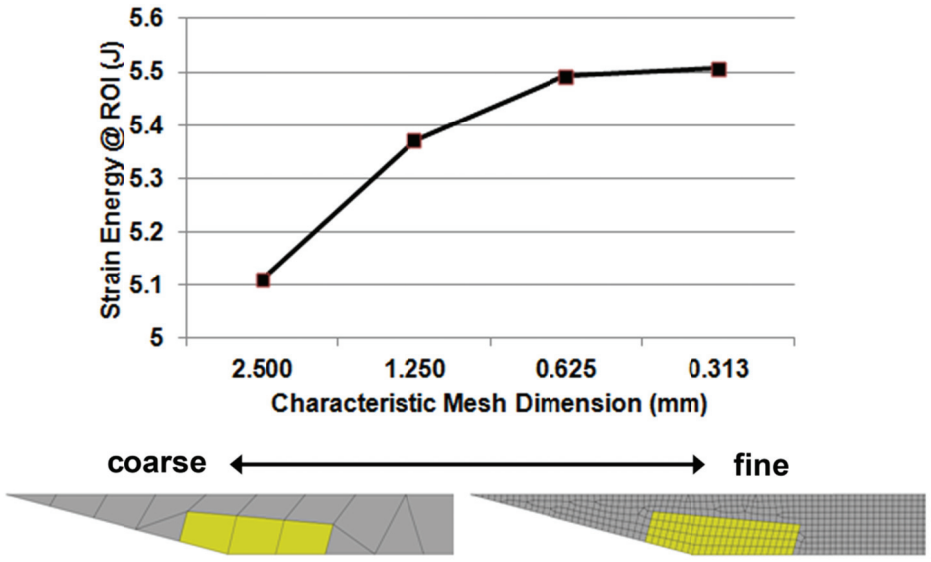

Figure 3.3. Strain energy and convergence rates at the interface corner ROI. Convergence is achieved as finer mesh is applied. Two examples of coarser (left) and finer (right) mesh configurations are shown below the abscissa.

In Figure 3.4, the largest in-plane principal stresses calculated from the Cauchy stress tensor are compared against a number of different stretch ratios. The mixed formulation elements utilized for the simulation appear to detect the singular behavior of the stress at the oblique interface corner of the PVM scarf enthesis. Larger stretch ratios

applied to the PVM model appear to create a more locally concentrated, as well as greater stress singularity.

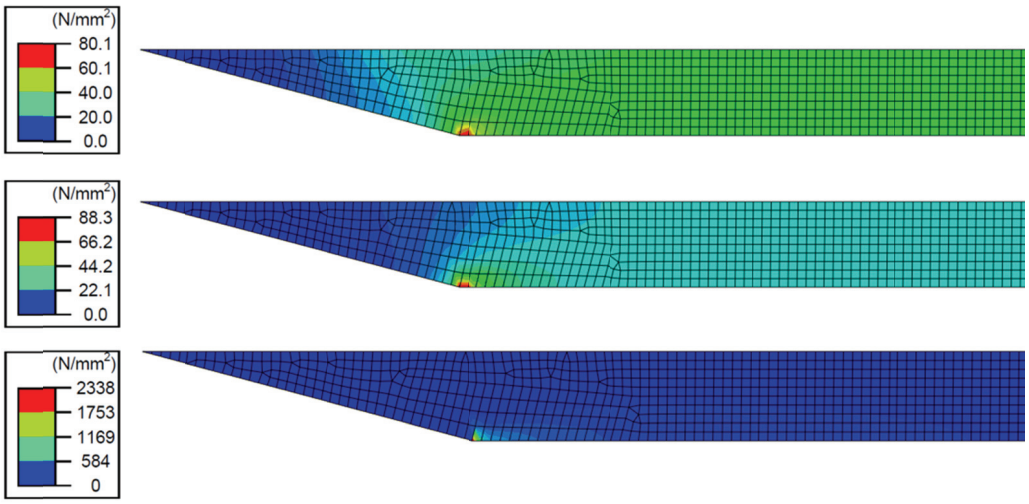

Figure 3.4. The largest in-plane principal stress were interpolated based on the integration points, and plotted on the deformed configurations at values of stretch ratio = 1.14 (top), 1.73 (middle), and 2.55 (bottom). For reference, Scarf Angle = 15°, Bending = 0°.

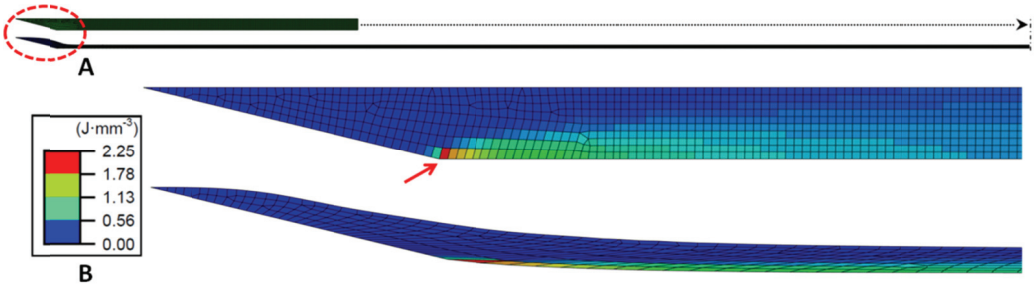

Figure 3.5. (A) PVM FE model before (top) and under second stage deformation (bottom) at a stretch ratio of 3.25. (B) Contour plots of the element-wise strain energy per unit reference volume near the PVM enthesis (red dotted circle) on the undeformed (top) and deformed (below) configurations when Scarf Angle = 15°, Stretch Ratio = 3.0, Bending = 0°, and both material properties have their highest values. Arrow indicates the area with maximum strain energy value along the inferior margin.

The scarf enthesis' oblique interface corner exhibited a greater strain energy concentration than any other region of the PVM (Figure 3.5). In general, the inferior margin seemed to transmit external loading to a visibly greater extent than the superior margin did. The mid-substance of the PVM displayed no conspicuous strain energy concentration. This suggests that the most susceptible location of the PVM to birth-associated loading conditions is indeed the inferior margin of the scarf enthesis at its oblique corner.

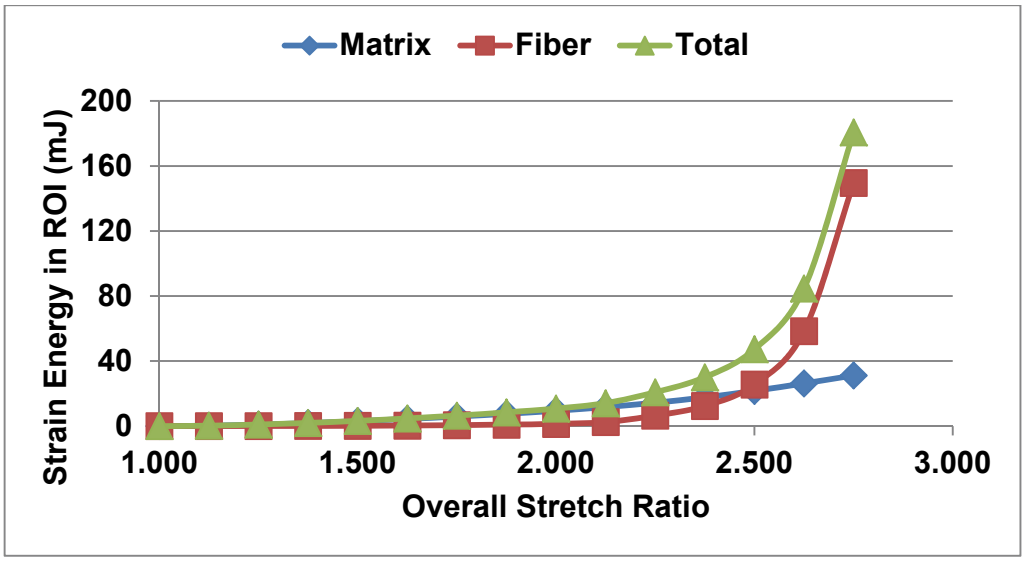

Figure 3.6. Strain energy carried by matrix and collagen fibers in the oblique interface corner ROI. Collagenous fiber contribution shows an exponential increase and becomes dominant when the stretch ratio is more than about 2.5.

The matrix transferred most of the external energy applied to the model under lower values of stretch, while the collagen fibers become the dominant load carrier when the stretch ratio of the model becomes sufficiently large (Figure 3.6). This result may be

explained by the exponential function in the material model, which sharply increases with stretch ratio.

The linear regression analysis shows that the five input variables explained up to 75% of variation in the output variable, Area Ratio. The Area Ratio was most sensitive to the variations in Stretch Ratio ($p < 0.001$), followed by Bending ($p < 0.001$) and Scarf Angle ($p = 0.003$, Table 3.2). However, the two material parameters turned out to be statistically insignificant.

Table 3.2. Results of the sensitivity analysis conducted using the regression model along with the relevant p-values. The asterisk denotes statistically significant values.

Input Variable	**Parameter Estimate from Linear Fit, $\hat{\beta}$**	**P-value**
Scarf Angle	9.662e-02	0.00333 *
Bending	-1.681e-01	5.26e-07 *
Stretch Ratio	-8.416e-01	< 2e-16 *
ECM Property	3.642e-02	0.26474
Collagen Property	-3.555e-02	0.27631

The sensitivity analysis showed that the smaller Scarf Angle, the larger Stretch Ratio, and the greater the degree of PVM enthesial strain energy concentration that was found (Fig. 3.7). Bending the PVM in the superior direction (-15 °) caused a greater concentration of strain energy than the cases with an absence of bending (0 °) or inferior-directed Bending (15 °).

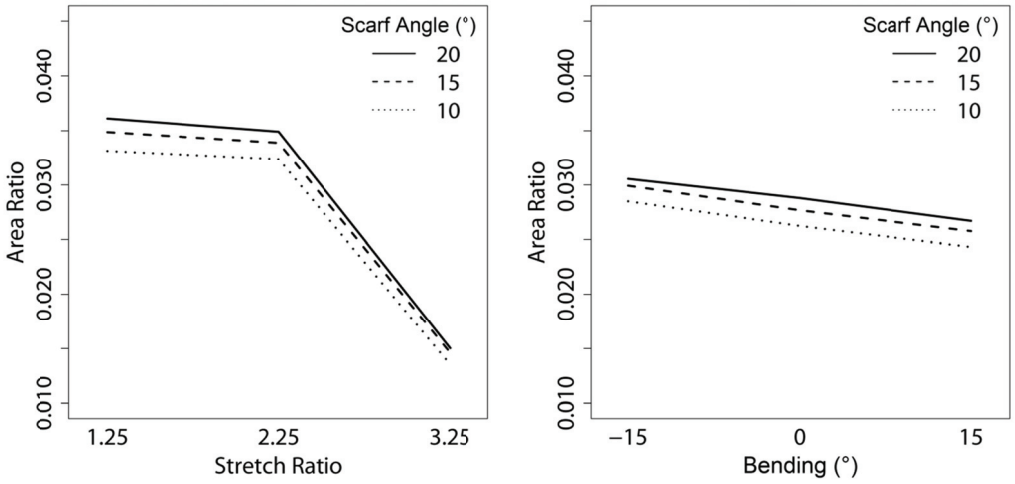

Figure 3.7. Interaction plots of Area Ratio with Scarf Angle against Stretch Ratio (left) and Bending (right).

Finally, when polynomial terms were added to the regression model, the coefficient of determination considerably improved to 0.98. The equation below shows the second degree model after sorting only the significant terms. When Scarf Angle, Bending, and Stretch Ratio were included in the second degree model, the magnitude of influence remained almost identical to that of the first degree model. The Stretch Ratio showed some interaction with Scarf Angle and Bending and its quadratic term also affected the response. Ripening (softening) of the matrix and stiffer collagen fibers both increased the strain energy concentration.

$$y_i = 0.62 + 0.097 \cdot x_{i(\text{Scarf Angle})} - 0.17 \cdot x_{i(\text{Bending})} - 0.84 \cdot x_{i(\text{Stretch Ratio})}$$
$$- 0.025 \cdot x_{i(\text{Scarf Angle})} \cdot x_{i(\text{Stretch Ratio})} - 0.19 \cdot x_{i(\text{Bending})} \cdot x_{i(\text{Stretch Ratio})}$$
$$- 0.62 \cdot x_{i(\text{Stretch Ratio})}^{2} + 0.036 \cdot x_{i(\text{Matrix Stiffness})} - 0.036 \cdot x_{i(\text{Collagen Stiffness})}$$

3.1.4 Discussion

A novel aspect of this study is the analysis of the behavior of the medial PVM origin from the pubic bone by an analogy with a traditional mechanical joint, namely scarf joint. The results demonstrate, for the first time, that the geometry of the PVM scarf enthesis gives rise to a local strain energy concentration at the oblique corner of its inferior margin, rendering it vulnerable to injury when large stretch is imposed (Fig. 3.5), as is the case during vaginal birth (Lien et al. 2004). An increase in the Stretch Ratio, Bending, or Scarf Angle all increased the strain energy concentration at that location (Table 3.2). Finally, the FE simulation of the transversely isotropic material PVM model showed that, as the tensile loading applied to the PVM scarf enthesis increases, more energy is stored by the collagen constituent rather than by the matrix (Fig. 3.6).

A number of simulation studies have attempted to explain why the PVM is the most frequently damaged part of the levator ani muscle during the vaginal birth (Lien et al. 2004; Hoyte et al. 2008; Parente et al. 2008; Li et al. 2010). These studies have consistently showed that the shorter original length of the PVM compared to other parts of the levator ani muscle, as well as the geometrical constraint requiring it to wrap around the fetal head give rise to the large PVM stretch ratio during birth. However, no explanation has been given for why the PVM fails near its origin, and not at its mid-substance or at the distal end. The present paper provides a possible explanation in that regard: namely, the oblique interface between the PVM and the pubic bone creates a local region of the enthesis that is susceptible to injury during vaginal birth due to its geometrical singularity. In a first vaginal delivery, this is the first time in a woman's life that her left or right PVM ever experiences such large and abnormal stretch (Lien et al.

2004). Because the strain energy concentration on the inferior interface corner occurs regardless of the magnitude of stretch ratio applied to the model, the PVM scarf enthesis by itself is likely to cause muscle damage when it exceeds a given injury tolerance.

From an obstetrical point of view, among the three statistically significant input parameters, the input parameter, Scarf Angle, is determined innately by the angle at which the muscle attaches to the bone. The Bending and Stretch Ratio, on the other hand, are governed by how the PVM is stretched as the fetal head pushes the muscles downward as it passes along the curve of Carus, a locus describing the centerline of the vaginal birth canal (Lien et al. 2004; Jing, D. et al. 2012). Our results predict that women with more acute scarf entheses are likely to experience more localized energy concentrations. Therefore, if a morphological measurement could reliably be made of the scarf enthesis angle prior to birth women might be screened for risk of injury. The study also shows that a negative angle of Bending, in the direction of perineal descent during the second stage of labor, reduces the strain energy concentration. This may be counterintuitive because factors inducing inferior rotation, such as forceps delivery, are known to be increase the risk of the levator ani muscle injury due to vaginal birth (Kearney et al. 2006). However, forceps delivery also places a large distraction force on the PVM, so this may be the dominant effect.

As with the material model used for the simulation of the current research, the mechanical response of the collagen fibers is often modeled with an exponential function partly because the fiber is crimped without any loading and tensed after a certain amount of tension (Gasser et al. 2006; Natali et al. 2005). This behavior leads to sudden stiffening of a muscle and to a sharp increase in the stored strain energy at the higher stretch ratio

regime (Fig. 3.6). If hormonal or enzymatic processes causing softening of the tissue are either impractical or do not occur naturally, then another possibility for avoiding the PVM rupture might be to physically reduce the stretch ratio of the PVM itself. Indeed ‘fusible link hypothesis' (Ashton-Miller and DeLancey 2009) assumes that the U-shaped PVM may be protected from overstretching and/or tearing by the presence of compliance in the perineal body that links the distal ends of the left and right PVM. Therefore, incorporating the perineal body into the model and testing this hypothesis directly is worthy of future research.

Limitations of this study include the simplified model geometry. Although the levator ani muscle runs around the pelvic side wall, the PVM portion of the levator ani muscle, where defects have been noted after vaginal delivery unlike the other subparts (DeLancey et al. 2003; Margulies et al. 2006), resides lateral to the vagina locally without significant curvature. Therefore, we chose to focus the analysis into this local region and simplified the geometry of the PVM into two-dimension in this first simulation of the specific birth injury mechanism. Second, the findings were restricted to time-independent phenomena. Based on the stress relaxation tests performed either on the human vaginal tissue or the levator ani muscle, at least a 40 % reduction in stress would occur in these tissues within approximate 15 minutes (Jing, D. 2010; Pena et al. 2010). If a normal range in duration of the second stage of vaginal delivery is considered, well below 50 % stress relaxation could occur. Therefore, one may argue that some results of this study likely overestimate the reported mechanical quantities. Notwithstanding this limitation, the location in which the strain energy concentration occurs is not affected by the energy dissipation over time, as long as there is no highly anisotropic dissipative behavior in the

tissue. Third, while the use of a fiber-reinforced matrix is a reasonable model of the enthesis, given the histology we have described, the use of such a model to represent the striated PVM muscle is a simplification that is probably only valid for the PVM under passive stretch, which is likely the case at the end of the second stage of labor. A future study might include a multi-scale model of the PVM under stretch. Fourth, we have not considered hormonal effects, which can "ripen" the PVM tissue allowing it to stretch more easily, or the effect of volitional contraction of the PVM, which would stiffen it (McMahon 1984). The fact that the PVM of most women remains intact during a vaginal delivery hints that local protective factors might mitigate the local stress/strain energy concentration at the scarf enthesis. One of these could be reinforcement of the oblique corner of the scarf enthesis by more, or stronger, collagen fibers. Fifth, an analytical solution of stress and deformation fields around the oblique scarf interface corner, which has not been investigated to our knowledge, could benefit from more comprehensive information in regard to the input parameters. The strength of the singularity, or the upper bound of the stress field, is required for the comparison with the FE simulation result. Despite its preliminary character, the research reported here would seem to reasonably describe the response of the PVM scarf enthesis both with mixed formulation elements that have been proved to be valid for detecting stress/strain energy singularity, and with a rather qualitative manner using the output variable, Area Ratio.

The response of a PVM scarf enthesis at its interface to the pubic bone appears to have considerable importance for understanding injury mechanisms to the PVM during vaginal delivery. A better understanding of the injury mechanism could lead to improved injury prevention strategies in the future. The results should also have relevance for the

injury of scarf entheses found elsewhere in the body such as chronic avulsion injury of the deltoid insertion to the humeral tuberosity especially in adolescents, where comparable histological characteristics can be found as a fibrous enthesis as with the PVM scarf enthesis (Kim et al. 2011; Benjamin et al. 1986; Donnelly et al. 1999).

3.1.5 References

Kearney, R., Miller, J. M., Ashton-Miller, J. A., DeLancey, J. O. L. (2006). Obstetric factors associated with levator ani muscle injury after vaginal birth. *Obstet. Gynecol., 107*(1), 144-149. doi: 10.1097/01.AOG.0000194063.63206.1c

DeLancey, J. O., Morgan, D. M., Fenner, D. E., Kearney, R., Guire, K., Miller, J. M., Hussain, H., Umek, W., Hsu, Y., Ashton-Miller, J. A. (2007). Comparison of levator ani muscle defects and function in women with and without pelvic organ prolapse. *Obstet. Gynecol., 109*(2 Pt 1), 295-302. doi: 10.1097/01.AOG.0000250901.57095.ba

DeLancey, J. O., Kearney, R., Chou, Q., Speights, S., Binno, S. (2003). The appearance of levator ani muscle abnormalities in magnetic resonance images after vaginal delivery. *Obstet. Gynecol., 101*(1), 46-53. doi: S0029784402024651

Dietz, H. P., Gillespie, A. V., Phadke, P. (2007). Avulsion of the pubovisceral muscle associated with large vaginal tear after normal vaginal delivery at term. *Aust. N. Z. J. Obstet. Gynaecol., 47*(4), 341-344. doi: 10.1111/j.1479-828X.2007.00748.x

Kim, J., Ramanah, R., DeLancey, J. O., Ashton-Miller, J. A. (2011). On the anatomy and histology of the pubovisceral muscle enthesis in women. *Neurourol. Urodyn., 30*(7), 1366-1370. doi: 10.1002/nau.21032

Benjamin, M., Kumai, T., Milz, S., Boszczyk, B. M., Boszczyk, A. A., Ralphs, J. R. (2002). The skeletal attachment of tendons--tendon "entheses". *Comp Biochem Physiol A-Mol Integr Physiol, 133*(4), 931-945. doi: 10.1016/S1095-6433(02)00138-1

Williams, M. L. (1952). Stress singularities resulting from various boundary conditions in angular corners of plates in extension. *J Biomech Eng-Trans ASME, 19*(4), 526-528.

Lubkin, J. L. (1957). A theory of adhesive scarf joints. *J Biomech Eng-Trans ASME, 24*, 255-260.

Liu, D., Fleck, N. A. (1999). Scale effects in the initiation of cracking of a scarf joint. *Int J Fracture, 95*(1-4), 67-88. doi: 10.1023/A:1018635914556

Qian, Z. Q., Akisanya, A. R. (1999). An investigation of the stress singularity near the free edge of scarf joints. *Eur J Mech A-Solid, 18*(3), 443-463. doi: 10.1016/S0997-7538(99)00118-7

Chaudhuri, R. A., Chiu, S. H. J. (2009). Three-dimensional asymptotic stress field in the vicinity of an adhesively bonded scarf joint interface. *Compos Struct, 89*(3), 475-483. doi: 10.1016/j.compstruct.2008.10.002

Geubelle, P. H., Knauss, W. G. (1994). Finite strains at the tip of a crack in a sheet of hyperelastic material: III. General bimaterial case. *J Elasticity, 35*(1-3), 139-174. doi: 10.1007/BF00115541

Long, R., Krishnan, V. R., Hui, C.-Y. (2011). Finite strain analysis of crack tip fields in incompressible hyperelastic solids loaded in plane stress. *J Mech Phys Solids, 59*(3), 672-695. doi: 10.1016/j.jmps.2010.12.005

Dempsey, J. P., Sinclair, G. B. (1981). On the singular behavior at the vertex of a bi-material wedge. *J Elasticity, 11*(3), 317-327. doi: 10.1007/bf00041942

Marks, L. W., Gardner, T. N. (1993). The use of strain energy as a convergence criterion in the finite element modelling of bone and the effect of model geometry on stress convergence. *J. Biomed. Eng., 15*(6), 474-476. doi: 10.1016/0141-5425(93)90061-3

Benzley, S. E. (1974). Representation of singularities with isoparametric finite elements. *Int J Numer Methods Eng, 8*(3), 537-545. doi: 10.1002/nme.1620080310

Brink, U., Stein, E. (1996). On some mixed finite element methods for incompressible and nearly incompressible finite elasticity. *Comput. Mech., 19*(2), 105-119. doi: 10.1007/BF02824849

Wilcox, C. H. (1979). Uniqueness theorems for displacement fields with locally finite energy in linear elastostatics. *J Elasticity, 9*(3), 221-243. doi: 10.1007/bf00041096

Chaudhuri, R. (2000). A tale of two saints: St. Venant and 'St. Nick': does St. Venant's principle apply to bi-material straight-edge and wedge-singularity problems? *Compos. Sci. Technol., 60*(12-13), 2503. doi: 10.1016/S0266-3538(00)00044-0

Brooks, S. V., Zerba, E., Faulkner, J. A. (1995). Injury to muscle fibres after single stretches of passive and maximally stimulated muscles in mice. *J. Physiol.-London, 488 (Pt 2)*, 459-469.

Wang, J. L., Parnianpour, M., ShiraziAdl, A., Engin, A. E. (1997). Failure criterion of collagen fiber: Viscoelastic behavior simulated by using load control data. *Theor. Appl. Fract. Mech., 27*(1), 1-12.

Gasser, T. C., Ogden, R. W., Holzapfel, G. A. (2006). Hyperelastic modelling of arterial layers with distributed collagen fibre orientations. *J. R. Soc. Interface, 3*(6), 15-35. doi: 10.1098/rsif.2005.0073

Subit, D., Masson, C., Brunet, C., Chabrand, P. (2008). Microstructure of the ligament-to-bone attachment complex in the human knee joint. *J. Mech. Behav. Biomed. Mater., 1*(4), 360-367. doi: 10.1016/j.jmbbm.2008.02.002

Jing, D. (2010). *Experimental and theoretical biomechanical analyses of the second stage of labor.* PhD. thesis, University of Michigan.

Simo, J. C., Armero, F. (1992). Geometrically nonlinear enhanced strain mixed methods and the method of incompatible modes. *Int J Numer Methods Eng, 33*(7), 1413-1449. doi: 10.1002/nme.1620330705

Ashton-Miller, J. A., DeLancey, J. O. (2009). On the biomechanics of vaginal birth and common sequelae. *Annu Rev Biomed Eng, 11*, 163-176. doi: 10.1146/annurev-bioeng-061008-124823

Lien, K. C., Mooney, B., DeLancey, J. O., Ashton-Miller, J. A. (2004). Levator ani muscle stretch induced by simulated vaginal birth. *Obstet. Gynecol., 103*(1), 31-40. doi: 10.1097/01.AOG.0000109207.22354.65

R Devolopment Core Team. (2011). *R: A language and environment for statistical computing.* Vienna, Austria: R Foundation for Statistical Computing.

Hoyte, L., Damaser, M. S., Warfield, S. K., Chukkapalli, G., Majumdar, A., Choi, D. J., Trivedi, A., Krysl, P. (2008). Quantity and distribution of levator ani stretch during simulated vaginal childbirth. *Am. J. Obstet. Gynecol., 199*(2), 198 e191-195. doi: 10.1016/j.ajog.2008.04.027

Parente, M. P., Jorge, R. M., Mascarenhas, T., Fernandes, A. A., Martins, J. A. (2008). Deformation of the pelvic floor muscles during a vaginal delivery. *Int. Urogynecol. J., 19*(1), 65-71. doi: 10.1007/s00192-007-0388-7

Li, X., Kruger, J. A., Nash, M. P., Nielsen, P. M. (2010). Anisotropic effects of the levator ani muscle during childbirth. *Biomech. Model. Mechanobiol., 10*(4), 485-494. doi: 10.1007/s10237-010-0249-z

Jing, D., Ashton-Miller, J. A., Delancey, J. O. (2012). A subject-specific anisotropic visco-hyperelastic finite element model of female pelvic floor stress and strain during the second stage of labor. *J. Biomech., 45*(3), 455-460. doi: 10.1016/j.jbiomech.2011.12.002

Natali, A. N., Pavan, P. G., Carniel, E. L., Lucisano, M. E., Taglialavoro, G. (2005). Anisotropic elasto-damage constitutive model for the biomechanical analysis of tendons. *Med. Eng. Phys., 27*(3), 209-214. doi: 10.1016/j.medengphy.2004.10.011

Margulies, R. U., Hsu, Y., Kearney, R., Stein, T., Umek, W. H., DeLancey, J. O. (2006). Appearance of the levator ani muscle subdivisions in magnetic resonance images. *Obstet. Gynecol., 107*(5), 1064-1069.

Pena, E., Calvo, B., Martinez, M. A., Martins, P., Mascarenhas, T., Jorge, R. M., Ferreira, A., Doblare, M. (2010). Experimental study and constitutive modeling of the viscoelastic mechanical properties of the human prolapsed vaginal tissue. *Biomech. Model. Mechanobiol., 9*(1), 35-44. doi: 10.1007/s10237-009-0157-2

McMahon, T. A. (1984). *Muscles, reflexes, and locomotion*. Princeton, N.J.: Princeton University Press.

Benjamin, M., Evans, E. J., Copp, L. (1986). The histology of tendon attachments to bone in man. *J. Anat., 149*, 89-100.

Donnelly, L. F., Helms, C. A., Bisset, G. S., 3rd. (1999). Chronic avulsive injury of the deltoid insertion in adolescents: imaging findings in three cases. *Radiology, 211*(1), 233-236.

3.2 A 3-D Levator Ani Muscle Model

3.2.1 Introduction

Vaginal delivery is the single most important risk factor for developing pelvic organ prolapse (Mant et al. 1997; Leijonhufvud et al. 2011). These studies show that compared with nulliparous women, the relative-risk for developing prolapse requiring hospital admission was four in women with one vaginal birth and eight in women with two births. Birth-related injuries occur immediately in the process of the delivery during the second stage phase but the prolapse only becomes manifest decades later in life.

Studies with MR imaging and pelvic floor ultrasound have demonstrated the occurrence of the trauma to the levator ani muscle (LA) after vaginal birth; these have been reported to occur in 20-30 % of women who have delivered vaginally (DeLancey et al. 2003; Kearney et al. 2006; Dietz and Simpson 2008). In women with prolapse, 55% show evidence of major injury (with more than 50 % of the muscle injured) while in women with normal support, only 16% have evidence of this type of injury (DeLancey et al. 2007).

To investigate the biomechanical factors relevant to LA injury and the forces it is subjected to during vaginal birth, researchers have used finite element (FE) models to simulate the biomechanics of the late second stage (Lien et al. 2004; Hoyte et al. 2008; Parente et al. 2008; Li et al. 2010). It is known from an earlier study that the most medial portion of the LA, known as the pubovisceral muscle (PVM), undergo the highest stretch

ratio of 3.26 by the end of the second stage of labor. In a recent study the additional role of the distensibility of the perineal body has been added (Jing et al. 2012). It was shown that decreasing the stiffness of the perineal body helped to mitigate the stretch of the PVM enthesis.

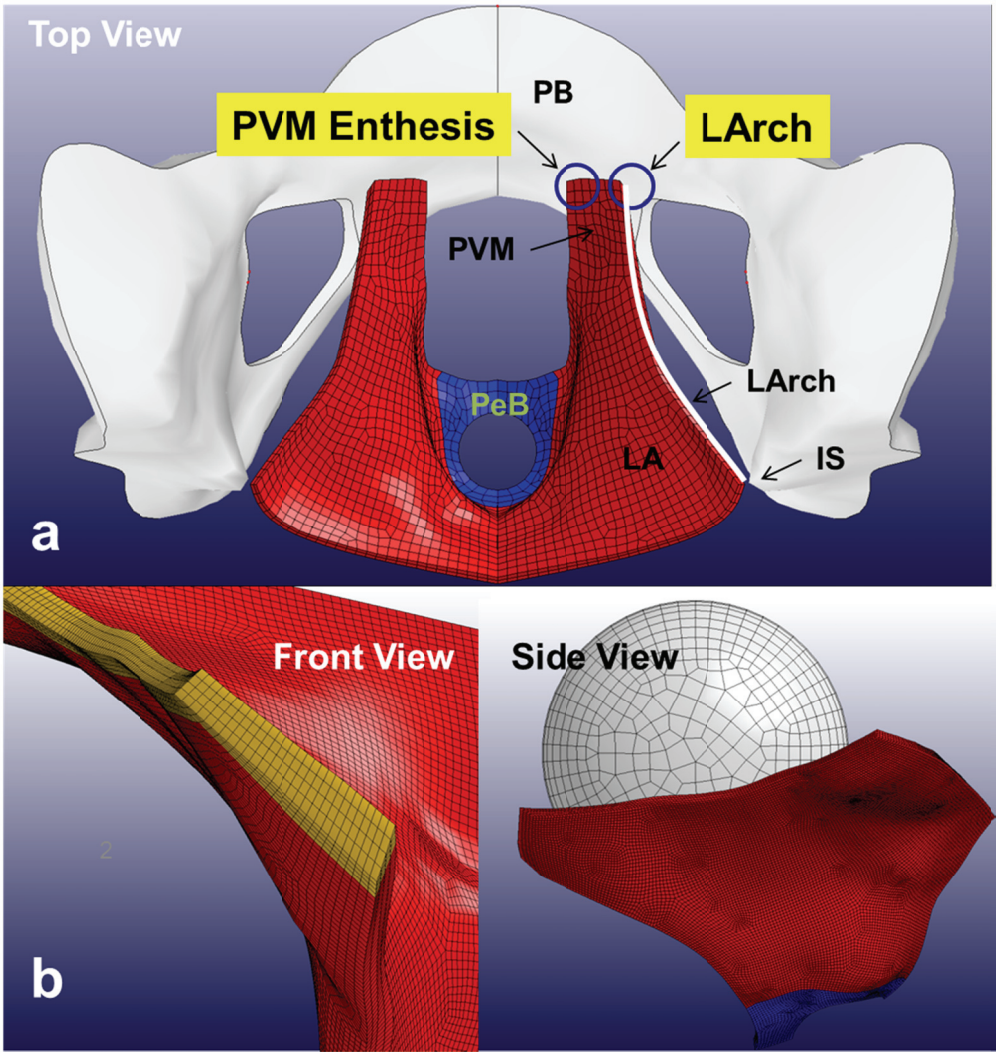

Figure 3.8. 3-D pelvic floor FE model. **(a)** Top view with the pubic bone (PB) for orientation. Lateral edges of the levator ani (LA) are supported by the levator arch (LArch), a catenary structure from the ischial spine (IS) to the anterior PB. (PVM: pubovisceral muscle; PeB: perineal body; R: rectum)**. (b)** Fetal head was modeled as a sphere.

The site of the LA injury has been identified as the pubic portion of the LA (Margulies et al. 2007). The factors that explain why the injury occurs at this location are not fully understood. In previous computer model studies, the detailed location of the putative injury site was also not fully explored because the anatomy was too simplified. We modeled the levator ani muscle with solid elements in order to better examine phenomena occurring in thickness direction. So this report describes a detailed computer model of the LA to better understand why injuries occur at the pubic origin of the LA during the 2nd stage of vaginal birth.

3.2.2 Methods

A three-dimensional (3-D) geometrical model of the pelvic floor was created based on Magnetic resonance (MR) scans of a healthy nulliparous 37-year-old woman, who satisfied the following criteria: no previous vaginal delivery, no symptoms of urinary incontinence, normal support on pelvic examination and normal anatomy of the levator ani muscles. The model for this study was focused on capturing anatomy in the LA injury zone associated with childbirth. Characteristic landmarks were identified in three-dimensionally aligned MR scans using 3D Slicer (The Brigham and Women's Hospital, Boston, MA, USA) software. These included the LA, the fascia arch (FArch, otherwise known as the arcus tendineus fascia pelvis), the levator arch (LArch; otherwise known as the arcus tendineus levator ani), the perineal body (PeB), and the pubic bone (PB) (Fig. 3.8). These structures were integrated with the MR based LA contour to

generate a geometrically smooth 3-D surface with the help of a commercial 3-D modeling tool, Rhinoceros 3D (Version 4, Robert McNeel & Associates, Seattle, WA, USA). The smoothly patched surface models were then imported into LS-DYNA (Version 971 R5, Livermore Software Technology Corporation, Livermore, CA, USA), an engineering multiphysics simulation software package to conduct the finite element (FE) simulation under implicit and explicit solvers. A previous study from our group has identified significant gradient in through-thickness stress and strain distributions when two heterogeneous materials meets at an oblique angle (Kim et al. 2011a). To understand and quantify this phenomenon through thickness, solid (also known as brick) elements were employed to represent the LA structure for FE simulation. This contrasts with previous FE analyses of the pelvic floor that have been performed by thin membrane elements (Lien et al. 2004; Parente et al. 2008; Jing et al. 2012).

The fetal head was approximated to a sphere of 8.5 cm in diameter after taking the fetal head molding effect into consideration. The applied size corresponds to about the 50th percentile in fetal head diameter. As a simplified second stage labor progress, the motion of the fetal head was prescribed to descend through the birth canal at constant velocity. Regions of higher stress, strain, and strain energy were identified. The simulation was initiated from the moment the fetal head made a contact with LA, and terminated once the two structures were fully engaged. We tested the hypothesis that the regions of highest stress and strain would occur in the locations that have previously been shown to exhibit defects after vaginal birth (see above).

The mechanical behavior of the LA was represented by a transversely isotropic hyperelastic material model, which provides an isotropic Mooney-Rivlin matrix

reinforced fibers having a strain energy contribution in a defined orientation. In addition, the viscoelastic behavior was represented by implementing a three-term Prony series for the relaxation function (Puso and Weiss 1998). A specific form of strain energy function takes the following form:

$$W = C_1\left(\tilde{I}_1 - 3\right) + C_2\left(\tilde{I}_2 - 3\right) + F(\lambda) + \tfrac{1}{2}K\left[\ln(J)\right]^2$$

where, λ is the deviatoric part of the stretch along the current fiber direction, $\overline{I}_1$ and $\overline{I}_2$ are the deviatoric invariants of the right Cauchy deformation tensor. J and K are the volume ratio and the bulk modulus, respectively. The anisotropic nature is explained by the third term, the derivative of which can be written in the following formulas:

$$\frac{\partial F}{\partial \lambda} = \begin{Bmatrix} 0 & \lambda < 1 \\ \frac{C_3}{\lambda}\left[\exp\left(C_4(\lambda - 1)\right) - 1\right] & \lambda < \lambda^* \\ \frac{1}{\lambda}(C_5\lambda + C_6) & \lambda \geq \lambda^* \end{Bmatrix}$$

where λ^* means the stretch ratio at which the fibers were assumed to be straightened.

The material parameters were based on a biaxial *in vitro* tensile tests of female PVM (Jing et al. 2008). Then the adjustment was made to limit the ultimate tensile stress (UTS) of the PVM and its surrounding structures under 100 MPa after taking the fact that reported UTS values of human soft tissue into account (Woo and Levine 1998). Finally, the reduced relaxation function that describes time-dependent phenomena of the tissue was represented by the following Prony series:

$$G(t) = \sum_{i=1}^{3} S_i \exp\left(\frac{t}{T_i}\right)$$

The parameters of the material properties used for the simulation are shown in Table 3.3 and 3.4.

Table 3.3. Transversely isotropic hyperelastic material parameter values (Units: MPa) used in this study.

	C_1	C_2	C_3	C_4	C_5
LA	0.013402	0.300785	978.1935	8.80E-05	0.086122
LArch, PeB	0.201222	0.287072	978.3199	5.88E-06	0.005755

Table 3.4. Viscoelastic material parameter values (unitless) used in this study

	S_1	T_1	S_2	T_2	S_3	T_3	S_4	T_4
LA	0.32186	5.2E-14	0.19137	3.3E-05	0.21385	3.3E02	0.27292	2.0E04
LArch, PeB	0.34428	5.2E-14	0.21380	3.3E-05	0.22786	3.9E02	0.21405	2.0E04

3.2.3 Results

We identified two specific areas of increased stress/strain on the proximal PVM, namely the origin of the levator arch (LArch) and the pubovisceral muscle enthesis to the pubic bone (Enthesis). Figure 3.9 shows the posterior margin of the levator ani muscle when the fetal head fully engages with the levator ani muscle. The PVM enthesis and the LArch seem to be the locations where higher local principal Green-Lagrange strain and principal Cauchy stress values occur, respectively.

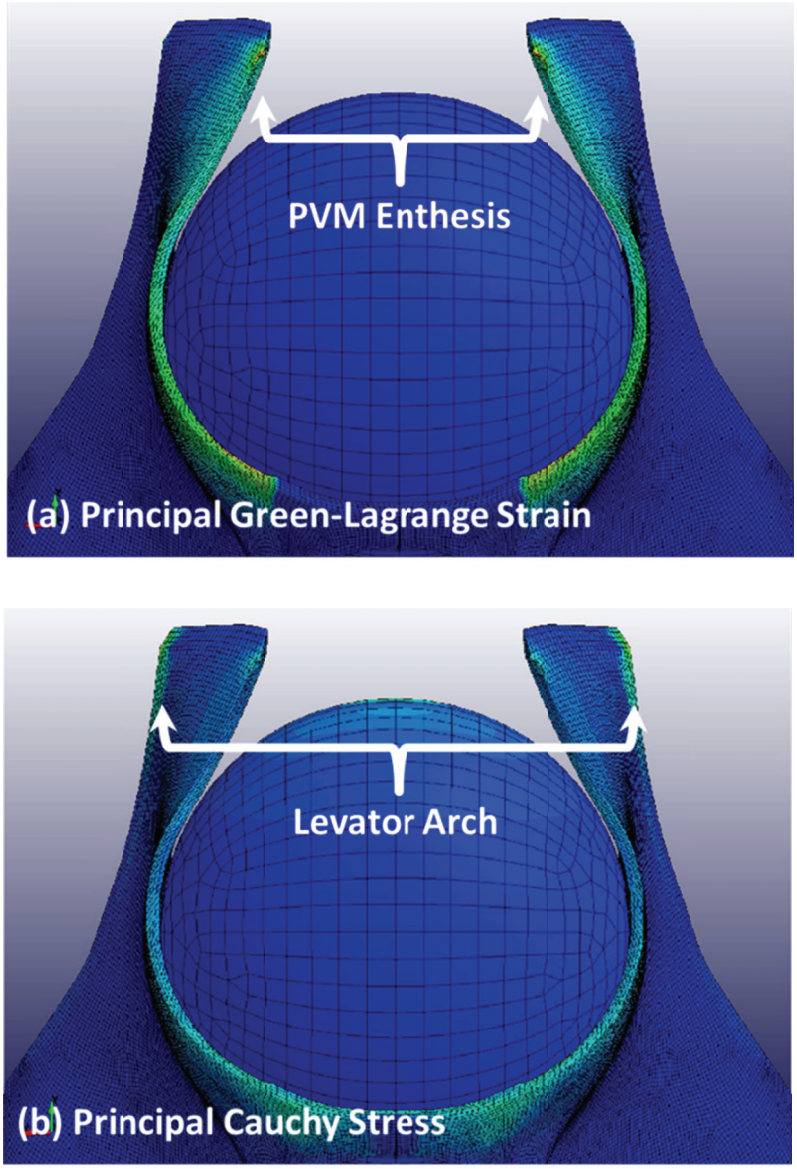

Figure 3.9. Maximum principal Green-Lagrange strain (a) and maximum principal Cauchy stress (b) contours in the 2nd-stage of labor. Note stress concentrations at the LArch when the fetal head fully interacts with the levator ani (LA). The PVM enthesis also exhibits a marked strain concentration, especially at the inferior obtuse attachment to the pubic bone.

A quantitative sense of the loading on these two foci relative to progress during the 2nd stage of labor can be found in Figure 3.10. As soon as the fetal head makes contact with the LA, the maximum principal Green-Lagrange strain on the PVM enthesis

sharply increases. On the other hand, the elongation of the levator arch does not seem to be conspicuous. Once the fetal head further descends and gets fully engaged with the LA, the levator arch starts to be loaded much greater than the PVM enthesis.

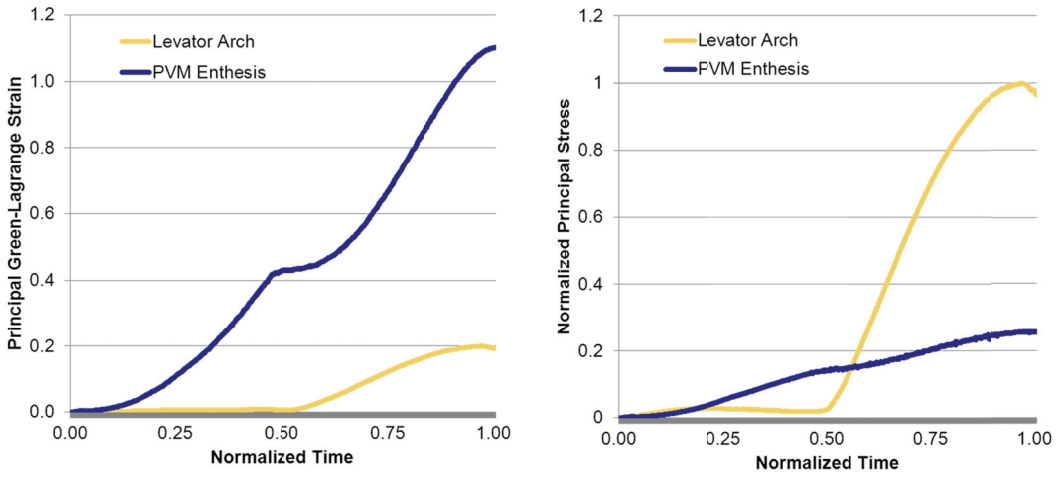

Figure 3.10. Plot of the maximum principal Green-Lagrange strain and maximum principal Cauchy stress at the levator arch and PVM Enthesis versus the progression of the 2nd stage of labor. Note that abscissa was normalized by duration of the simulation, and principal stress was normalized by the maximum value since cadaveric tissue properties have limited physical representation of physiological tissue characteristics. While the PVM is always elongated more than the levator arch, loading is concentrated more to the levator arch than to the PVM especially during the later stage of the 2nd stage.

3.2.4 Discussion

This biomechanical model reveals that the pubic origins of both the LArch and PVM are both at elevated risks for injury during the second stage due to excessive stress and strain. The findings of high stress and strain in these regions are consistent with the injury patterns seen in MRI images of women with levator injury (Margulies et al. 2007).

This is the first biomechanical explanation of why the injury occurs at this specific location and in a particular sequence.

The findings of this study add to a growing body of information about the location and causes of the LA injury; these injuries are strongly associated with prolapse later in life. Two different morphological types exist in women with the LA defect. Some women reveal distorted anatomy ("architectural distortion") while others experience loss of muscle but in whom the overall location of structures remains intact (Margulies et al. 2007). Further analysis of women with architectural distortion has shown that there is a downward shift in the LArch below its' normal location in women with architectural distortion (Larson et al. 2011). Because the LArch is the point of origin for much of the LA, this could prove a critical defect. The present study reveals high stress and strain concentrations at the origin of the LArch during birth, suggesting a possible injury mechanism. This high stress is logical because all of the PVM between the ischial spine and the origin of the LArch to the pubic bone is attached to the LArch. Therefore any forces exerted on the LA must be carried by the two small attachment points that are the focus of the present study. The second finding, namely that the medial portion of the PVM where it attached directly to the pubic bone (Kim et al. 2011a; Kim et al. 2011b) is also under stress can help to explain those women where the levator arch remains intact (i.e., no architectural distortion) but who lose muscle in this region.

These observations can be shown in the conceptual model shown in Fig. 3.11 that integrates LA defect, architectural distortion, apical support, and pelvic organ prolapse. Of course, muscle damage is only one part of the pelvic organ support system and the importance of other factors such as apical support and fascial integrity is revealed by the

fact that roughly half of women with prolapse do not have major damage to the pelvic floor muscles. Several studies have demonstrated a correlation between pelvic organ prolapse and a defect in apical support, the LA structure itself, and a subsidiary morphological distortion in MR images (DeLancey et al. 2007; Margulies et al. 2007; Huebner et al. 2008; Chen et al. 2009).

Figure 3.11. A putative pelvic organ prolapse disease model shows why the factors analyzed in the present study are significant. Vaginal delivery is the single most important risk factor for pelvic organ prolapse, whose precursor includes LA defect, architectural distortion, and apical support. This study has value because it provides evidence of where, when, and why injuries occur at the origin of the PVM and the LArch.

The biomechanics of vaginal delivery and its effect on the LA structure have been discussed in broad perspective in several earlier computer simulation studies from our group (Lien et al. 2004; Jing et al. 2012). Recently, more specific research on where and why the LA injury would happen due to vaginal delivery have been conducted (Kim et al. 2011a; Larson et al. 2011). These studies not only revealed using a 3-D computer model the appearance of the LA after the origin of the LArch was detached, but also showed

significantly higher stress and strain at the origin of the PVM from the pubic bone due to the oblique nature of the interface in a simplified FE simulation (Chapter 3.1). This study attempted to integrate these detailed findings into a larger scale computer simulation where birth injury mechanisms can be examined and captured with all of the largely effective factors - the thickness of the LA structure, the fetal head, and the pubic bone - put together.

The present study has a number of limitations. The present model uses a simplified loading condition by which fetal head descent was specified at a given velocity along the admissible space surrounded by the LA and the space of Retzius. This modeling approach differs from actual vaginal delivery since phasic uterine contractions and voluntary pushes usually drive a fetal head down along the birth canal (Rempen and Kraus 1991). The results are likely conservative because the simulation represents delivery in a single push, but momentary increases in resulting from voluntary pushes still need to be considered. It should also be noted that the anatomical representation of the LA structure remains to be improved. The fiber orientation of the puborectal portion of the LA (PRM), which is known to show about 55 degrees difference on the sagittal plane from that of the PVM (Betschart et al. 2012), was not accurately implemented in this study. However, considering PRM takes its origin from the periphery of the perineal membrane, the effect of this angle on the Enthesis and the LArch is expected to be small. Finally, the bio-tissue properties of this study were taken from human cadaveric specimens, which do not represent physiological conditions of the pelvic floor muscles. Nonetheless, to the best of our knowledge, there is no data of the human tissue viscoelastic properties available in literature.

3.2.5 References

Mant, J., Painter, R., Vessey, M. (1997). Epidemiology of genital prolapse: observations from the Oxford Family Planning Association Study. *Br. J. Obstet. Gynaecol., 104*(5), 579-585.

Leijonhufvud, A., Lundholm, C., Cnattingius, S., Granath, F., Andolf, E., Altman, D. (2011). Risks of stress urinary incontinence and pelvic organ prolapse surgery in relation to mode of childbirth. *Am. J. Obstet. Gynecol., 204*(1), 70 e71-77.

DeLancey, J. O., Kearney, R., Chou, Q., Speights, S., Binno, S. (2003). The appearance of levator ani muscle abnormalities in magnetic resonance images after vaginal delivery. *Obstet. Gynecol., 101*(1), 46-53. doi: S0029784402024651

Kearney, R., Miller, J. M., Ashton-Miller, J. A., DeLancey, J. O. L. (2006). Obstetric factors associated with levator ani muscle injury after vaginal birth. *Obstet. Gynecol., 107*(1), 144-149. doi: 10.1097/01.AOG.0000194063.63206.1c

Dietz, H. P., Simpson, J. M. (2008). Levator trauma is associated with pelvic organ prolapse. *BJOG, 115*(8), 979-984. doi: 10.1111/j.1471-0528.2008.01751.x

DeLancey, J. O., Morgan, D. M., Fenner, D. E., Kearney, R., Guire, K., Miller, J. M., Hussain, H., Umek, W., Hsu, Y., Ashton-Miller, J. A. (2007). Comparison of levator ani muscle defects and function in women with and without pelvic organ prolapse. *Obstet. Gynecol., 109*(2 Pt 1), 295-302. doi: 10.1097/01.AOG.0000250901.57095.ba

Lien, K. C., Mooney, B., DeLancey, J. O., Ashton-Miller, J. A. (2004). Levator ani muscle stretch induced by simulated vaginal birth. *Obstet. Gynecol., 103*(1), 31-40. doi: 10.1097/01.AOG.0000109207.22354.65

Hoyte, L., Damaser, M. S., Warfield, S. K., Chukkapalli, G., Majumdar, A., Choi, D. J., Trivedi, A., Krysl, P. (2008). Quantity and distribution of levator ani stretch during simulated vaginal childbirth. *Am. J. Obstet. Gynecol., 199*(2), 198 e191-195. doi: 10.1016/j.ajog.2008.04.027

Parente, M. P., Jorge, R. M., Mascarenhas, T., Fernandes, A. A., Martins, J. A. (2008). Deformation of the pelvic floor muscles during a vaginal delivery. *Int. Urogynecol. J., 19*(1), 65-71. doi: 10.1007/s00192-007-0388-7

Li, X., Kruger, J. A., Nash, M. P., Nielsen, P. M. (2010). Anisotropic effects of the levator ani muscle during childbirth. *Biomech. Model. Mechanobiol., 10*(4), 485-494. doi: 10.1007/s10237-010-0249-z

Jing, D., Ashton-Miller, J. A., Delancey, J. O. (2012). A subject-specific anisotropic visco-hyperelastic finite element model of female pelvic floor stress and strain during the second stage of labor. *J. Biomech., 45*(3), 455-460. doi: 10.1016/j.jbiomech.2011.12.002

Margulies, R. U., Huebner, M., DeLancey, J. O. (2007). Origin and insertion points involved in levator ani muscle defects. *Am. J. Obstet. Gynecol., 196*(3), 251 e251-255.

Kim, J., DeLancey, J. O., Ashton-Miller, J. A. (2011a). *Why does the pubovisceral muscle fail at its enthesis, and not elsewhere, during the second stage of labor? A computational study*. Paper presented at the 35th Annual Meeting of the American Society of Biomechanics, Long Beach, CA.

Puso, M. A., Weiss, J. A. (1998). Finite element implementation of anisotropic quasi-linear viscoelasticity using a discrete spectrum approximation. *J. Biomech. Eng., 120*(1), 62-70.

Jing, D., Lien, K. C., Ashton-Miller, J. A., DeLancey, J. O. (2008). *Visco-hyperelastic properties of the pelvic floor muscles in healthy women*. Paper presented at the North American Congress on Biomechanics, Ann Arbor, MI.

Woo, S. L., Levine, R. E. (1998). Ligament, tendon and fascia. In J. Black & G. W. Hastings (Eds.), *Handbook of biomaterial properties* (pp. 59-65). London, UK: Chapman & Hall.

Larson, K., Luo, J., Yousuf, A., Ashton-Miller, J., Delancey, J. (2011). Measurement of the 3D geometry of the fascial arches in women with a unilateral levator defect and “architectural distortion”. *Int. Urogynecol. J.*(In Press). doi: 10.1007/s00192-011-1528-7

Kim, J., Ramanah, R., DeLancey, J. O., Ashton-Miller, J. A. (2011b). On the anatomy and histology of the pubovisceral muscle enthesis in women. *Neurourol. Urodyn., 30*(7), 1366-1370. doi: 10.1002/nau.21032

Huebner, M., Margulies, R. U., DeLancey, J. O. (2008). Pelvic architectural distortion is associated with pelvic organ prolapse. *Int. Urogynecol. J. Pelvic Floor Dysfunct., 19*(6), 863-867. doi: 10.1007/s00192-007-0546-y

Chen, L., Ashton-Miller, J. A., DeLancey, J. O. (2009). A 3D finite element model of anterior vaginal wall support to evaluate mechanisms underlying cystocele formation. *J. Biomech., 42*(10), 1371-1377. doi: 10.1016/j.jbiomech.2009.04.043

Rempen, A., Kraus, M. (1991). Pressures on the fetal head during normal labor. *J. Perinat. Med., 19*(3), 199-206.

Betschart, C., Kim, J., Ashton-Miller, J. A., DeLancey, J. O. (2012). *Muscle Fiber Direction of the Levator Ani and External Anal Sphincter Muscle in MRI*. Paper presented at the 33rd Annual Scientific Meeting of the American Urogynecologic Society, Chicago, IL.

CHAPTER 4

System for Measuring *In Vivo* Fetal Head Displacement and Perineal Deformation during the Second Stage of Vaginal Delivery

4.1 Introduction

Vaginal delivery is known to be the most influential factor for causing levator ani muscle injury that is associated with the pelvic organ prolapse, later in a woman's life (Dietz and Lanzarone 2005; Kearney et al. 2006; DeLancey et al. 2007). This type of injury may be attributed to excessive deformation during vaginal delivery particularly at the end of the second stage of labor. Several computational birth simulation studies have identified the largest stretch ratio at the part of the levator ani muscle, namely the pubovisceral muscle, which can be stretched to over three times its original length.(Lien et al. 2004; Hoyte et al. 2008; Parente et al. 2008; Li et al. 2010) However, the specific factors or cascade of events lead to levator ani muscle injury and subsequent dysfunctions later in life remain unknown. A major impediment to this research is a paucity of measurement strategies for quantifying the second stage events of labor that are potentially correlated with levator ani muscle damage. At the bedside, healthcare providers often make multiple intuitive and somewhat subjective assessments regarding the second stage progress which guide labor management. However, details of the assessment are not typically captured in the medical record. Unlike the first stage of

labor, with well-defined markers of events and progress such as cervical dilation, the complex dynamics of the second stage are typically summed up simplistically as length of time from complete cervical dilation to expulsion of the baby. Therefore, a direct comparison of the biomechanical computer simulations to the experimental measurements has not been made for validation purposes. Moreover, this lack of fundamental information on perineal surface deformation during delivery has prevented researchers from a deeper understanding of how, when and why levator ani muscle injury is most likely to occur.

The goal of this experimental study, therefore, was to develop and test a system using computer vision technology to document the details of the deformation of the perineal skin during the end phase of second stage of labor.

4.2 Methods

The approval of the University of Michigan Medical School Institutional Review Board was obtained for the human studies that will be described in this article. This system passed the electrical safety inspection administered by the Biomedical Engineering Unit at the University of Michigan before being deployed to the hospital.

The main components of the system were two webcams mounted in a plastic housing and connected to a laptop computer (Fig. 4.1). They were set on a wheeled cart in order to be quickly set aside in case clinicians needed rapid access to the patients. This configuration helped occupy a relatively small space and minimize interference with clinical activities by the healthcare providers. Since the cameras were pre-calibrated in a

fixed position relative to each other, there was no need for additional calibration process in preparation of the experiments. A laptop computer served as a wide viewfinder to the clinicians as well as a power source that brought an additional benefit of circumventing hospital electrical safety requirements. A custom recording program written in C++ in conjunction with the OpenCV library (Bradski and Kaehler 2008) was also installed in the laptop and allowed the users to conveniently choose to record only the moments of interest.

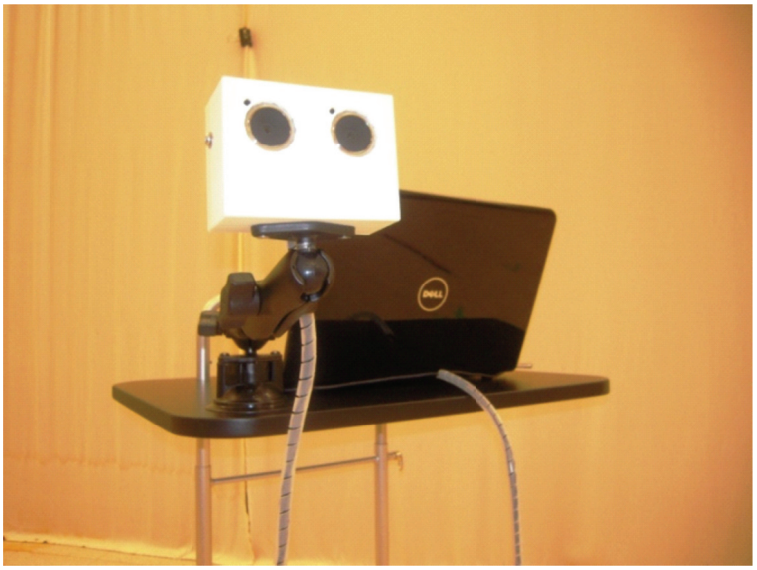

Figure 4.1. Picture of the measurement "Pixie" system consisting of a dual webcam assembly connected to a laptop.

During delivery, the measurement system was placed at the foot of the bed facing the perineum at a range of between 30 to 50 inches. This placement yields a large enough field of view to include the entire perineal surface as well as the proximal thighs for the frame-by-frame registration purpose (which will be described in more detail later in this

Section). Prior to the recording, approximately 15 dot markers were drawn with a surgical marker over the perineal skin and the thighs. Four points were placed on the perimeter of the vaginal opening for the antero-posterior (AP) and lateral (LA) diameters, around six points within the boundary covering the protruding perineal surface area during birth, and four points on each side of the back of the thighs for registration purposes. The duration of the recording in the two subjects was 16 and 106 minutes. After the intervals that did not contain active pushing phase were deleted, the resulting lengths of the recording times were 15 and 30 minutes, respectively.

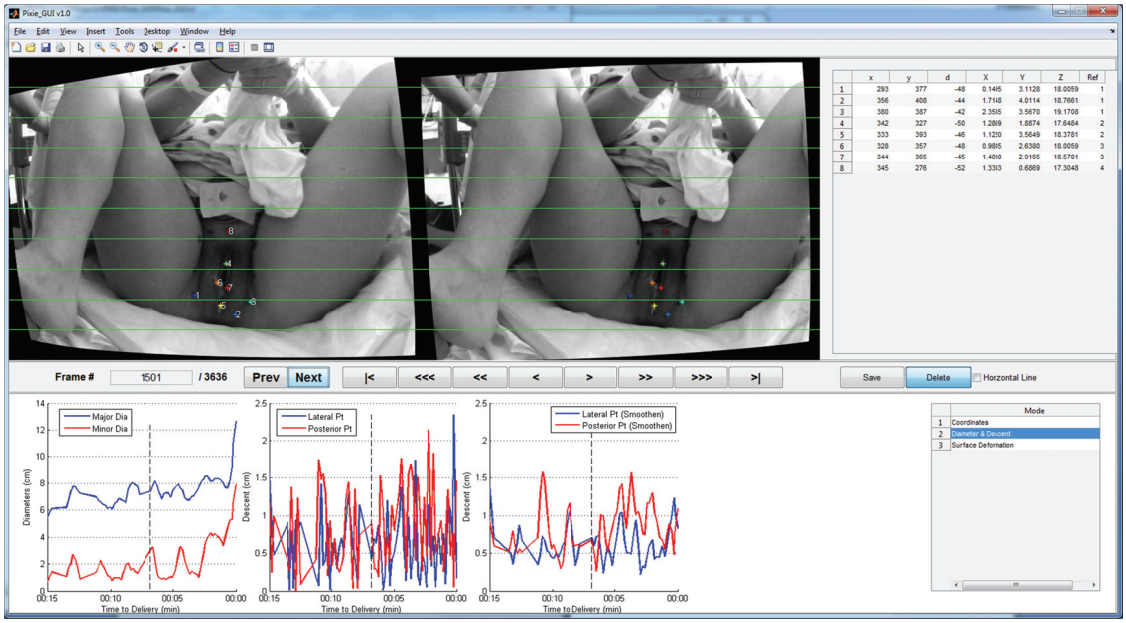

Figure 4.2. The graphic user interface of the post-processing software. Two views from each of the cameras were provided along with other information regarding the three-dimensional coordinates of the markers, diameters, amount of perineal descent, and principal stretches/spatial directions.

Upon completion of the intrapartum recording, post-processing was conducted using custom software written in MATLAB R2011b (MathWorks, Natick, MA) (Fig. 4.2). This software enabled automatically selection of the ink markers to the sub-pixel accuracy level on the planar image from which three-dimensional coordinates were calculated. However, manual selection of the markers on some frames was performed as well, because the patient care had been prioritized during the testing and it often led to the inevitable occlusions of the scene by clinicians' hands or limbs. The frames on which the three-dimensional reconstruction was performed were selectively chosen by the data processor (Jinyong Kim), yet they were checked by experienced clinicians (Lisa Kane Low and John O. L. DeLancey) that all the pushing phases were correctly identified.

Three measurements were made. First, the time histories of anterior-posterior (AP) and lateral (LA) vertex diameters were plotted from the four ink markers located around the vaginal opening (Fig. 4.3a). Based on this measurement, the rate of stretch in the final volitional pushing of mothers was also estimated. To validate the present system measurement results, comparison with the AP vertex diameter measured *in vivo* in six primipara (Jane Walder, RN, personal communication, March 14, 2002). The perineal surface deformation was then computed based on the triangular meshes that were created by connecting the ink markers on the protruding perineal surface (Fig. 4.3b). The triangular meshes were assumed to be a planar membrane as many curved, thin bodies are. The deformation state for a membrane was then be represented by the position of points on the two-dimensional surface, thus making the formulation of the membrane behavior simple, even for large displacement response (Buechter and Ramm 1992; Taylor et al. 2005) (Fig. 4.4). In the plane of the triangle, the deformation gradient **F** is given by

$$\mathbf{F} = \mathbf{j}\mathbf{J}^{-1} \quad ,$$

where **J** is the Jacobian transformation for the reference configuration ($\mathbf{J}^{-1}$ is used to denote the inverse of **J**) and **j** that for the current configuration, which can be determined as

$$\mathbf{J} = \begin{bmatrix} \left(\Delta\tilde{\mathbf{X}}^{21}\right)^{\mathrm{T}}\mathbf{M}_1 & \left(\Delta\tilde{\mathbf{X}}^{31}\right)^{\mathrm{T}}\mathbf{M}_1 \\ \left(\Delta\tilde{\mathbf{X}}^{21}\right)^{\mathrm{T}}\mathbf{M}_2 & \left(\Delta\tilde{\mathbf{X}}^{31}\right)^{\mathrm{T}}\mathbf{M}_2 \end{bmatrix} = \begin{bmatrix} \left\|\Delta\tilde{\mathbf{X}}^{21}\right\| & \left[\left(\Delta\tilde{\mathbf{X}}^{21}\right)^{\mathrm{T}}\left(\Delta\tilde{\mathbf{X}}^{31}\right)\right] / \left\|\Delta\tilde{\mathbf{X}}^{21}\right\| \\ 0 & \left\|\mathbf{M}_3\right\| / \left\|\Delta\tilde{\mathbf{X}}^{21}\right\| \end{bmatrix} \quad ,$$

and

$$\mathbf{j} = \begin{bmatrix} \left(\Delta\tilde{\mathbf{x}}^{21}\right)^{\mathrm{T}}\mathbf{m}_1 & \left(\Delta\tilde{\mathbf{x}}^{31}\right)^{\mathrm{T}}\mathbf{m}_1 \\ \left(\Delta\tilde{\mathbf{x}}^{21}\right)^{\mathrm{T}}\mathbf{m}_2 & \left(\Delta\tilde{\mathbf{x}}^{31}\right)^{\mathrm{T}}\mathbf{m}_2 \end{bmatrix} = \begin{bmatrix} \left\|\Delta\tilde{\mathbf{x}}^{21}\right\| & \left[\left(\Delta\tilde{\mathbf{x}}^{21}\right)^{\mathrm{T}}\left(\Delta\tilde{\mathbf{x}}^{31}\right)\right] / \left\|\Delta\tilde{\mathbf{x}}^{21}\right\| \\ 0 & \left\|\mathbf{m}_3\right\| / \left\|\Delta\tilde{\mathbf{x}}^{21}\right\| \end{bmatrix} \quad .$$

where $\Delta\tilde{\mathbf{x}}^{ij} = \tilde{\mathbf{x}}^{i} - \tilde{\mathbf{x}}^{j}$ and $\hat{\mathbf{X}}^{i}$, $\tilde{\mathbf{x}}^{i}$ denote nodal values of the reference coordinates and the current coordinates, with the definition of $\|\mathbf{a}\| = \sqrt{\mathbf{a}^{\mathrm{T}}\mathbf{a}}$. Accordingly, we defined the unit vectors on a surface coordinate system as

$$\mathbf{M}_1 = \frac{\Delta\hat{\mathbf{X}}^{21}}{\left\|\Delta\hat{\mathbf{X}}^{21}\right\|} \quad ,$$

$$\mathbf{M}_3 = \Delta\hat{\mathbf{X}}^{21} \times \Delta\hat{\mathbf{X}}^{31} \quad ,$$

$$\mathbf{M}_2 = \frac{\mathbf{M}_3}{\left\|\mathbf{M}_3\right\|} \times \mathbf{M}_1 \quad .$$

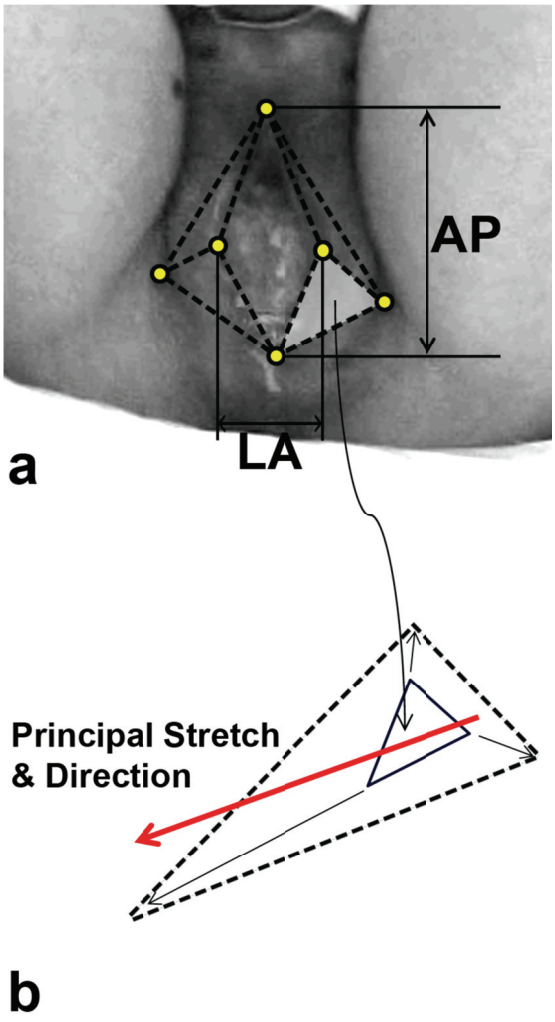

Figure 4.3. (a) Prior to recording, ink-based markers were placed on the perineum (indicated here with yellow dots). Antero-posterior (AP) and lateral (LA) diameters were defined as distances of the four points around the vaginal opening. (b) Triangular meshes from undeformed configuration at the beginning of the 2nd-stage (solid line) and deformed configuration during a push (dash line), are used to calculate the magnitude and direction of the most dominant components of the deformation (red arrow, often referred to as the principal stretch and direction).

Notice that the first unit vector was aligned along the 1-2 side. Current quantities may be deduced by replacing upper case letters by lower case ones. Using these definitions, the left Cauchy-Green deformation tensor **b** may be expanded as

$$\mathbf{b} = \mathbf{F}\mathbf{F}^{\mathrm{T}} \quad .$$

The principal spatial direction $\hat{\mathbf{n}}_a$ and the principal stretches λ_a could then be calculated in the convenient form of their spectral decomposition, i.e.

$$\mathbf{b} = \sum_{a=1}^{3} \lambda_a^2 \hat{\mathbf{n}}_a \otimes \hat{\mathbf{n}}_a \quad .$$

We created a perineal surface deformation map by superimposing $\hat{\mathbf{n}}_a$ and λ_a on the recorded images in order for a faster and more intuitive understanding of the perineal surface motion during delivery.

Figure 4.4. Description of coordinates for triangular element. Note that X_i, x_i, i = 1,2,3 are the global Cartesian coordinate system and Y_i, y_i, i = 1,2,3 are a surface coordinate system, with upper case letters refer to the reference frame and lower case ones the current frame.

The unit vectors on the surface coordinate system were denoted as $\mathbf{M}_i$, $\mathbf{m}_i$, i = 1,2,3, respectively.

4.3 Results

Two female volunteers, who were 20 and 32 years old, respectively, were invited to participate and their second stage of vaginal delivery was recorded by a custom-made computer-vision measurement system. The duration of the measurement of the recorded subjects were 16 and 106 minutes, and then the period that did not contain active pushing phase were trimmed out. The lengths of the processed recording time, therefore, were 15 and 30 minutes.

Figure 4.5. Temporal changes in AP and LA diameters during the final ten minutes (Min) of the 2nd-stage of labor. Six and eight pushing efforts (asterisks) were observed from subjects during this recording period, respectively. There was an inevitable interruption by a practitioner recorded (h) in one of the recordings. Note that significant increase in diameters at the last pushing when the fetal head passed out of the vaginal opening.

Figure 4.5 shows time course of diametric changes during the last ten minutes of the 2nd stage vaginal delivery. Substantial changes in both of the diameters were concentrated in the final pushing phase. Diametric changes and the pushing pattern seemed to be in phase, proving the validity of the measurement method.

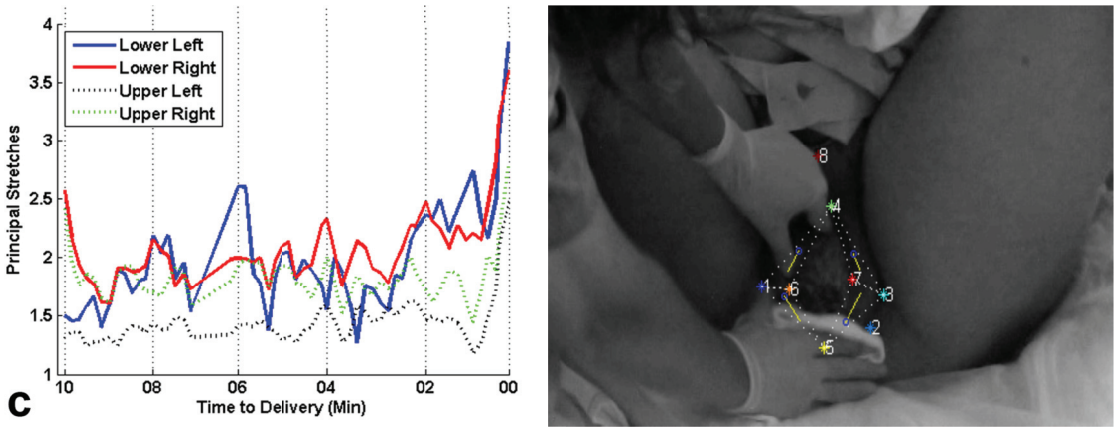

Figure 4.6. (Left) Principal stretches of the four triangularly meshed regions on the perineum during the final ten minutes (Min) of the 2nd-stage of labor. (Right) Directions of principal stretch are superimposed on the triangular mesh during final push. The directions were concentric to the vaginal opening.

Figure 4.6 demonstrates the perineal surface deformation patterns from the recording. The deformation during the final push is up to twice that of earlier pushes in the 2nd-stage of labor, reaching greater than 3.5 of its original length. The rates of stretch ratio during the final push were 2.30 (/min) and 1.11 (/min), respectively. The directions on which the principal stretches lie were concentrically distributed with respect to the center of the vaginal opening. Spatial resolution of the ink dot markers placed during the measurement seemed to be adequate. The results were helpful in differentiating local stretch magnitude and direction, although any generalization of the deformation pattern was not able to make due to small subject sample size.

4.4 Discussion

The current study has demonstrated the capabilities of a system to track the detailed time course of the perineal surface deformation during the second stage of labor using a novel computer vision-based measurement system. This system enabled objective representations of the deformation in terms of various geometric quantities. Unlike a simple metric such as the vaginal opening diameter, stretch rate, perineal descent and principal stretches and directions of the perineal surface could be documented for the first time. Near the end of the second stage of vaginal delivery appeared to be the moment when all the quantities reached the maximum values - stretch rate was as high as 2.30 (/min), diameters of the opening became 12.5 cm (AP) and 7.9 cm (LA), and more than 3.5 times the original length of principal stretch occurred in the direction tangent to the vaginal opening perimeter.

Based on the observation that circumferential stretch was very noticeable, which seemingly relates to the posterior protrusion of the superficial perineal surface, one might argue that perineal descent might not be worth measuring. The perineal descent, however, has been reported by a number of investigators to relate to anatomical characteristics as well as pelvic organ prolapse symptoms (Boulay et al. 2009; Broekhuis et al. 2010). Moreover, biomechanical analyses have shown perineal descent was caused by the posterior rotation of the pubovisceral portion of the levator ani muscle relative to its pubic bone origin, as evidenced by clinical observation as well (Lien et al. 2004; Jing 2010).

Perineal deformation was expressed as the principal spatial direction and the amount of principal stretch. Since these quantities can be plotted on every mesh from interconnected points of more than three points on the perineal surface, they would be likely to reveal the regional difference in the surface deformation as the newborn is delivered. It has the potential to answer a lot of open questions. For example, it is known that levator defects occur more commonly on the right side so it might be important to know which side demonstrates greater perineal stretch (Margulies et al. 2007; March et al. 2012).

When it comes to the mechanism of muscle stretch injury, stretch rate might be an important factor for determining whether the muscle exceeds a critical limit because muscle is known to behave in a viscoelastic manner. The level of stress on the muscle is proportional to the rate at which the muscle is stretched as well as the absolute amount of stretch itself. Therefore, recording stretch rate at the end of second state is expected to be a valuable for further research. Moreover, an improved understanding of this information can aid the clinician in potentially directing the amount of effort and timing of pushing to reduce undue stress and stretch as much as is possible to reduce rapid deformation of the perineum.

There are several limitations that should be kept in mind when interpreting the results of this study. The measurement accuracy is limited by the consumer-level webcams used in the system. However, the small size of the cameras and the simple electrical configuration were weighted heavily as design requirements because we needed to make the system unobtrusive. This was based on feedback from the clients themselves. An early prototype had been far too large and imposing for women to feel comfortable.

We believe this present measurement accuracy was sufficient to capture the intrapartum perineal deformation pattern. Also, the ease of use of the cameras and the ability to place them in a location to not be disruptive but to actually gain clear recordings was of value to this system Furthermore, the study included only two subjects and the difference between nulliparous and parous women could not be evaluated. Recruiting subjects for this study had been extremely challenging due to the subjects' privacy concerns. Although we assured clients that no private information would be identified, patients were highly reluctant to participate in the study due to concerns both for privacy during the birth experience. This seemed of particular significance to first time mothers who had a lot of questions about what the actual process of birth would be like and were thus reluctant to include other elements in the room which they feared could be a distraction. Other limitations concern the paucity of real-time processing, which might lead to a faster interpretation of the second stage events for practitioners. A major reason for this limitation was the lack of source information that is easily detected by image processing routine. For example, materials like self-growing powder materials might be adequate to improve the system to a fully automated one.

Intrapartum documentation of the events of second stage labor resulting in vaginal delivery is a challenging and intricate measurement task, because extensive care is usually required during this period and the safety of mother and fetus must be prioritized before anything else. At the same time, injury prevention research has been constrained by the paucity of details on the second stage kinematics. We believe that this study has successfully addressed this research gap by using a unique quantitative, instrumented

measurement system to assess progress and pelvic floor deformation during the second stage of labor.

4.5 References

Dietz, H. P., Lanzarone, V. (2005). Levator trauma after vaginal delivery. *Obstet. Gynecol., 106*(4), 707-712. doi: 10.1097/01.AOG.0000178779.62181.01

Kearney, R., Miller, J. M., Ashton-Miller, J. A., DeLancey, J. O. L. (2006). Obstetric factors associated with levator ani muscle injury after vaginal birth. *Obstet. Gynecol., 107*(1), 144-149. doi: 10.1097/01.AOG.0000194063.63206.1c

DeLancey, J. O., Morgan, D. M., Fenner, D. E., Kearney, R., Guire, K., Miller, J. M., Hussain, H., Umek, W., Hsu, Y., Ashton-Miller, J. A. (2007). Comparison of levator ani muscle defects and function in women with and without pelvic organ prolapse. *Obstet. Gynecol., 109*(2 Pt 1), 295-302. doi: 10.1097/01.AOG.0000250901.57095.ba

Lien, K. C., Mooney, B., DeLancey, J. O., Ashton-Miller, J. A. (2004). Levator ani muscle stretch induced by simulated vaginal birth. *Obstet. Gynecol., 103*(1), 31-40. doi: 10.1097/01.AOG.0000109207.22354.65

Hoyte, L., Damaser, M. S., Warfield, S. K., Chukkapalli, G., Majumdar, A., Choi, D. J., Trivedi, A., Krysl, P. (2008). Quantity and distribution of levator ani stretch during simulated vaginal childbirth. *Am. J. Obstet. Gynecol., 199*(2), 198 e191-195. doi: 10.1016/j.ajog.2008.04.027

Parente, M. P., Jorge, R. M., Mascarenhas, T., Fernandes, A. A., Martins, J. A. (2008). Deformation of the pelvic floor muscles during a vaginal delivery. *Int. Urogynecol. J., 19*(1), 65-71. doi: 10.1007/s00192-007-0388-7

Li, X., Kruger, J. A., Nash, M. P., Nielsen, P. M. (2010). Anisotropic effects of the levator ani muscle during childbirth. *Biomech. Model. Mechanobiol., 10*(4), 485-494. doi: 10.1007/s10237-010-0249-z

Bradski, G., Kaehler, A. (2008). *Learning OpenCV: computer vision with the OpenCV library*. Sebastopol, CA: O'Reilly Media.

Buechter, N., Ramm, E. (1992). Shell theory versus degeneration—a comparison in large rotation finite element analysis. *Int J Numer Methods Eng, 34*(1), 39-59. doi: 10.1002/nme.1620340105

Taylor, R., Oñate, E., Ubach, P.-A. (2005). Finite Element Analysis of Membrane Structures. In E. Oñate & B. Kröplin (Eds.), *Textile Composites and Inflatable Structures* (Vol. 3, pp. 47-68). Dordrecht, The Netherlands: Springer.

Boulay, C., Prudhomme, M., Prat-Pradal, D., Pouderoux, P., Duval-Beaupère, G., Pélissier, J. (2009). Perineal Descent Predicted by a Pelvic Bone Factor: The Pelvic Incidence Angle. *Dis. Colon Rectum, 52*(1), 119-126. doi: 10.1007/DCR.0b013e3181972447

Broekhuis, S., Hendriks, J., Fütterer, J., Vierhout, M., Barentsz, J., Kluivers, K. (2010). Perineal descent and patients' symptoms of anorectal dysfunction, pelvic organ prolapse, and urinary incontinence. *Int. Urogynecol. J., 21*(6), 721-729. doi: 10.1007/s00192-010-1099-z

Jing, D. (2010). *Experimental and theoretical biomechanical analyses of the second stage of labor.* PhD. thesis, University of Michigan.

Margulies, R. U., Huebner, M., DeLancey, J. O. (2007). Origin and insertion points involved in levator ani muscle defects. *Am. J. Obstet. Gynecol., 196*(3), 251 e251-255.

March, M. I., Warsof, S. L., Chauhan, S. P. (2012). Fetal biometry: relevance in obstetrical practice. *Clin. Obstet. Gynecol., 55*(1), 281-287. doi: 10.1097/GRF.0b013e3182446e9b

CHAPTER 5

General Discussion

5.1 Summary and Significance

This dissertation has clinical significance in that it explains more concretely how the birth-related injury occurs and progresses. Hypotheses on injury mechanisms were first suggested based on the findings from the cadaveric examinations (Chapters 2.1 and 2.3) around the putative injury areas that had been found from a number of imaging researches (Tunn et al. 1999; Hoyte et al. 2001; DeLancey et al. 2003; Dietz and Lanzarone 2005). We noticed the geometrical similarities between the birth-injury zones and the other engineering structures. For example, an oblique interface between the pubovisceral muscle and the pubic bone was compared with a scarf joint, and then general characteristics of the scarf joint was applied to design a biomechanical analysis in order to understand the mechanical behavior of the pubovisceral muscle origin (Chapter 3.1). The simulation results demonstrated that the oblique corner of the muscle enthesis is more vulnerable to stretch-induced injury due to the unique geometry of the scarf enthesis. At the lateral margin of the pubovisceral muscle origin, on the other hand, was the levator arch, which is essentially a thick collagenous fiber connecting the pubic bone and the ischical spine. We were able to find out the way the levator arch supports the

levator ani muscle resembles how a catenary cable bears the weight of a suspension bridge. This insight, along with the fundamental information on the levator ani fiber orientation (Chapter 2.2), was applied to create a refined anisotropic 3-D finite element model and the srisks of damage occurrence at these locations were considered (Chapter 3.2). This biomechanical consideration provided with reasonable explanation of why the injury occurs at this specific location and in a particular sequence. Finally, as a potential verification tool for emerging pelvic floor biomechanics studies (Li et al. 2010; Pu et al. 2011; Brandao et al. 2012; Jing, D. et al. 2012), a new method of in vivo measurement of the second stage of vaginal delivery was suggested (Chapter 4).

Figure 5.1. Structural analogy of two attachment types to hanging beaded curtains. (Left) Direct attachment is thought of a series of bead strings that are individually hung to the wall. Therefore, local damage is not necessarily propagated to the next. Note that orange points to the aponeurosis, which connects the levator ani muscle fascicles (red) to the pubic (Right) Catenary attachment is different in that beads are suspended by a catenary cable (blue). So, single detachment at one of the fixation of the catenary cable could lead to complete collapse of the entire unit. This catenary cable corresponds to the levator arch (LArch).

To give a brief summary on the mechanisms of the levator ani muscle injury during vaginal birth that was refined by a number of studies in this thesis, we can make a structural analogy of the proposed injury mechanism to the behavior of a hanging beaded curtain. The type 1 injury could be compared to a regular beaded curtain, where beaded strings are independently attached (Fig. 5.1 left). Therefore, if one of the strips was pulled and detached, adjacent string would not be affected. However, if the vertical beaded strings are linked to another cable connecting two points and one of the points were separated, the entire structure would collapse in a rather catastrophic manner. This corresponds to the type 2 injury.

5.2 Limitations

The approaches used in this thesis have several limitations.

First of all, despite women experience noticeable remodeling of their tissues throughout their entire body during pregnancy (Myers et al. 2009; Wells et al. 2012), the finite element simulation results were based on human cadaver tissues (Jing, D. 2010). Therefore, mechanical behavior of *in vivo* pregnant human soft tissues was not able to be captured. There is, however, no available information on either uniaxial or biaxial properties of the pregnant human levator ani muscle to the best of our knowledge, and this approach was considered the closest approximation available to us at the present time. Further research on the measurement of the change in the levator ani muscle properties before and during pregnancy would greatly benefit the quality of analysis of the vaginal delivery.

Second, moderate number of samples hindered from deducing stronger conclusions in a few chapters, including Chapters 2.1, 2.3, and 4. Acquiring nulliparous or young anatomy is extremely rare in the donation program. Comparisons of the morphology at the birth-injury zones between young and elderly women or between nulliparous and primiparous women would potentially reveal a lot of unknown characteristics that could help better understand underlying injury mechanisms. Also, recruiting pregnant women for intrapartum measurement was very challenging mainly because privacy issues were brought up. If more subject were to be participated in this kind of study, valuable dataset such as the amount of the perineal and the fetal head descent would be able to measured.

Finally, the modeling strategy for the vaginal delivery biomechanics model was limited to a subject-specific setting. A subject-specific geometry model for finite element analysis is very advantageous because accuracy of the model could be focused and relatively easily achieved. So, better results for a given circumstances are expected to be deduced. On the other hand, a parametric modeling, where a modeling is established by a finite number of parameters that determines the overall shape of a model, might potentially be more suitable to generalize how the output of a biomechanics model could be apportioned to different sources of inputs. A subject-specific modeling would also be applied to different scenarios by slightly modifying the geometry as well as the properties of the model. But, the more the number of the input parameter combinations are tested, the less effective and efficient the processing could be.

5.3 References

Tunn, R., DeLancey, J. O., Howard, D., Thorp, J. M., Ashton-Miller, J. A., Quint, L. E. (1999). MR imaging of levator ani muscle recovery following vaginal delivery. *Int. Urogynecol. J. Pelvic Floor Dysfunct., 10*(5), 300-307.

Hoyte, L., Schierlitz, L., Zou, K., Flesh, G., Fielding, J. R. (2001). Two- and 3-dimensional MRI comparison of levator ani structure, volume, and integrity in women with stress incontinence and prolapse. *Am. J. Obstet. Gynecol., 185*(1), 11-19. doi: 10.1067/mob.2001.116365

DeLancey, J. O., Kearney, R., Chou, Q., Speights, S., Binno, S. (2003). The appearance of levator ani muscle abnormalities in magnetic resonance images after vaginal delivery. *Obstet. Gynecol., 101*(1), 46-53. doi: S0029784402024651

Dietz, H. P., Lanzarone, V. (2005). Levator trauma after vaginal delivery. *Obstet. Gynecol., 106*(4), 707-712. doi: 10.1097/01.AOG.0000178779.62181.01

Li, X., Kruger, J. A., Nash, M. P., Nielsen, P. M. (2010). Anisotropic effects of the levator ani muscle during childbirth. *Biomech. Model. Mechanobiol., 10*(4), 485-494. doi: 10.1007/s10237-010-0249-z

Pu, F., Xu, L., Li, D., Li, S., Sun, L., Wang, L., Fan, Y. (2011). Effect of different labor forces on fetal skull molding. *Med. Eng. Phys., 33*(5), 620-625. doi: 10.1016/j.medengphy.2010.12.018

Brandao, S., Da Roza, T., Mascarenhas, T., Duarte, S., Ramos, I., Parente, M., Jorge, R. N. (2012). Moment of inertia as a means to evaluate the biomechanical impact of pelvic organ prolapse. *Int. J. Urol.* doi: 10.1111/j.1442-2042.2012.03219.x

Jing, D., Ashton-Miller, J. A., Delancey, J. O. (2012). A subject-specific anisotropic visco-hyperelastic finite element model of female pelvic floor stress and strain during the second stage of labor. *J. Biomech., 45*(3), 455-460. doi: 10.1016/j.jbiomech.2011.12.002

Myers, K., Socrate, S., Tzeranis, D., House, M. (2009). Changes in the biochemical constituents and morphologic appearance of the human cervical stroma during pregnancy. *Eur. J. Obstet. Gynecol. Reprod. Biol., 144 Suppl 1*, S82-89. doi: 10.1016/j.ejogrb.2009.02.008

Wells, S. M., Pierlot, C. M., Moeller, A. D. (2012). Physiological remodeling of the mitral valve during pregnancy. *American journal of physiology. Heart and circulatory physiology, 303*(7), H878-892. doi: 10.1152/ajpheart.00845.2011

Jing, D. (2010). *Experimental and theoretical biomechanical analyses of the second stage of labor*. PhD. thesis, University of Michigan.

CHAPTER 6

Conclusions

The major findings in this dissertation are as follows:

- **Chapter 2.1:** Morphology of the pubovisceral muscle (PVM) origin from the pubic bone shows different patterns in the medial region to the lateral margin. Unlike the medial region which demonstrates an enthesis where there are multiple muscle fibers that individually attaches to the pubic periosteum by short connective tissue slips, the central portion is very thin and aponeurotic. The very lateral margin is comprised of the levator arch, which is a relatively thick collagenous bundle. This suggests that vaginal loading is transferred mainly through both the thick, direct medial enthesis as well as the lateral levator arch attachment.
- **Chapter 2.2:** In living women, a magnetic resonance imaging study demonstrated three distinct fiber directions in the levator ani muscle subdivisions; namely the pubovisceral muscle (PVM), puborectal muscle (PRM), iliococcygeal muscle (ICM) as well as external anal sphincter (EAS). We conclude that the 58° difference in fiber orientation between the PVM and the PRM reflects the former acting primarily to elevate perineal structures (a 'lifter') and the latter increasing levator hiatus closure creating the vaginal high pressure zone (a 'closer').
- **Chapter 2.3:** The medial portion of the pubovisceral portion of the levator ani muscle originates tangentially from the pubic bone through a fibrous entheses. Collagenous

fibers, which lie between the pubovisceral muscle and the pubic bone and connect each other, mainly arise from the periosteum of the pubic bone. In a longitudinal cross-section, the amount of the connective tissue and muscular tissue becomes equal at approximately 8 mm from the pubic bone.

- **Chapter 3.1:** The oblique interface between the pubic bone and PVM, along with heterogeneous material properties of the enthesis, causes a noticeable strain energy concentration at the inferior margin of the interface corner when the PVM is placed under tension. This suggests a likely injury initiation point during the late second stage of vaginal birth. The severity of the strain energy localization was inversely proportional to the scarf angle of the PVM as well as the posterior bending, but proportional to the amount of stretch applied to the PVM.
- **Chapter 3.2:** The pubic origins of both the levator arch and PVM are shown both to be at risk for injury during the second stage of vaginal birth due to excessive stress and strain. This is the first biomechanical explanation of why it is the pubic origins of these structures that can be injured during vaginal birth.
- **Chapter 4:** This objective measurement method can document the dynamic, multi-dimensional changes of the perineum during the 2nd-stage of labor. The method potentially allows stretch and deformation patterns to be correlated with the occurrence of perineal lacerations.

CHAPTER 7

Suggestions for Future Work

- For an anatomical/histological study, more cadaver specimens need to be acquired in order to draw more general conclusions on the morphological patterns at the birth injury sites. Quantification of the variations in (a) the shape of the levator arch, (b) the levator arch material properties including ultimate tensile strength could be addressed. Comparison of the morphological variations against advancing age and increasing parity is also needed.
- For a computer simulation study, measurement of the elastic and viscoelastic material properties of the pregnant pelvic floor muscle should be conducted. Although many kinds of tissue property data are currently available, the lack of information of the pregnant effect on the pelvic floor soft tissue hinders investigators from emulating a more realistic vaginal birth simulation.
- Parametric modeling of the pelvic floor would allow biomechanical models to predict the injury location and pattern during vaginal delivery. Until now, all the previously reported vaginal birth biomechanics models were subject-specific models, which made hard to deduce generalized conclusions. With the accumulation of the information from the previous models, some meaningful results might be generated.
- The stereophotogrametry proved itself to be a reasonable technique that can be efficiently used to measure the deformation during vaginal delivery. Although the

occlusion of the scene may be an inevitable event for this experiment setting, alternative light source which can penetrate through the skin might be adequate for the configuration. Finer distribution of the marker is another obstacle to overcome for an even more meaningful study.

APPENDIX

APPENDIX A

Consumer Camera-Based System for Measuring Fetal Head and Pelvic Floor Displacements During the Second Stage of Labor

A.1 Introduction

Pelvic floor dysfunction is a major health problem for women, which requires approximately 11% of American women to be surgically treated annually (Wilson et al. 2001). In particular, vaginal delivery is considered to be a major risk factor for developing pelvic floor dysfunction (Mant et al. 1997). The circumferential length of the circumvaginal tissue at the second stage is expected to increase four times the initial periphery, and this process often causes injuries to the striated muscles of the levator ani (Brooks et al. 1995). However, the level of stretch in levator ani muscles during birth, accompanying displacements in the whole pelvic floor, has not yet been quantified experimentally.

There are several methodologies for studying the causes and the characteristics of pelvic floor dysfunction, including magnetic resonant imaging (MRI) (Hoyte et al. 2001) and computerized finite element methods (FEM) model (Lien et al. 2005). Although MRI allows for examining the three-dimensional pelvic floor geometry both inside and outside the human body, there are limitations that exist because MRI devices are immobile and costly. On the other hand, a 3-D FEM pelvic floor model has been used to evaluate the levator ani muscle stretch induced during the second stage of simulated labor (Lien et al.

2004). However, the results from computer models are often compared with experimental measurements to verify the predictions, therefore, achieve a stronger authenticity (Pan 1990).

As an alternative, stereophotogrammetric methods have been used to reconstruct 3-D object coordinates from photographs for medical purposes (Mitchell and Newton 2002). Photogrammetric techniques are comparatively advantageous in that they are easier to repeatedly produce, process and exploit for large amounts of high-resolution data in a geometrically consistent, robust and accurate way. An application by Wojtys et al. (2000) set a precedent by using a structured light imaging system for making non-contact optical measurements of the 3-D shape of the surface of the back in 2,270 boys and girls.

The purpose of this study, therefore, is to describe an experimental apparatus and method for measuring fetal head and pelvic floor displacements during the second stage of labor. Since, this system incorporates the stereophotogrammetric principle into a set of consumer-level digital cameras which are on a movable frame, low-cost measurements can be made in varied locations without compromising accuracy and precision.

A.2 Methods

To meet the requirements of the clinical environment, a specialized mobile camera stand needed to be designed (Figure A.1). The apparatus is mainly comprised of three Olympus Stylus 800 Digital cameras (Olympus America Inc., Center Valley, PA), aluminum frames (80/20 Inc., Columbia City, IN), and a custom projector with a strobe flash. The stand can be drawn and placed at the foot of the bed, and then stored on a

small footprint when not in use. Lead plates, outriggers and a shock-isolating mount were attached to minimize vibrations from the ground. Also, to help an experimenter activate the system with minimal movement, a foot switch was connected to a circuit box, which is responsible for receiving the triggering signal as an input, and firing the cameras and the flash synchronously.

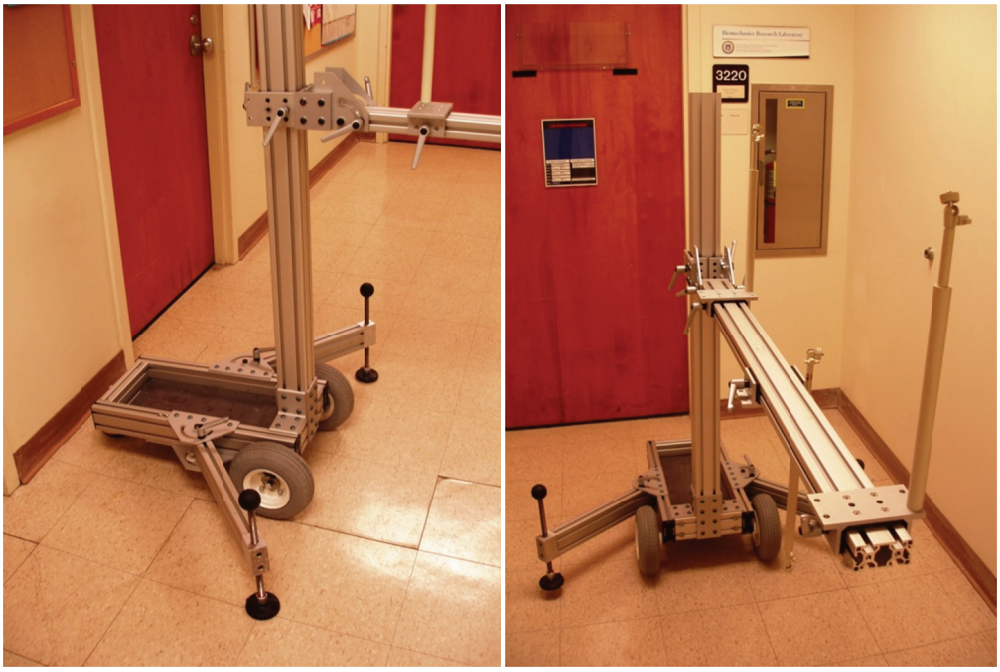

Figure A.1. A mobile camera stand made of aluminum frames. Cameras and a flash can be attached to measure the time course of the second stage of labor.

The flash was designed to project a grid of circular dots on a surface to be used as markers. These markers were utilized to associate the points on one picture to the points on the other picture and, finally, to reconstruct the 3-D perineal geometry. This process was done in the PhotoModeler^{TM} (EOS Systems Inc., Vancouver, Canada) commercial software package by using data uploaded from sets of triple planar images to a PC.

Given that the uterus contracts once every three minutes, the system is expected to measure the change in the vertex location at rest and at the height of every push by asking the experimenter to trigger the cameras. Then, the major and minor vaginal diameters versus time are going to be measured in either a one-shot mode or in a burst mode. The burst mode will be useful for documenting the time-dependent behavior of the tissues on pelvic floor, especially if we can measure the intrauterine pressure.

Pilot calibration tests were performed to determine the level of accuracy and precision of the measuring system. The calibration procedure was based on the method of bundle adjustment (Triggs 2000) and calculated automatically by PhotoModeler^{TM} with the use of a special calibration grid. We used the '1 in N' unit to denote the precision value, which is widely being adopted in the field of photogrammetry.

Finally, the whole procedure was examined and tested through delivery simulation and face reconstruction. Delivery simulation made use of both a mock-up of the vertex and vagina (Figure A.2) and ink reference points to imitate the actual process of laboring. The vertex is gradually supposed to come out through the vagina and to be captured as the fetus is pushed away. Additionally, a face of a man was tagged with dot-shaped stickers and stored in images by the system. The position vectors of the dots were calculated and then used to generate a facial surface.

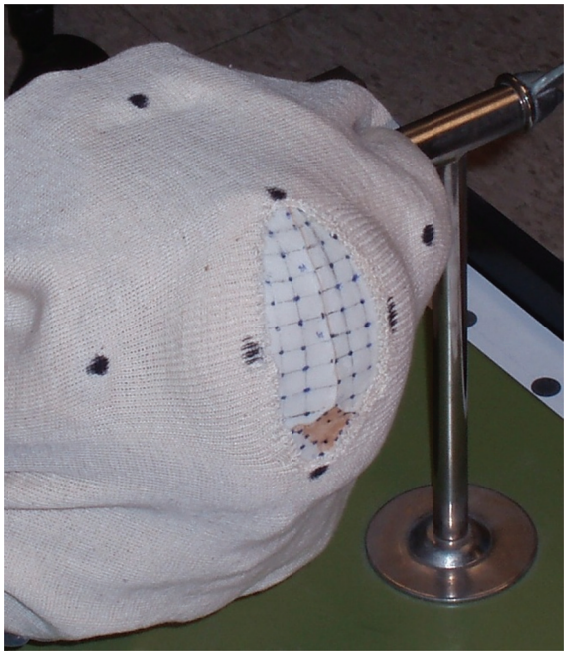

Figure A.2. A mock-up of the vertex and the vagina used to simulate laboring process.

A.3 Results

Pilot calibration tests show that we could locate a flat plane to within up to 1:28,900 of the 75 cm field of view or, in other units, a precision of 0.026 mm. This means that there is as much as 0.026 mm between an expected and calculated value. The precision values appeared to depend on the location of the target, the position of the cameras, and the focus settings, as well. Among these parameters, we consistently found that setting the cameras in ‘auto focus’ mode yielded a better result than ‘manual focus’ mode. (Figure A.3)

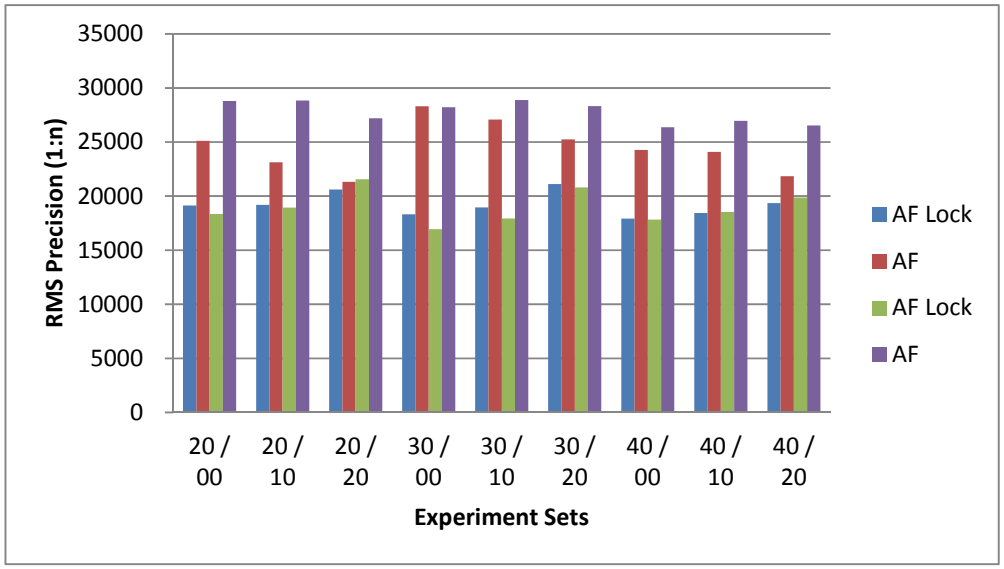

Figure A.3. Precision values for 'auto focus' modes in different camera angle settings. The numbers before slash in the x axis mean the angle between the upper two cameras from the target. And the numbers following slash indicate the angle between the horizontal line connecting the upper cameras and the lower camera.

The results from the delivery simulations and the face reconstruction are shown above (Figure A.4). The left is one of the sample measurements we were trying to achieve from actual experiment settings. This shows three locations of the reconstructed vertex at different time points, from which the major and minor diameter can be measured. Also, the face of the author can be seen on the right after the pictures of the face were taken and then reconstructed. These results prove that even a geometric figure having complicated morphology can be realistically reconfigured. Due to these preliminary findings, we expect that the major and minor diameters of fetal heads can be measured from this form of images. Both results support that this system can be successfully used for measuring the time course of vertex descent during the second stage of labor.

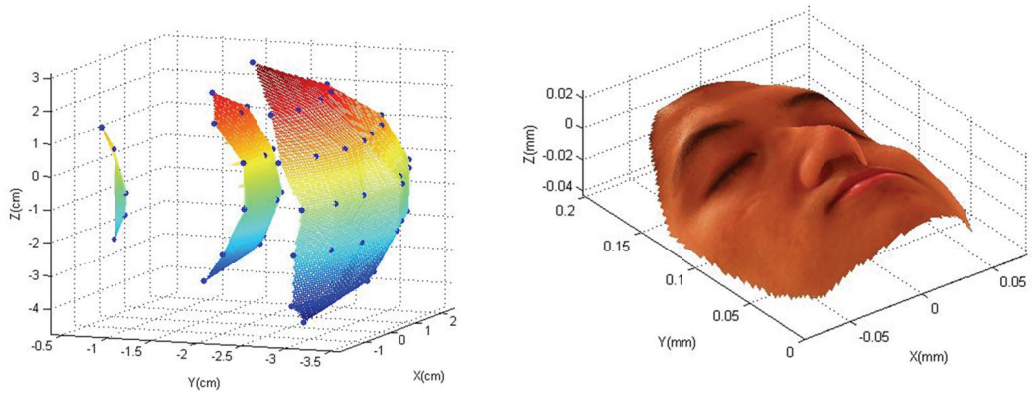

Figure A.4. Reconstructed images in the pilot tests generated by the same process that will be used in the actual experiments. Possible trajectory of the vertex (Left), Face of a person (Right)

A.4 Discussion

The average precision value, the parameter study for finding a better position and camera setting, the points cloud and the reconstructed surface appear to support that this system is able to provide reliable measurements for fetal head and pelvic floor displacement during the second stage of labor. In particular, the precision value of 1:28,900 proves that this system has the capability of distinguishing very close points in pelvic floor area. Given that the voluntary push period lasts about 90 seconds and the interval between the continuous shots takes approximately 9 seconds, we are expecting to achieve 10 sets of images in a push period. This amount of data is thought to be sufficient to document the time-dependent behavior of voluntary pushes.

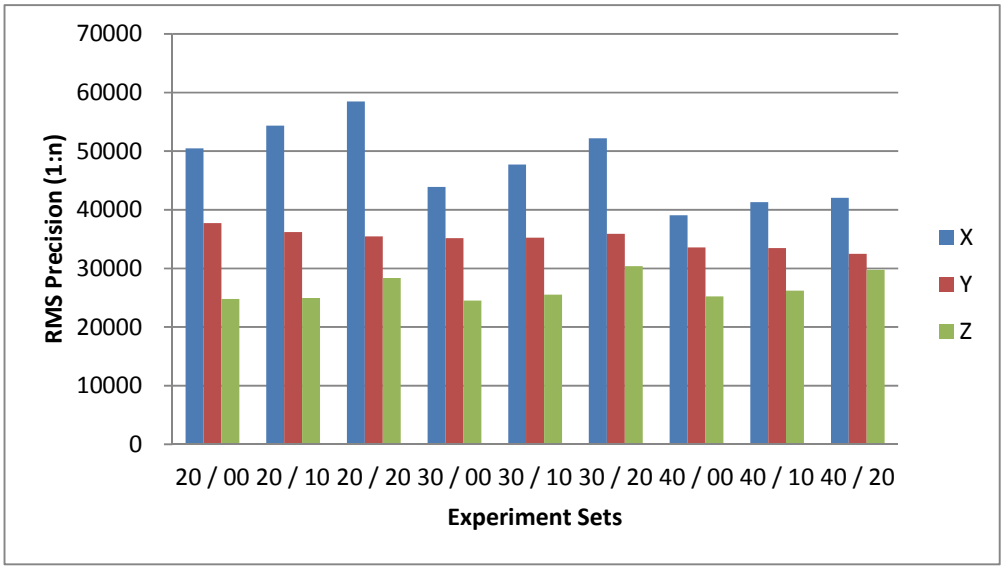

Figure A.5. RMS precision values in three different axes. X and Y axes constitute the transverse plane of the target object. And, Z direction is toward the cameras.

We acknowledge several methodological limitations can possibly occur. First, it should be noted that this system has a better resolution in a transverse plane than in a sagittal plane (Fig. A.5). This result is consistent with the general results measured by the stereophotogrammetric techniques, which shows the worst records in the most-perpendicular plane to the image planes of the cameras. It might be possible to improve the overall accuracy if one of the cameras is repositioned in the sagittal plane. An experiment testing this aspect is worth trying as a further step.

Second, we would like to point out that central area is the best location to be measured in the most accurate manner (Fig. A.6). Therefore, in the actual experiments, the target needs to be positioned in the middle of the viewport generated by the three cameras.

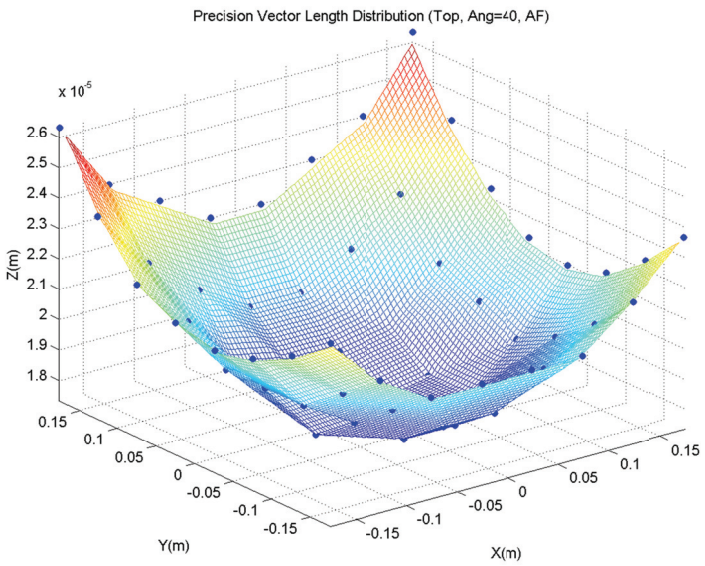

Figure A.6. Distribution of RMS precision value over a plane target. Note that X-Y plane corresponds to the transverse plane, which means that Z axis is parallel to the direction from the plane made by the three cameras to the target object.

Third, the findings of this study assume that there are fixed reference points. However, due to the requirements of the clinical environment, mounting reference points is very restrictive. Currently, several ink markers are planned to be located on the back of the thigh of the subjects and then utilized as a reference points. Hence, further study on the reference point is required.

Finally, the limitations of this study are clear in that the level of accuracy of the system depends on the performance of the cameras. If cameras that have better resolution, such as digital SLR cameras (DSLR camera), are incorporated into the system, of course, they would yield improved precision. However, there is a possible drawback to the DSLR camera it that these might cause anxiety or discomfort to the subjects who are emotionally sensitive at this time in their lives. Furthermore, considering that the current

set of cameras is producing accurate enough results, we could exclude the usage of DSLR cameras.

A.5 Conclusions

A working stereophotogrammetry apparatus was designed, built, calibrated and tested ready for use to make 3-D measurements of perineal geometry and perienal/vertex displacements during vaginal birth. The resolution and precision of the measurements proved adequate for the proposed research project.

A.6 References

Brooks SV, Zerba E, Faulkner JA (1995) Injury to muscle fibres after single stretches of passive and maximally stimulated muscles in mice. J Physiol-London 488 (Pt 2):459-469

Hoyte L, Schierlitz L, Zou K, Flesh G, Fielding JR (2001) Two- and 3-dimensional MRI comparison of levator ani structure, volume, and integrity in women with stress incontinence and prolapse. Am J Obstet Gynecol 185 (1):11-19. doi:10.1067/mob.2001.116365

Lien KC, Mooney B, DeLancey JO, Ashton-Miller JA (2004) Levator ani muscle stretch induced by simulated vaginal birth. Obstet Gynecol 103 (1):31-40. doi:10.1097/01.AOG.0000109207.22354.65

Lien KC, Morgan DM, Delancey JO, Ashton-Miller JA (2005) Pudendal nerve stretch during vaginal birth: a 3D computer simulation. Am J Obstet Gynecol 192 (5):1669-1676. doi:10.1016/j.ajog.2005.01.032

Mant J, Painter R, Vessey M (1997) Epidemiology of genital prolapse: observations from the Oxford Family Planning Association Study. Br J Obstet Gynaecol 104 (5):579-585

Mitchell HL, Newton I (2002) Medical photogrammetric measurement: overview and prospects. ISPRS Journal of Photogrammetry and Remote Sensing 56 (5?6):286-294. doi:10.1016/s0924-2716(02)00065-5

Pan JY (1990) Verification of FEM analysis of load-deflection methods for measuring mechanical properties of thin films. IEEE 4th Technical Digest on Solid-State Sensor and Actuator Workshop:70-73. doi:10.1109/solsen.1990.109823

Triggs B (2000) Bundle Adjustment ? A Modern Synthesis. vol 1883. Springer. doi:10.1007/3-540-44480-7_21

Wilson L, Brown JS, Shin GP, Luc KO, Subak LL (2001) Annual direct cost of urinary incontinence. Obstet Gynecol 98 (3):398-406

Wojtys EM, Ashton-Miller JA, Huston LJ, Moga PJ (2000) The association between athletic training time and the sagittal curvature of the immature spine. Am J Sports Med 28 (4):490-498